EFFECTS OF ADDITIVES ON MECHANICAL MILLING AND HYDROGENATION OF MAGNESIUM POWDERS

A THESIS SUBMITTED TO

THE GRADUATE SCHOOL OF NATURAL AND APPLIED SCIENCES

OF

THE MIDDLE EAST TECHNICAL UNIVERSITY

BY

MURAT GÜVENDİREN

IN PARTIAL FULFILLMENT OF THE REQUIREMENTS FOR THE DEGREE OF

MASTER OF SCIENCE

IN

THE DEPARTMENT OF METALLURGICAL AND MATERIALS ENGINEERING

FEBRUARY 2003

Approval of the Graduate School of Natural and Applied Sciences

Prof. Dr. Tayfur ÖZTÜRK
Director

I certify that this thesis satisfies all the requirements as a thesis for the degree of Master of Science.

Prof. Dr. Naci SEVİNÇ
Head of Department

This is to certify that we have read this thesis and that in our opinion it is fully adequate, in scope and quality, as a thesis for the degree of Master of Science.

Prof. Dr. Tayfur ÖZTÜRK
Supervisor

Examining Committee Members

Prof. Dr. Naci SEVİNÇ

Prof. Dr. Vedat AKDENİZ

Prof. Dr. Şakir BOR

Prof. Dr. İnci EROĞLU

Prof. Dr. Tayfur ÖZTÜRK

ABSTRACT

EFFECTS OF ADDITIVES ON MECHANICAL MILLING AND HYDROGENATION OF MAGNESIUM POWDERS

Güvendiren, Murat
M.S., Department of Metallurgical and Materials Engineering
Supervisor: Prof. Dr. Tayfur Öztürk

February 2003, 132 pages

A study is carried out on hydrogen storage in magnesium-based powders. For this purpose magnesium hydride powders are processed via mechanical milling with the use of additives, namely V, Al_2O_3 and graphite.

Scanning electron microscopy (SEM) and X-ray line broadening studies are carried out to identify the role of additives on structural refinement. The results show that the highest structural refinement is achieved with graphite addition. As powders are exposed to high temperatures during sorption the structural refinement of sorbed systems are also examined. The results indicate that there is a recovery of as-milled structure upon sorption.

Sorption experiments are carried out within the temperature range of 300-400°C. At least three hydriding/dehydriding cycles found to be necessary for reproducible results. Pressure-composition isotherms indicate that the equilibrium hydrogen pressures are in the range of 3-6 atm., and the highest hydrogen storage capacity

achieved in this study is 6.25 wt.% H with graphite addition. The highest sorption rate is also obtained with MgH_2-graphite system.

It is concluded that hydrogen storage capacity and reaction rates are acceptable for practical applications. However, temperatures within which these values are obtained are rather high.

Keywords: Magnesium hydride, hydrogen storage, sorption kinetics, mechanical milling, structural refinement, additives in milling.

ÖZ

HİDROJEN DEPOLAMA AMACIYLA MAGNEZYUM TOZLARININ ÖĞÜTÜLMESİNDE KATKI MADDELERİNİN ETKİSİ

Güvendiren, Murat
Y. Lisans, Metalurji ve Malzeme Mühendisliği Bölümü
Tez Yöneticisi: Prof. Dr. Tayfur Öztürk

Şubat 2003, 132 sayfa

Bu çalışmada hidrojen depolama amacıyla magnezyum tozları mekanik olarak alaşımlandırılmıştır. Bu amaçla magnezyuma V, Al_2O_3 ve grafit ilaveleri yapılarak tozlar mekanik olarak alaşımlandırılmıştır.

Katkı maddelerinin yapısal incelmedeki rolü tarama elektron mikroskobu (SEM) ve x-ışınları kırınım genişleme yöntemi kullanılarak incelenmiş ve en etkin incelmenin grafit ilavesi ile elde edildiği görülmüştür. Tozlar emilim/geribırakım sırasında nispeten yüksek sıcaklıklara maruz kaldığından, öğütme sonundaki incelme korunamamış ve tozlarda yapısal toparlanma gözlenmiştir.

Emilim/geribırakım deneyleri 300-400°C lik sıcaklık aralığında gerçekleştirilmiştir. Tekrarlanabilir sonuçlar için en az üç emilim/geribırakım döngüsünün gerekli olduğu tespit edilmiştir. Basınç kompozisyon eşsıcaklık diyagramları denge hidrojen basıncının 3-6 atm aralığında olduğunu göstermiştir. Çalismada en yüksek hidrojen depolama kapasitesi ağırlıkça yüzde 6.25 olarak

grafit ilavesi ile elde edilmiştir. En hızlı emilim/geribırakım yine grafit ilaveli sistemde elde edilmiştir.

Sonuç olarak çalışmada elde edilen hidrojen depolama ve emilim/geribırakım hızları tatmin edici düzeydedir. Ancak bu değerlerin elde edildiği sıcaklık aralığının (300-400°C) düşürülmesine ihtiyaç duyulmaktadır.

Anahtar Kelimeler: Magnezyum hidrür, hidrojen depolama, emilim/geribırakım kinetiği, makanik alaşımlandırma, yapısal incelme, katkı maddeleri.

To My Grandparents
And To Memnune Kayacan

ACKNOWLEDGEMENTS

I am grateful to Prof. Dr. Tayfur Öztürk for his guidance and insight throughout the preparation of this thesis. This study could not be completed in such a short period without his encouragement, analytical thoughts and experience in summing up conclusions.

I would like to acknowledge the contribution of members of the research group to this study for their cooperation and informative discussions.

Thanks are due to the staff of Metallurgical and Materials Engineering Department for their help in various stages of the study, and special thanks go to Nacmi Avcı for his assistance in X-ray diffraction work.

I would like to express my gratitude to Erdal Güvendiren for his sincere help and guidance, and special thanks are due to the staff of Fişeksan Co.

I would like to sincerely thank to Esra Arıkan for her help and understanding during the intensive period of experiments.

I am truly indebted to my family; İffet Güvendiren, Erdal Güvendiren and Berna Güvendiren, for their great encouragement, patience and support all through my education. I could not achieve this success without my family.

I gratefully acknowledge to METU Research Fund (Project number BAP 02-07-47) and TUBITAK (MISAG 213) for providing the financial support for this study.

TABLE OF CONTENTS

LIST OF TABLES

TABLES

LIST OF FIGURES

FIGURES

CHAPTER I

INTRODUCTION

In recent decade there has been considerable interest in hydrogen as an alternative source of energy. Although hydrogen is readily available and nonpolluting, it has not been exploited as an energy source due to storage problems. Many applications in fields such as fuel cells, thermodynamic devices, etc. require an efficient and safe storage of hydrogen.

One of the storage methods that gain importance in recent years is metal hydrides, i.e. storing hydrogen in solid state. In this respect magnesium hydrides are particularly attractive due to their high storage capacity and low density. However, the main disadvantages of magnesium are the high stability of the hydride, i.e. high temperatures and pressures are needed for sorption (absorption and desorption), slow reaction kinetics, low cycle life and problems in fabrication.

The current study aims to improve the sorption rate as well as to decrease the sorption temperature and pressure so as to make it suitable for practical applications. For these purpose a variety of additives have been added to magnesium and processed via mechanical milling.

The work is made up of following parts; a detailed review on recent studies on magnesium based hydrides for hydrogen storage is presented in Chapter II. Chapter III gives the experimental procedures including the materials used, powder fabrication and set-up for sorption experiments. Experimental results and discussions are presented in Chapter IV. Finally, the conclusions derived from the current work are given in Chapter V.

CHAPTER II

LITERATURE REVIEW

2.1. INTRODUCTION

In the present decade public interest is aroused in the possibilities of diversifying energy resources due to the shortages of petroleum supplies, continuous increase in the world energy needs and environmental pollution. Therefore, the investigations focused on finding renewable, efficient and clean energy supplies.

Hydrogen, which is a promising medium for both energy transmission and storage, may be a solution. It is essentially nonpolluting, the major by-product of combustion is H_2O, and it can be generated from readily available and abundant raw materials. In fact, hydrogen not only offers the possibility of easy production and transportation, but also the capacity to be stored in large quantities. In addition it produces more energy per unit weight than any other fuel. The comparison of energy density of various fuels is given in Table 2.1. (Selvam et al., 1986)

Hydrogen can be utilized in a number of ways. Combustion of hydrogen in an internal combustion engine and combining hydrogen with oxygen in a fuel cell to produce electricity are the most common methods. Beside automotive applications, thermal engines, air conditioning systems and heat exchangers are also involved in methods of utilization. (Selvam et al, 1986)

Although hydrogen has unique properties, it has not yet been widely exploited for use as a fuel due to the greatest disadvantage of storing it economically and efficiently.

Hydrogen has been traditionally stored in the form of liquid and compressed gas in storage tanks. The major disadvantages in gas storage are the high compressed gas pressures (greater than 150 atm), large volumes and additional weight of the tank and safety risks. In terms of liquid storage the need of special care, extremely low temperatures (-253°C), high evaporation rates and high cost of the process (liquefaction requires 25% of the available heat from combustion of hydrogen) are the main disadvantages (Ivey and Northwood, 1983). Therefore, neither of the conventional methods offers an efficient way of storage.

The reversible reaction of hydrogen with metals, alloys or intermetallic compounds is considered to be a convenient way of hydrogen storage (Selvam et al., 1986).

2.2 METAL HYDRIDES

Metal-hydride reaction can be given as follows:

$$M + (x/2)\ H_2 = MH_x$$

Metal-hydride reactions are reversible, and the forward reaction can be exothermic or endothermic depending on the system. The reaction is highly pressure dependent i.e. hydrogen pressure of the system determines the direction of the reaction.

Two basic properties that make metal hydrides attractive are their high and reversible storage capacity per mole of compound, and high energy stored by unit volume.

Hydrogen content and energy density of various hydrogen storage media are given in Table 2.2. (Bolcich et al., 1994)

Table 2.1. Energy density of various fuels (Selvam et al., 1986).

FUEL	Energy density (heat of combustion) ($MJ.kg^{-1}$)
Hydrogen	141.90
Methane	55.55
Ethane	51.92
Propane	50.39
Gasoline	47.27
Natural Gas	47.21
Kerosene	46.00
Crude Oil	45.55
Benzene	42.29
Coal	31.38
Ethanol	29.70
Methanol	22.69
Ammonia	20.54
Wood	17.12

Table 2.2. Hydrogen content and energy density of several hydrogen storage media (Bolcich et al, 1994).

Medium	Hydrogen Content (Wt%)	Volumetric Density (H atoms L^{-1}) ($x10^{19}$)	Energy Density ($MJ\ kg^{-1}$)	Energy Density ($MJ\ L^{-1}$)
Gaseous H_2 (150 atm)	100.00	0.5	141.90	1.02
Liquid H_2 (-253 °C)	100.00	4.2	141.90	9.92
MgH_2	7.65	6.7	9.92	14.32
VH_2	2.10	11.4	—	—
Mg_2NiH_4	3.60	5.9	4.48	11.49
$TiFeH_{1.95}$	1.95	5.5	2.47	13.56
$LaNiH_{6.7}$	1.50	7.6	1.94	12.77
$ZrMn_2H_{3.4}$	1.75	6.0	—	—
$ZrMn_2Fe_{0.8}H_{3.4}$	1.38	4.8	—	—

It can be seen from Table 2.2 that metal hydrides can store much more hydrogen atom per unit volume than gaseous and liquid storage.

The most common applications of metal hydrides are hydrogen storage, which can be classified as large and medium sized stationary storage, small stationary storage and mobile transportation. Sandrock (1999) pointed out that the important property for stationary storage is the low cost of the hydride former because the process requires large amounts of hydride former. On the other hand for mobile storage the amount of hydrogen stored per unit weight is important.

Metal hydrides are also potential candidates for thermodynamic energy storage devices such as hydride compressors, hydride heat engines (Dantzer, 1997; Groll et al., 1994; Reiser et al., 2000; Sandrock, 1999). Groll et al. (1994) reported that metal hydrides are efficient for refrigerators and heat pumps. Bogdanovic et at. (1995) reported a pilot reversible high temperature steam generator based on MgH_2/Mg system. Metal hydrides have been used successfully as actuators, temperature sensors and detectors (Dantzer, 1997; Sandrock, 1999). Metal hydrides may also be used in fuel cells (Liu et al., 1997; Choi et al., 2000; Cui et al., 2000; Wu et al., 2000).

Recently, investigations are focused on mobile storage for hydride vehicles based on fuel cells and internal combustion engines (Schulz et al., 1999; Dantzer, 1997).

2.3. STORAGE CRITERIA FOR METAL HYDRIDES

Many investigations have been made on hydride forming metals to determine the important parameters in selecting the proper system for hydrogen storage. (Douglas and Derek, 1983; Jain and Vijay, 1987; Selvam et al., 1986, 1988; Bolcich et al., 1994; Dantzer, 1997). The researchers are in agreement that the candidate material has to meet stringent requirements that can be summarized as follows:

i) High hydrogen storage capacity per unit weight
ii) Fast metal-hydrogen reaction kinetics
iii) Minimum degradation upon hydriding/dehydriding cycling
iv) Resistance to poisoning (O_2, H_2O, CO, CO_2)
v) Low hydriding/dehydriding hysteresis
vi) Easy alloy fabrication and low cost

Douglas and Derek (1983), and Selvam et al. (1986) summarized the major alloy types that to some extent meet the above requirements. They grouped the systems as follows: AB (FeTi, ZrNi, TiAl), AB_2 (ZrC_2, $ZrMn_2$, $LaNi_2$, Zr (Fe_xV_{1-x})), AB_3 & A_2B_7 (VFe_3, $CeCo_7$, Th_2Fe_7), AB_5 ($LaNi_5$, $LaCo_5$, $CeCo_5$), and Mg and Mg-based compounds (Mg, Mg_2Cu, Mg_2Ni).

Of the systems investigated in the literature, magnesium is considered to be the best hydrogen storage material when cost, weight, storage capacity and material availability are considered (Selvam et al., 1986; Liang et al., 1999a).

2.4. MAGNESIUM AND MAGNESIUM BASED HYDRIDES

Magnesium has the highest hydrogen capacity per unit weight, 7.6 wt%, than any other metal. The low density (of 1.745 g/cm^3 at RT) of Mg is another promising parameter as compared to other hydrogen storing metals. Magnesium reacts with hydrogen according to the following reaction:

$$Mg + H_2 = MgH_2$$

The forward reaction is exothermic (ΔH = -74.5 kJ mol H_2^{-1}, Selvam et al 1986). The formed hydride is stable i.e dehydriding occurs at higher temperatures (above 400°C).

Magnesium has 2 valance electrons that can be easily lost, which make it strongly electropositive. Therefore, it can readily react with O_2, CO_2 and form a stable oxide film, MgO or react with H_2O to form $Mg(OH)_2$. The oxide (MgO) film may acts as a protective coverage for further oxidation. However, this is not the case in $Mg(OH)_2$. Above 440°C $Mg(OH)_2$ is unstable and decomposes into MgO and water. (Raymor, 1959)

Fabrication of Mg is also difficult due to its high vapour pressure and low melting point. The change in Mg vapour pressure with temperature is given in Table 2.3 (Skol'skaya, 1961). The variation of melting temperature of Mg with pressure is reported in Figure 2.1 (Okamoto, 1988).

There is no complete phase diagram for the Mg-H system available in the literature. San-Martin and Manchester (1988) related this to the fact that the equilibrium pressure of the H surrounding the metal is always a significant thermodynamic variable in metal-hydrogen system. However, they proposed an assessed Mg-H phase diagram and Mg-H isotherm, Figure 2.2 and 2.3, respectively.

Table 2.3. Vapour pressure of Mg at different temperatures (Skol'skaya, 1961).

Temperature (°C)	Vapour Pressure (atm)	Vapour Pressure (mm Hg)
337	$1,3x10^{-6}$	1x10-3
417	$6,6x10^{-6}$	5x10-3
437	$1,3x10^{-5}$	1x10-2
492	$6,6x10^{-5}$	5x10-2
515	$1.3x10^{-4}$	0.1
572	$6.6x10^{-4}$	0.5
602	$1.3x10^{-3}$	1
651	$2.9x10^{-3}$	2.2
672	$6.6x10^{-3}$	5
723	$1.3x10^{-2}$	10
837	$6.6x10^{-2}$	50
890	$1.3x10^{-2}$	100
977	$3.2x10^{-1}$	250
1057	$6.6x10^{-1}$	500
1102	1	760

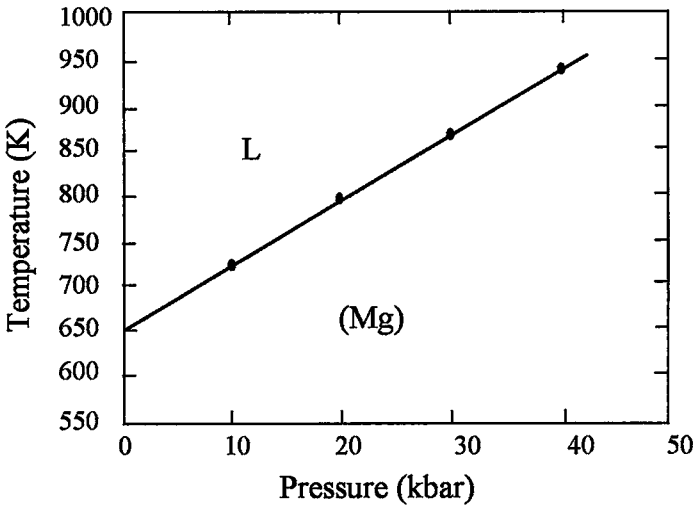

Figure 2.1. Variation of melting temperature of Mg with pressure. (Okamoto, 1988)

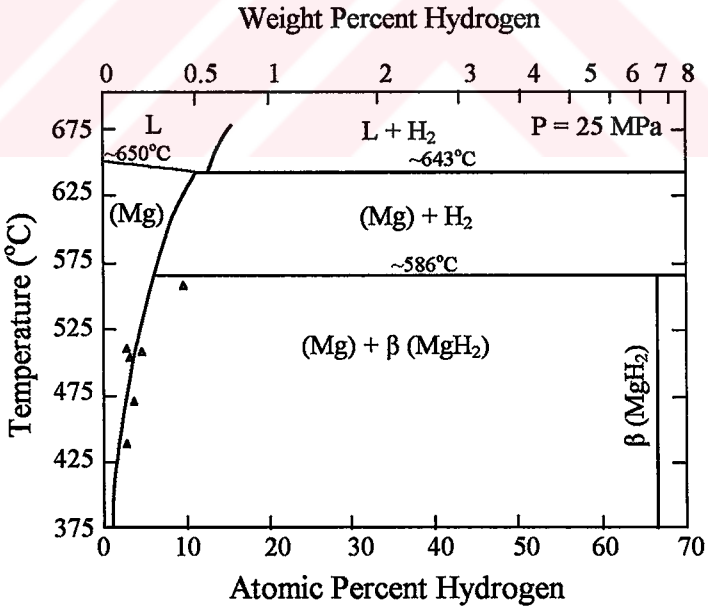

Figure 2.2. Assessed Mg-H phase diagram. (San-Martin and Manchester, 1988)

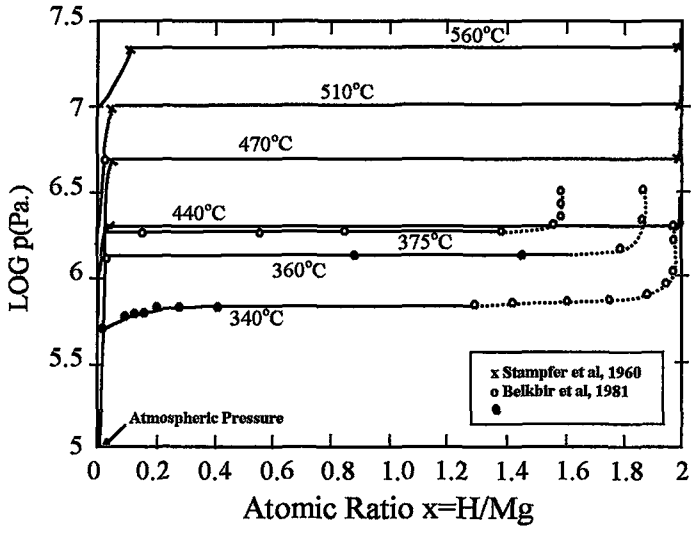

Figure 2.3. Assessed Mg-H isotherms. The open and full circles refer to formation and decomposition isotherms, respectively. (San-Martin and Manchester, 1988)

2.5. HYDROGEN SORPTION KINETICS

There have been many investigations on sorption kinetics of Mg and Mg based hydrides in order to identify a suitable model and a rate-limiting step for absorption and desorption (Karty et al., 1979, Luz et al., 1980; Uchida et al., 1984; Vigeholm et al., 1983, 1987; Douglas and Derek, 1983; Suda and Kobayashi, 1980).

Karty et al. (1979) investigated pure Mg and Mg-Mg_2Cu systems and found that the rate determining steps for hydriding and dehydriding are hydrogen diffusion through growing dense-MgH_2 and Mg layers respectively.

Luz et al. (1980) investigated the diffusion process in hydriding. They found that upon hydriding of Mg the diffusing species is the hydrogen anion (H^-), but not the Mg cation (Mg^{+2}).

Rudman (1983), Vigeholm (1983), Bobet et al. (2000) proposed nucleation and growth theory for hydriding and dehydriding, i.e. Johnson-Mehl-Avrami (JMA) equation.

$$F = 1 - \exp\{-(K.t)^n\} \qquad \textbf{2.1}$$

In this equation F denotes the transformed fraction, K is the rate constant and n is the reaction exponent.

Vigeholm et al (1983) suggested that the mechanism involve surface nucleation and growth with a pressure dependent concentration of nuclei. They further pointed out that for first hydrogenation, regardless of other factors, the specific surface is important to the reaction kinetics. They found that smooth surface resulted in slow reaction whereas the cracked irregular surface absorbs hydrogen immediately.

Martin et al. (1996) reinvestigated the reaction models within the context of sorption kinetics of hydrogen storage, and suggested several intermediate processes for the overall reaction of the formation and decomposition of metal hydrides (Figure 2.4). According to Martin et al. (1996) the intermediate processes for hydride formation are physisorption of hydrogen molecules (1), dissociation of hydrogen molecules and chemisorption (2), surface penetration of hydrogen atoms (3), diffusion of hydrogen atoms through the hydride layer (4) and finally hydride formation at the metal/hydride interface (5). On the other hand, for dehydriding hydride decomposition at the metal hydride interface (1), diffusion of hydrogen atoms through the α phase (2), surface penetration of hydrogen atoms (3), recombinations of chemisorbed hydrogen atoms and physisorption (4) and desorption of the gas phase (4) are the steps in dehydriding. They further suggested that in hydriding the slowest step might be chemisorption whereas dehydriding that is the surface penetration.

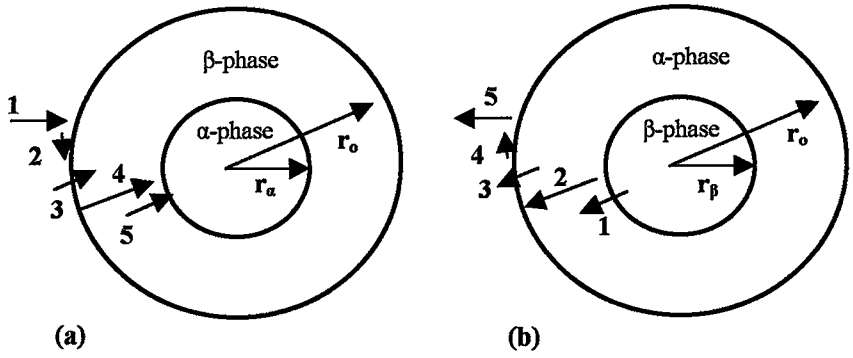

Figure 2.4. Schematic representation of the over all reaction of (a) hydride formation, (b) hydride decomposition. α and β phases denote metal and hydride phase respectively. "r" is the radius. (Martin et al., 1996)

Renner and Grabke (1972), Douglass (1975), Zaluski et al. (1997) proposed that the important parameters that affect absorption is the rate of hydrogen dissociation at the surface and the capability of hydrogen to penetrate the surface and the rate of hydrogen diffusion into the bulk metal and through the hydride already formed.

Schlapbach (1980) suggested that dissociative chemisorption and associative desorption are not necessarily rate determining steps until the segregation stops and the active surface is covered.

Genossar and Rudman (1979) pointed out the necessity of chemical reaction or hydrogen activation on contaminated metal surface layer in order for hydrogen sorption.

Hjort et al. (1996) worked on partially oxidized Mg films and found that thin oxide layers improve hydrogen uptake rate and they also stated that MgO_x is not an important diffusion barrier. However, Selvam et al. (1988) argued that very thin oxide layer that is sufficient to be ductile enough to adhere to particle would not be cracked and thus hinder the hydrogen absorption.

Liang et al. (1999a, b; 2000a, b) proposed a nucleation-growth type model for MgH_2-transition metal systems, and further investigated the pressure-temperature dependence of desorption kinetics of Mg-5 at.% V system in detail. They reported that for high temperature (523-673K) interface motion (Mg/MgH_2) is the rate determining step with high driving force (high hydrogen pressure) whereas nucleation and growth followed by long-range hydrogen diffusion is favoured for small driving force (low hydrogen pressures). On the other hand, below 523K they suggested that rate is determined by nucleation and growth of Mg in hydride phase.

Fernandez and Sanchez (2002) proposed nucleation and growth mechanism for Mg-H system with rate orders n=2 and n=0.5 to 1 (Equation 2.1) for hydrogen absorption and desorption, respectively. They further stated that rate determining steps in both desorption and absorption might be hydrogen diffusion through β-phase.

An alternative approach for sorption kinetics is based on shrinking core model, which involves a thin film formation and continues growth of this film with the expense of inner metal. (Vigeholm et al., 1987, Osovizky et al., 1996, Sharp et al., 1966, Hancock and Sharp, 1972, Stander, 1977a, 1977b, Bronfman et al., 1991, Mintz et al., 1985, 1980)

2.5.1. Activation

In hydrogen sorption, it is generally hard to obtain acceptable hydriding and dehydriding rates in the first three cycles even at high temperatures and pressures. The cause of this phenomenon has been intensively investigated over the last 20 years. Several processes have been reported that make hydride former accustomed to hydriding and dehydriding (Selvam et al., 1986; Bolcich et al., 1994; Bouaricha et al., 2001a, b, 2002). These processes usually involve treatments similar to hydriding/dehydriding cycling but involve the use of relatively high pressure and

vacuum, details of which depend on the nature of the hydride former and its fabrication method.

Activation is generally difficult in bulk hydride formers, i.e. pressures and temperatures are higher. For example for bulk Mg and Mg-alloys Selvam et al. (1988) reported a vacuum treatment with a subsequent hydriding/dehydriding process at temperatures in between 625-675K under a pressure range of 60-80 atm. However, for powdered hydride formers activation is relatively easy. For example, for powdered Mg-Ni alloy Bolcich et al. (1994) reported that several hydriding/dehydriding cycling is needed at a temperature of 573K under a pressure of 30 atm for activation. For powdered Ti-Ni alloy a vacuum treatment carried out at high temperatures was reported to be enough for activation. Bolcich et al. (1994) further reports that no activation was necessary for powdered $LaNi_5$ as the activation takes place in situ during fabrication of powders by hammer milling.

There have been extensive studies, over the last 10 years on mechanical milling of powders that yield micron, sub micron particles. Under such conditions the powders are easy to activate. For example, Zaluska et al. (1999) reported that for pure Mg after ball milling no special treatment was necessary but in order to reach full capacity of hydrogenation several hydriding/dehydriding cycles were necessary. They attribute this to the fact that during milling in addition to formation of smaller particles, surface contamination layer was broken and fresh surfaces are formed. Zaluski et al. (1997) and Spassov et al. (1999) reported better results for nanocrystalline metal hydrides such as Mg, Mg_2Ni, FeTi, $LaNi_5$ hydrides. Similarly, for nanocrystalline Mg-5 wt.% Ti, Mg-10 wt.% V and Mg-10 wt.% Fe Khrussanova et al (2001) stated that the achieved particle size of 30nm eliminates the need for activation. In addition for amorphous Mg-$FeTi_{1.2}$ Wang et al. (2002) showed that there is no need for activation.

Schulz et al. (1999) pointed out that the use of MgH_2 yields better results than pure Mg. This was due to brittle nature of MgH_2, which brakes down easily into finer particle size, whereas pure Mg is ductile and mechanical milling results in

excessive cold welding and formation of large agglomerates. Schulz et al. (1999) further explained that in addition to the decrease in average particle size (increase in specific surface area) milling of MgH_2 induces the formation of a new metastable phase, namely orthorhombic γ-MgH_2. According to Bastide et al. (1980) this β–phase has been transformed into the mixture of β and γ phase under a pressure of 8 Gpa, and transforms into equilibrium tetragonal structure when heated above 623K.

It is reported that (Dehouche et al., 2000; Schulz et al., 2001; Huot et al., 1999) no activation was necessary for mechanically milled nanocrystalline MgH_2, which may also be contributed to the formation of the metastable phase. Gennari et al (2001) proposed that the presence of γ-MgH_2 phase destabilizes the β–MgH_2 phase by reducing its desorption temperature. The case of mechanical milling of Mg (with or without additives) under hydrogen atmosphere i.e. reactive milling that ensures the formation of MgH_2 in the process yields also similar results (Huot et al., 1995, 2002; Tessier et al., 1998, 2000; Wang et al., 2000a, b; Zeng et al., 1999a, b; Gennari et al., 2001; Bobet et al., 2001; Song et al., 2002). Tessier and Akiba (1999) stated that in situ activated MgH_2 powders can be produced by mechanical milling of Mg powders under hydrogen atmosphere.

Gennari et al. (2001) pointed out that this might be due to the change in particle size in reactive milling. They showed that the milling produces slight decrease in particle size (150 microns) in the first milling stages (15 hrs), due to the presence of ductile Mg phase. However, after formation of hydride phase they observed a rapid decrease in particle size (5 microns).

The use of pure magnesium without resort to MgH_2 is also possible. For example Imamura et al (2002,1999,1996,1995) worked on mechanical milling of Mg with graphite in the presence of several solvents such as tetrahydrofuran (THF), benzene, cyclohexane. They obtained improved activation especially with THF.

In recent years there has been intensive studies on mechanical alloying of nanocrystalline MgH_2 with additives. These fall mainly into four categories: the transition metal additives (Ti, V, Mn, Fe, Ni) Liang et al. (1999a, b, c), Khrussanova et al. (2001), Dehouche et al. (2000), Huot et al. (1998a, b, 2002); C and Si additives Reule et al. (2000), Jacobson et al. (2002), Awasthi et al. (2002); metal oxides (CuO, Fe_3O_4, Cr_2O_3, VO) Oelerich et al. (2001a, 2001b), Song et al. (2002), Dehouche et al. (2002), Wang et al. (2000a), and intermetallics (FeTi, $LaNi_5$) Mandal and Srivasta (1994), Liang et al. (2000a, b, 1995), Cui et al. (1999), Khrussanova et al. (2000). They all yield the same result, i.e. reduced need for activation or no activation at al.

It has been pointed that with additives new phases might form during milling which may then act as catalyst and hence improve the kinetics and eliminate the need for activation. For MgH_2-transition metals such as Ti, V, Mn, Fe and Ni Liang et al. (1999a, b) reported the formation of $VH_{0.81}$, $MgNiH_4$ and Mg_2FeH_6 phases for Mg-V, Mg-Ni and Mg-Fe systems respectively. Similarly, MgH_2-Fe system, for instance, studied by Huot et al (1998a, b) and Khrussanova et al (2001) the formation of Mg_2FeH_6 was observed, however, formation of this phase is not desired due to high hydride stability.

Reule et al. (2000) found that mechanical alloying of MgH_2 with metallic additives ($La(Ni_{0.7}Fe_{0.3})_5$, Pd_3Fe) forms a composite structure in which MgH_2 covers additives in the form of thin film having regular thickness. According to Reule et al. (2000) this structure enables short diffusion paths and large hydride-additive interface, which may improve the sorption kinetics and eliminate activation.

It should be pointed out that a preliminary treatment is a common practice for almost all hydrogen studies. For those systems that do not require "activation", the general form of it is a vacuum treatment for desorption followed by not less than three cycles of absorption/desorption (Liang et al., 1999a; Oelerich et al., 2001a, 2001b; Imamura et al., 2002; Huot et al., 2002). Such a treatment is necessary to obtain stabilized kinetics in hydrogen sorption.

A summary of various MgH_2-additive systems investigated in the literature is given in Table 2.4. The reported structural changes with milling and reaction kinetics data are included in the table.

The need for activation has not been clearly defined up to now. Karty et al. (1979) and Rudman (1983) explain that the observed rapid increase in sorption kinetics after activation is due to the breaking of the passivating surface (surface oxide or hydroxide layer) formed during handling. Rudman further explains a two stage process for powdered hydride formers which includes the fracturing of particles as a result of transformation stresses during cycling thus formation of fresh surfaces and small particles i.e. first stage activation, and fragmentation of particles over the first 10 cycles i.e. termed as second stage activation. In addition, Rudman pointed out that fragmentation is minimal in ductile hydride formers, as in the case of magnesium, and thus kinetics are poor. Selvam et al. (1986) explain that protective layers, i.e. MgH_2 during hydriding and Mg during dehydriding, act as diffusion barrier for hydrogen even if the surface oxide layer is eliminated.

2.6. PCT DIAGRAM

Thermodynamic properties of metal-hydride systems can be best understood by a pressure-composition-temperature diagram, i.e. isothermal plots of equilibrium hydrogen pressures as a function of composition, Figure 2.5. Detailed explanation of PCT diagram within the context of hydrogen sorption is given by Douglas and Derek (1983), and by Dantzer (1997).

Douglas and Derek consider a two-component system, i.e. metal and hydrogen in which metal is initially present as solid. In this system, according to Gibbs' phase rule,

$$F = C - P + 2,$$

Table 2.4. Summary of various MgH_2-additive systems in the literature including the structural and kinetic characteristics.

Additive %	Starting Composite	Phases After Milling	Desorption Kinetics (T,P,t)	Phases After Desorption	Absorption Kinetics (T,P,t)	Phases After Sorption	Activation Energy ($kJ.mol^{-1}$)	Reference
None	β-MgH_2	γ-MgH_2 β-MgH_2	573K,0.5wt%,600s 523K,0.1wt%,600s 0.15 atm	Mg	573K,5wt%,1000s 523K,1wt%,1000s 508K,0.5wt%,200s 10 atm	β-MgH_2	120	Liang et al (1999b)
5at.% Ti	β-MgH_2 Ti	Mg γ-MgH_2 β-MgH_2 TiH_2	573K,5wt%,200s 523K,4-5wt%,600s 508K,4.5wt%,2500s 0.15 atm	Mg TiH_2	473K,5wt%,200s 373K,4wt%,200s 302K,2.5wt%,1000s 10 atm	β-MgH_2 TiH_2	71.1	Liang et al (1999b)
5at.% V	β-MgH_2 V	Mg γ-MgH_2 β-MgH_2 $VH_{0..81}$	573K,5.4wt%,300s 523K,5.5wt%,900s 508K,-5wt%,2500s 0.15 atm	Mg V	473K,5.5wt%,150s 373K,4.5wt%,200s 302K,2wt%,1000s 10 atm	β-MgH_2 $VH_{0..81}$	62.3	Liang et al (1999b)
5at.% Mn	β-MgH_2 Mn	Mg γ-MgH_2 β-MgH_2 Mn	573K,5wt%,500s 523K,1.5wt%,1500s 508K,0.5wt%,2500s 0.15 atm	Mg Mn	473K,5.5wt%,200s 373K,3wt%,1000s 302K,1wt%,1000s 10 atm	β-MgH_2 Mn	104.6	Liang et al (1999b)
5at.% Fe	β-MgH_2 Fe	γ-MgH_2 βMgH_2 Mg_2FeH_6	573K,5wt%,250s 523K,4.5wt%,1500s 508K,3.2wt%,2500s 0.15 atm	Mg Fe	473K,4wt%,200s 373K,3wt%,200s 302K,1.8wt%,1000s 10 atm	β-MgH_2 Fe	67.6	Liang et al (1999b)
5at.% Ni	β-MgH_2 Ni	γ-MgH_2 β-MgH_2 Mg_2NiH_4	573K,5wt%,3500s 523K,3.6wt%,1500s --- 0.15 atm	Mg Mg_2Ni	473K,5wt%,1000s 2.0wt%,200 373K,3wt%,1000s 302K,0.5wt%,200s 10 atm	βMgH_2 Mg_2Ni	88.1 69	Liang et al (1999b) Liang et al (1999c)
Ni-Ti	$Mg_{1.9}Ti_{0.1}Ni$	-	-	-	423K,3.3wt%,3000s 473K,3.0wt%,200 10 atm	ort-mono $Mg_{12}NiH_4$ $Mg_2NiH_{0.3}$	59	Liang et al (1999c)

"Table 2.4 (continued)"

Additive %	Starting Composite	Phases After Milling	Desorption Kinetics (T,P,t)	Phases After Desorption	Absorption Kinetics (T,P,t)	Phases After Absorption	Activation Energy	Reference
10wt.% Co	Mg Co	Co Mg MgH_2	623 K,>3w%,3000s	-	623 K,3w%,140min	-	-	Bobet et al (2000)
30wt.% $LaNi_5$	Mg $LaNi_5$	-	573K,5wt%,150s 523K,5wt%,1200s 0.015 MPa	-	423K,4.2wt%,1000s 302K,1.8wt%,2000s 10 atm	MgH_2 LaH_3 $MgNiH_4$ Mg	-	Liang et al (2000)
23wt.% LaH_3	β-MgH_2 LaH_3	-	573K,0.5wt%,500s 523K,0.2wt%,1500s 0.015 MPa	-	423K,3wt%,1000s 302K,1.3wt%,2000s 10 atm	-	-	
5mol.% CuO		-	473K,6wt%,1200s vacuum	-	473K,6wt%,300s 8.3 atm	-	-	Oelerich et al (2001a)
5mol.% Mn_2O_3		-	473K,5wt%,600s vacuum	-	473K,4.8wt%,120s 8.3 atm	-	-	Oelerich et al (2001a)
5mol.% Cr_2O_3		-	473K,4.5wt%,600s vacuum	-	473K,4.3wt%,120s 8.3 atm	-	-	Oelerich et al (2001a)
5mol.% Fe_3O_4		-	473K,4wt%,600s vacuum	-	473K,4.1wt%,120s 8.3 atm	-	-	Oelerich et al (2001a)

"Table 2.4 (continued)"

Additive %	Starting Composite	Phases After Milling	Desorption Kinetics (T,P,t)	Phases After Desorption	Absorption Kinetics (T,P,t)	Phases After Hydrogenation	Activation Energy	Reference
5mol.% V_2O_5		-	473K,4wt%,600s vacuum	-	473K,4wt%,300s 8.3 atm	-	-	Oelerich et al (2001a)
20wt.%, TiO_2	Mg TiO_2	-	----------	-	373K,3.5wt%,600s 353K,2.5wt%,600s 313K,2wt%,600s 20 atm	-	-	Wang et al (2000a)
1wt% YNi_2Al_3	Mg Yni_2Al_3	-	----------	-	623K,7wt%,7200s 10 atm	-	-	Khrussanova et al (2000)
10wt% YNi_2Al_3	Mg YNi_2Al_3	-	----------	-	623K,5.5wt%,7200s 10 atm	-	-	Khrussanova et al (2000)
10wt% Yni_4Al	Mg YNi_4Al	-	----------	-	623K,5wt%,7200s 10 atm	-	-	Khrussanova et al (2000)

where C is the number of components (C=2), P is the number of phases, and F represents the degrees of freedom. Douglas and Derek indicate that initially P=2 i.e. hydrogen gas and metal with dissolved hydrogen, and thus F=2. That means for a constant temperature hydrogen pressure in equilibrium with the solid phase changes with composition. The reaction can be given as

$$\tfrac{1}{2} H_2 \text{ (gas)} = H \text{ (in solution in metal)}$$

According to Sieverts' law the solubility of hydrogen is proportional to the square root of the hydrogen pressure, which denotes the initial steep slope in Figure 2.5 (Region A). Sieverts' law graph is given in Figure 2.6. (Mueller, Blakledge and Libowitz, 1968)

When the metal phase saturates with hydrogen, (at H/M = a; solubility limit at T3), i.e. the formation of a metal-hydride phase (P=3 and thus F=1), the pressure remains constant with composition, Figure 2.5 (Region B). That means equilibrium pressure remains constant as more hydrogen is introduced into the system. This constant equilibrium pressure is usually referred as plateau pressure.

Douglas and Derek further explains that the equilibrium pressure increases as additional hydrogen is added into the system since there is once again a single phase is present in the system i.e. F is again equal to 2. Thus the pressure changes again with composition, Figure 2.5 (Region C).

Several researchers (Mueller et al., 1968; Selvam et al., 1988; Tessier et al., 1998; Wang et al., 2000c, b; Bernhardt and Bohmammel, 2002) worked on metal hydride systems that have more than one hydride phase. They observed several plateau regions that correspond to the hydride phases present in the system. An example is given in Figure 2.7.

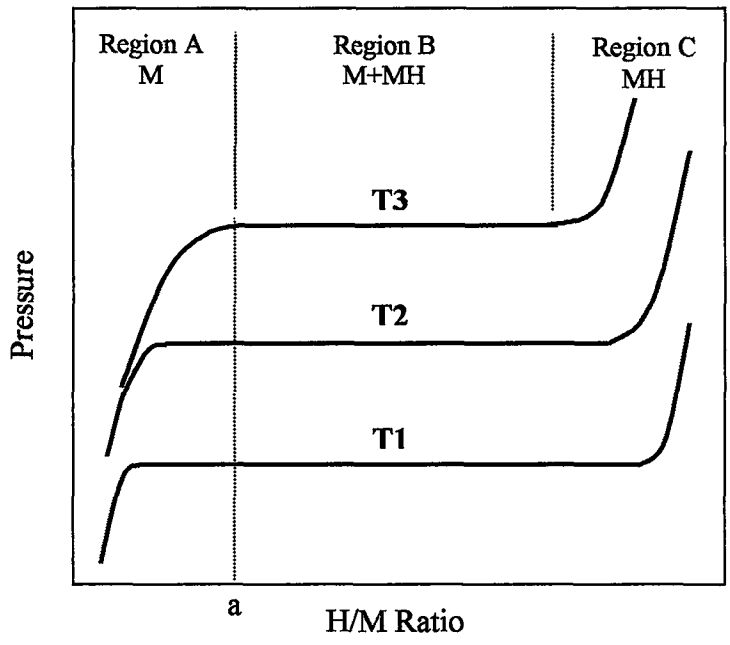

Figure 2.5. Typical pressure-composition isotherms at various temperatures. (T3>T2>T1)

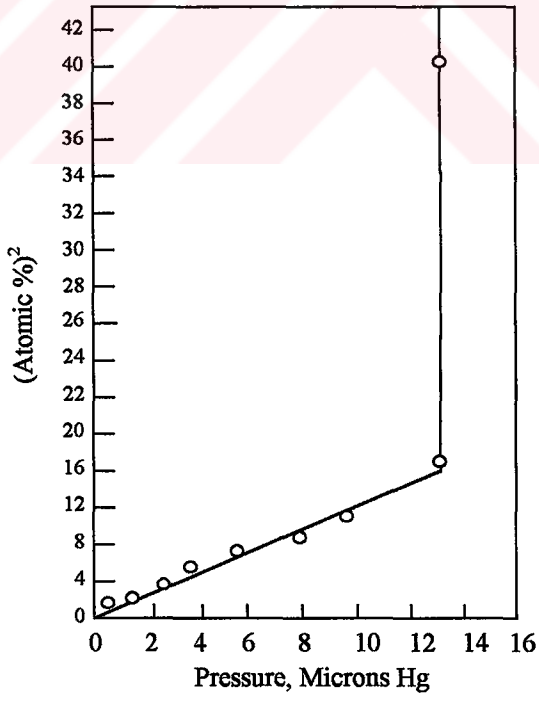

Figure 2.6. Sieverts' law graph for metal-hydrogen system. (Mueller, Blakledge and Libowitz 1986)

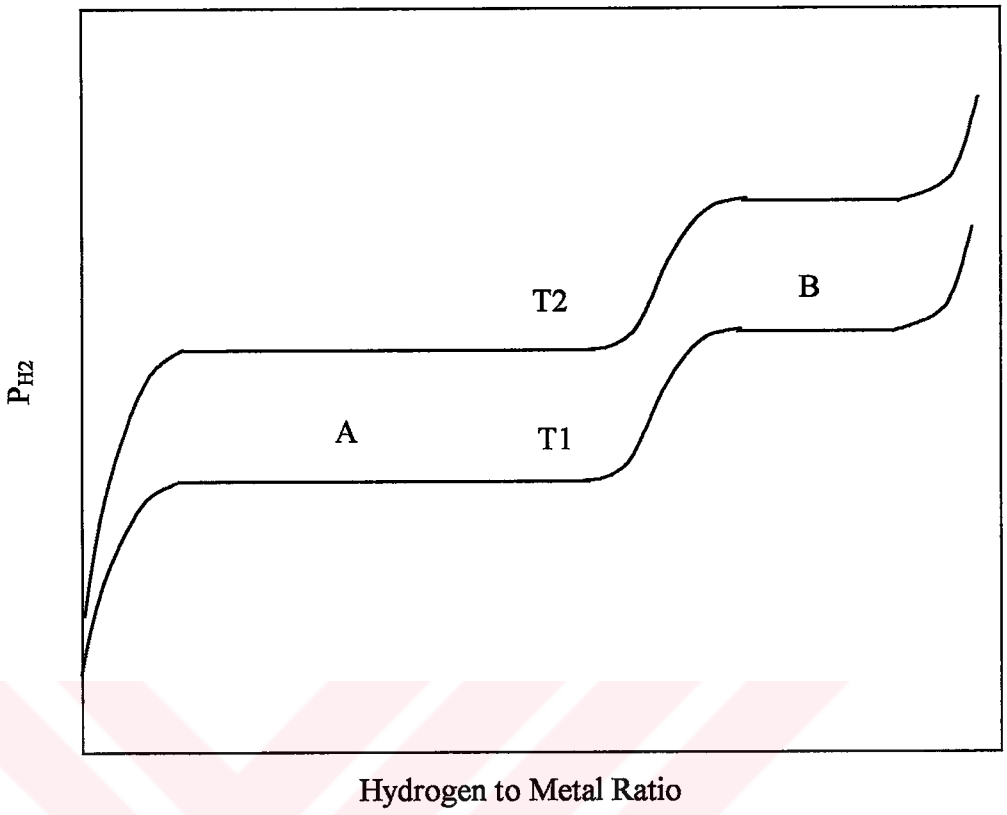

Figure 2.7. Typical pressure-composition isotherms for a system having two hydride phases. A and B denotes the plateau regions of the hydrides.

In many metal-hydrogen systems p-c isotherms show hysteresis, Figure 2.8. This is due to the fact that the plateau pressure for absorption is higher than that for desorption, Douglas and Derek (1983). The cause of hysteresis is not clearly understood. But three explanations are proposed; lattice expansion theory by Kuijpers et al. (1971) and Lundin et al. (1977), defect theory proposed by Libowitz et al. (1957) and that proposed by Flanagan et al. (1980).

According to Kuijpers et al (1971) and Lundin et al (1977), during absorption the formation of hydride causes an irreversible plastic deformation generating residual stresses in the matrix, and on desorption as hydrogen is released, the matrix relaxes as these stresses are relieved. Thus, desorption should occur at lower pressure. On the other hand, Libowitz et al. (1957) i.e. defect theory, explain hysteresis based on changes in vacancy concentration upon absorption and desorption. They

explain that a certain fraction of equilibrium vacancies are occupied with hydrogen upon absorption, whereas in desorption this will not be the case. Moreover, Flanagan et al. (1980) stated that dislocation and non-equilibrium defect densities vary in desorption and absorption based on the solvus behaviour in the palladium-hydrogen system; therefore, the absorption and desorption plateau pressures does not correspond to the equilibrium.

Dantzer (1997) points out that in real systems two types of isotherms exist, namely reproducible and non-reproducable (especially in intemetallic hydrides). He further explains that hysteresis and sloping plateau effects make it difficult to determine the reproducible stationary states for metal hydrides. According to Larsen and Livesay (1980) impurities, inhomogenities and stress could be the factors creating the sloping plateau.

2.6.1 Temperature Dependency

P-c isotherms at various temperatures are shown in Figure 2.5. Plateau pressure has a strong dependency on temperature. The plateau pressure increases with increase in temperature. This may be attributed to the heat of the reaction of the process (Boureau et al., 1979; Flangan, 1978; Ramakrishna et al., 1987).

$$Mg + H_2 = MgH_2$$

The temperature dependence of plateau pressure (P), linked with the reaction enthalpy ΔH, can be best represented by Van't Hoff equation after integration, i.e.

$$\ln P = \Delta H/RT - \Delta S/R$$

in which ΔS is entropy, R is the gas constant and T is the temperature.

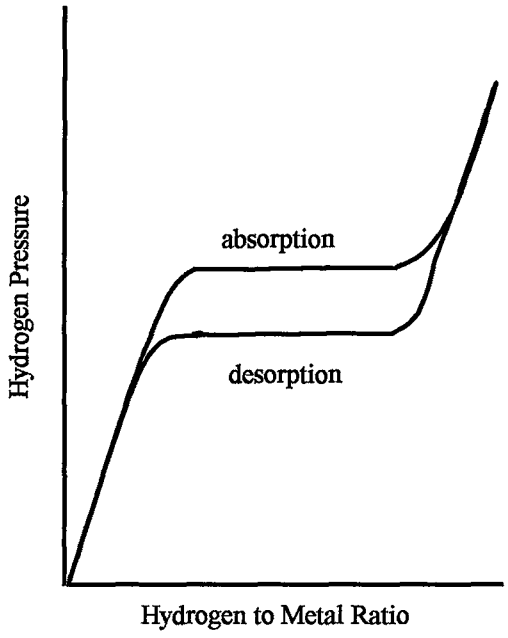

Figure 2.8. Pressure-composition isotherm diagram showing hysteresis in metal hydrogen system.

There are numerous studies based on temperature-dependent equilibrium hydrogen pressure of MgH_2 (Bogdanovic et al 1999; Bohmhammel et al 1998, 1999; Kapischke and Hapke 1998). However, reported values show considerable differences.

Two major properties of hydrides can be obtained from p-c isotherms; namely hydriding/dehydriding plateau pressures and the total amount of hydrogen stored by the metal (hydrogen to metal ratio). The factors affecting these two properties have been intensively investigated for many systems for the last few years, and attention is being focused on the effects of mechanical milling and/or mechanical alloying, and hydriding/dehydriding cycling on these properties (Dehouche et al., 2000, 2002; Inuni, 2002; Kadir, 2000, 1999).

2.6.2 The Effect of Mechanical Milling

Huot et al. (1999) compared the PCT curves obtained at 623K for ball milled and unmilled MgH_2. They observed an increase in desorption plateau pressure with milling (pressures were 3.5 and 5 atm for milled and unmilled powders respectively) while absorption plateau pressure (6 atm) remains constant with milling. They contributed this difference to slow desorption kinetics, i.e. real equilibrium is not reached. They further show that the maximum hydrogen content is slightly decreased after milling.

For MgH_2-Tm (Fe, Ni, Ti, V) system Liang et al. (1999b) observed only one plateau owing MgH_2 except for Ni addition, and absorption/desorption plateau pressures for these composites showed no differences as compared to pure Mg. Moreover, for MgH_2-V system Liang et al. (1999b) obtained a small hysteresis and sloping curve at 583K, pressures were 1 atm for desorption and 2 atm for absorption. However, for the same system Schulz et al. (2001) reported that hydrogen storage capacity decreases slightly in the first 20 hrs of milling (by 10%), such a decrease can not be due to the small amount of oxygen and iron impurities introduced during milling. On the contrary, in the case of MgH_2, they observe no change with milling time. Finally, Zaluska et al (1999) reported that there is no significant shift of the plateau pressures (573K-603K) after ball milling of MgH_2.

2.6.3 The Effect of Cycling

Inui et al. (2002) reported that for intermetallic hydrides absorption plateau pressure for the first cycle is greater than that of the second cycle due to introduction of lattice defects, which is independent of particle size. They related the extent of this decrease with initial particle size i.e. the pressure required to form cracks depends on particle size. As for desorption they observe no change in

pressure with cycling. They further reported that p-c isotherm is reproducible and does not depend on the number of cycling after the second cycle.

For MgH_2-V system Dehouche et al. (2000) reported that the measured plateau pressures (1 bar for desorption and 2.5 bar for absorption) and hysteresis remain stable after 2000 cycles at 573K; however, hydrogen capacity is slightly increased due to structural relaxation.

For Mg + Cr_2O_3, Al_2O_3 and CeO_3 (10wt.%) Song et al (2002) reported that all samples absorb and desorb less hydrogen with cycling due to agglomeration of particles during hydriding-dehydriding cycling.

CHAPTER III

EXPERIMENTAL PROCEDURES

3.1. MATERIALS

Pure magnesium hydride powder from Goldschmidt GmbH (95%MgH_2+5%Mg), vanadium (V) powder from ABCR GmbH & Co., graphite (C) and aluminum oxide (γ-Al_2O_3) powders from MERC are used in the experiments. The average particle sizes of the powders, i.e measured from SEM micrographs, are 20 μm, 13 μm, 60 μm and 5 μm for MgH_2, V, graphite and Al_2O_3, respectively. Several sets of powder composites are produced by mechanical milling.

Before experiments powders are separately heated to 120°C under vacuum in order to remove moisture absorbed by the powders. Then they are mixed under argon atmosphere. The synthesis of the samples is accomplished by mechanical milling of powder mixtures in an attritor mill for 3 hours under argon atmosphere in a glove box. All handlings are performed in a glove box under argon.

The systems investigated are given in Table 3.1.

Table 3.1. The systems investigated in the experiments.

System
MgH_2 without additive
MgH_2-5%G
MgH_2-5%V
MgH_2-10%V
MgH_2-5%V-5%G*

* 5%G is added in the last 15 minutes of milling.

3.2. ATTRITOR MILL

Schematic representation of attritor mill used for mechanical milling process is shown in Figure 3.1. Attritor mill is composed of a cylindrical housing with water circulation ducks, hardened steel crucible, impeller and stainless steel balls (6 mm in diameter). The attritor mill is operated at a speed of 515 rpm. Mechanical milling takes place in the inner hardened steel crucible (A), which was shrink-fitted in outer steel container (B). This inner steel container can be water cooled during milling.

3.3. GLOVE BOX

Due to high oxygen affinity of the powders used in the experiments a glove box was designed. It provides enough space for handling and storing the milled samples under inert atmosphere. Schematic representation of the glove box is given in Figure 3.2. Glove box is made of plexiglas having 10mm thickness. Dimensions of the glove box are 700mm×300mm×260mm. There are four openings in the system, which are for gloves (D), rotating impeller (C), sample transfer gate (A), gas-water inlets and outlets (B).

Attritor (F) is housed in this glove box on a fixer table (E). Two glove openings (D) having 130 mm diameter provides easy access in the glove box. The diameter of the opening for rotating impeller is 15mm. Sample transfer gate (A) that enables to transport powders in and out of the glove box is a brass container having two lids, one opens inside the glove box and the other opens outside. The diameter of the transport gate is 30mm. Three inlets are available at (B); two inlets for cooling water (in and out), and one for argon gas (in).

A gas flow meter (G) (Alborg Ins. FM032-01ST) is used to control argon flow into the glove box. A steel frame (H) of considerable mass is put on the glove box to help seal the upper cover.

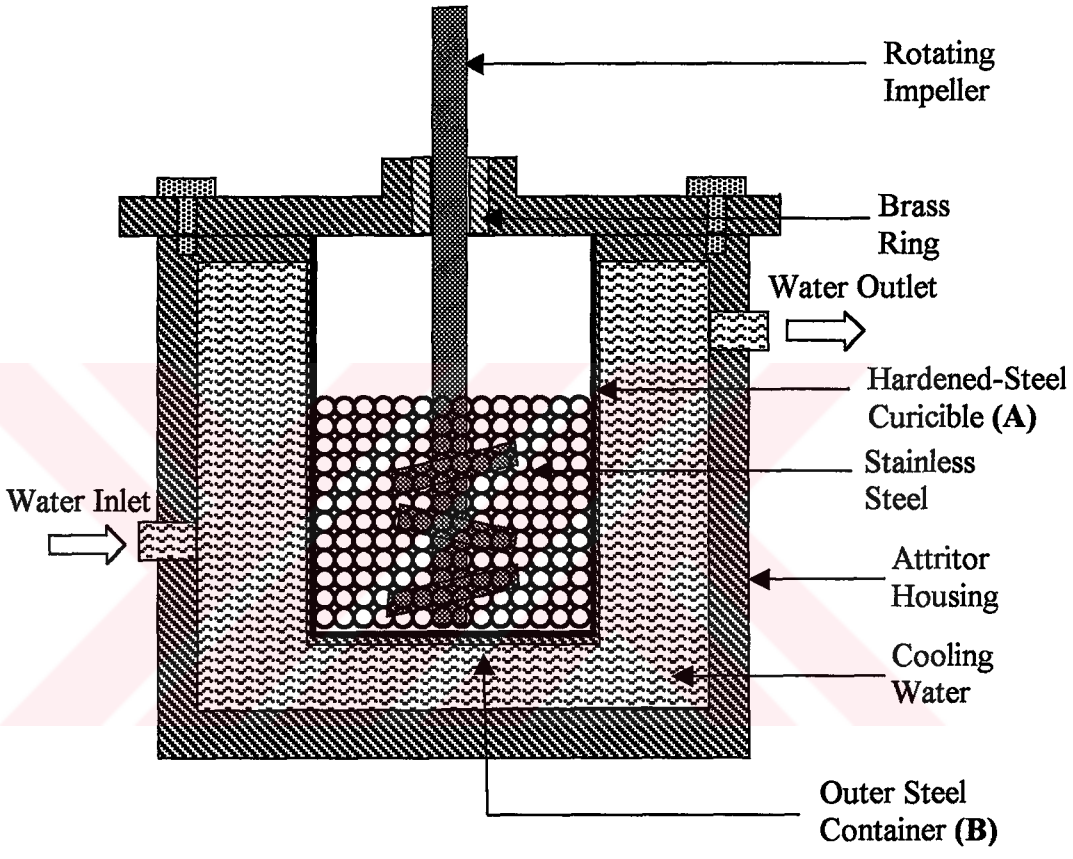

Figure 3.1. Schematic representation showing main parts of the attritor mill.

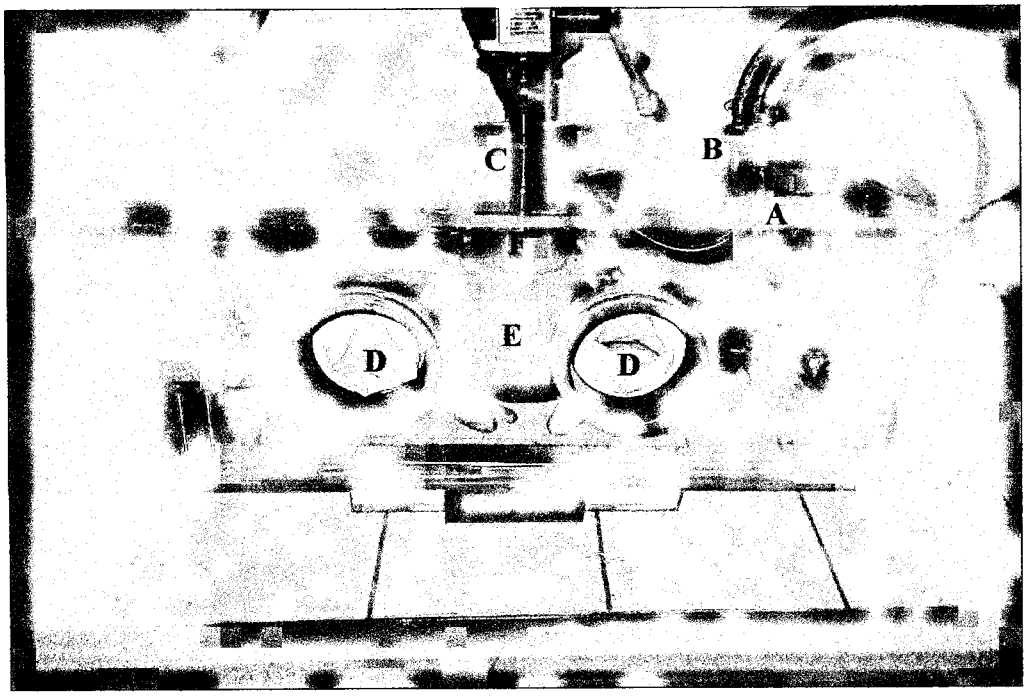

(a)

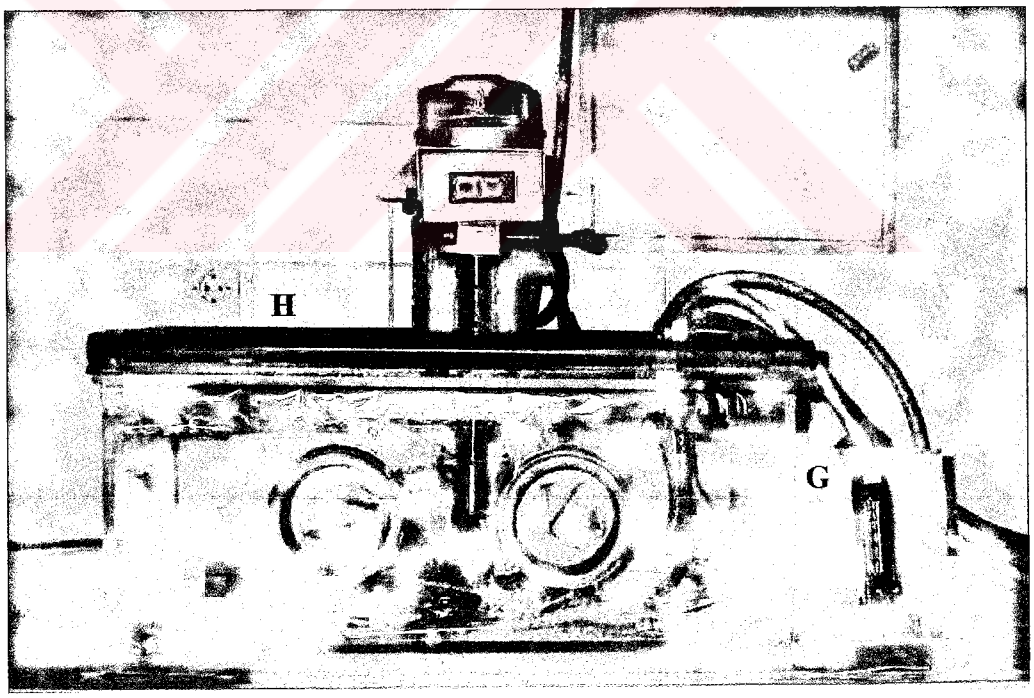

(b)

Figure 3.2. Glove box; (a) general view, (b) front view.

Milled powders are transported in and out of the glove box in a container shown in Figure 3.3. This container is in the form of a cylindrical box with a screw lid having a circular opening. The container is sealed in the glove box with aluminum foil fitted to the lid. When needed, aluminum foil can be burst by applying a sufficiently high positive pressure from outside or from inside, i.e. by a built-up of pressure due to hydrogen release.

3.4. MECHANICAL MILLING

The synthesis of the samples is accomplished in the glove box by mechanical milling of powder mixtures in an attritor mill under argon atmosphere. 1wt.% graphite is used as an anti-sticking agent during milling. The ball to powder ratio is 10:1. Argon flow is adjusted to 10 L/min, and cooling water flowed with a rate of 0.1 L/min during milling.

Powders are transferred into glove box through sample transfer gate. Glove box is then flushed with argon gas with a flow rate of 5-6 L/min for a period of typically 2hrs. First, impeller then stainless steel balls and finally powder mixture is placed into the attritor container. The attritor is closed and fixed to the fixer table tightly. Impeller is connected to a rotating shaft through a circular opening slightly larger than the impeller shaft. The space in between allows continuous flow of argon gas from the glove box to outside.

Typically attritor mill is operated for 3hrs at a speed of 515rpm. After milling the opening (C) is closed firmly (Figure 3.2 (a)). The lid of the container is opened and powders are separated from the steel balls. Powders are stored into small plastic bags. Milled powders of amount sufficient for sorption experiment (typically 0.3gr) are put into the container. The container is then filled with argon and closed. When needed the sample is taken out of the glove box through the transfer gate. All handlings are performed under argon atmosphere.

3.5. MEASUREMENT OF HYDROGEN SORPTION PROPERTIES

Photograph and schematic layout of the apparatus used for hydrogen sorption experiment can be seen in Figure 3.4 and Figure 3.5. This set-up was originally developed by Baybörü (2001). As improved in the current work set-up has three major components; reaction tube, vacuum pump and gas source.

A thick walled 316-L stainless steel tube, having a length of 280 mm and an outside diameter of 42 mm, is used as reaction tube, Figure 3.6. With the help of an additional 316-L stainless steel filler rod active volume of the chamber is reduced to approximately 94mL. Filler rod can be removed freely during sample loading. A mobile tube furnace, which is mounted on a runner to facilitate up and down positioning, is used to heat the reaction tube. The temperature of the furnace is controlled with a controller. To help maintain the stability of the furnace current to heating coil is fed through a variable A.C. regulator (AVR, X10208), Figure 3.7 Two thermocouples (chromel-alumel type) are used; one is placed near the heating coil used for control purpose, the other is placed inside the furnace in contact with the reaction tube to monitor the temperature of the reaction tube.

A digital pressure gauge (TIF 9685, TIF Instruments Inc.) is used to monitor pressure changes in the reaction tube. Pressure gauge is placed approximately 400 mm above the reaction chamber just below Gate (Figure 3.6). The gauge is mounted on an arm (stainless steel tube swaged down to a smaller size to reduce the internal diameter to approx. 1 mm) at a distance of 260 mm. The gauge has a range of 0-3500kPa with accuracy ±1 digit of reading.

A Turbomolecular pump system (Leybold AG PT 50) is used to evacuate the system to pressure levels as low as 4×10^{-4} mbar, though actual level reached was not measured in this work. Maximum volume flow rate of the pump is 6 m^3/h.

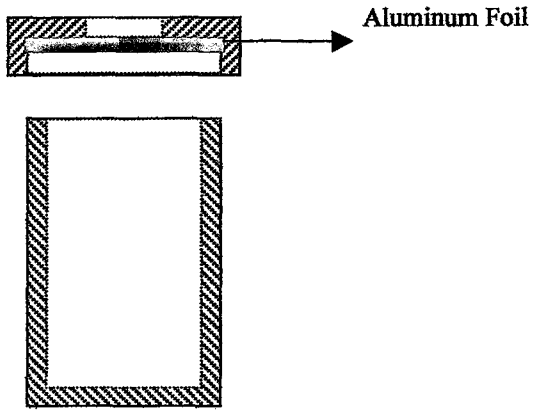

Figure 3.3. Sample transporter container

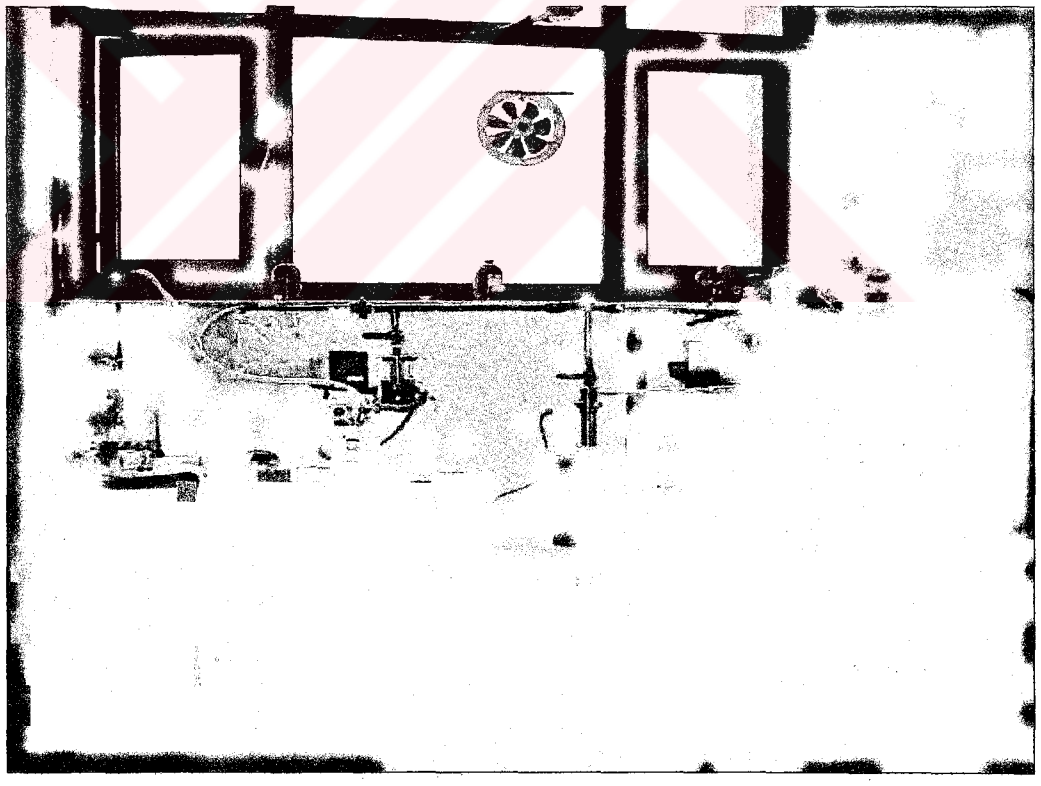

Figure 3.4. The photograph of the hydrogen sorption measurement system.

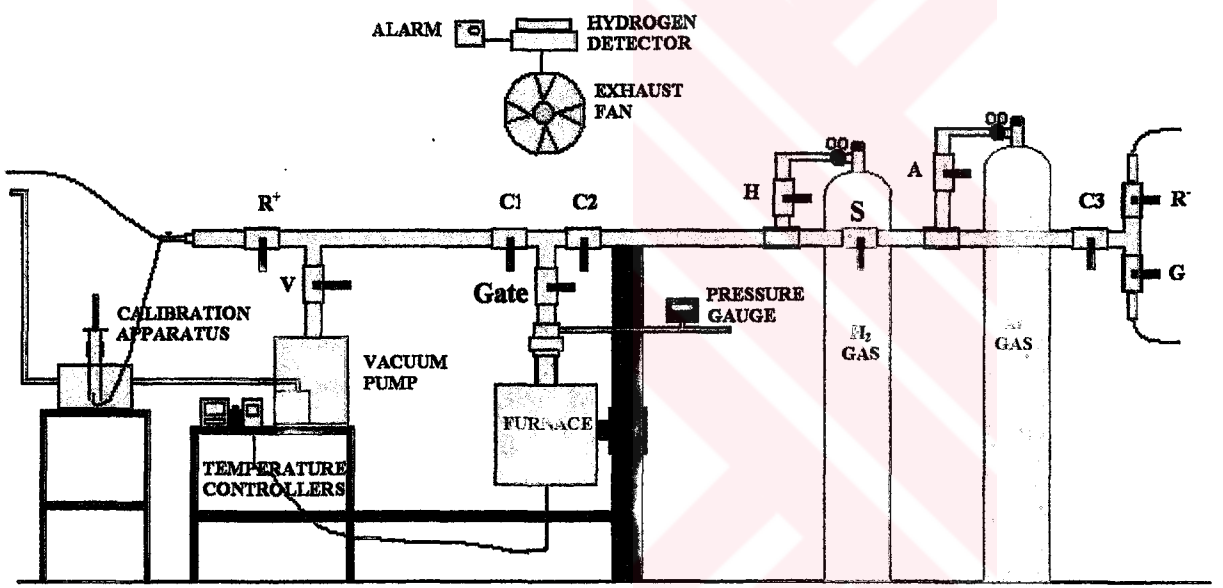

Symbol	Name
A	Argon Valve
C1, C2, C3	Control Valve
G	Glovebox Valve
H	Hydrogen Valve
R+, R-	Release Valve
S	Seperation Valve
V	Vacuum Valve

Figure 3.5. Schematic layout of the hydrogen sorption measurement system.

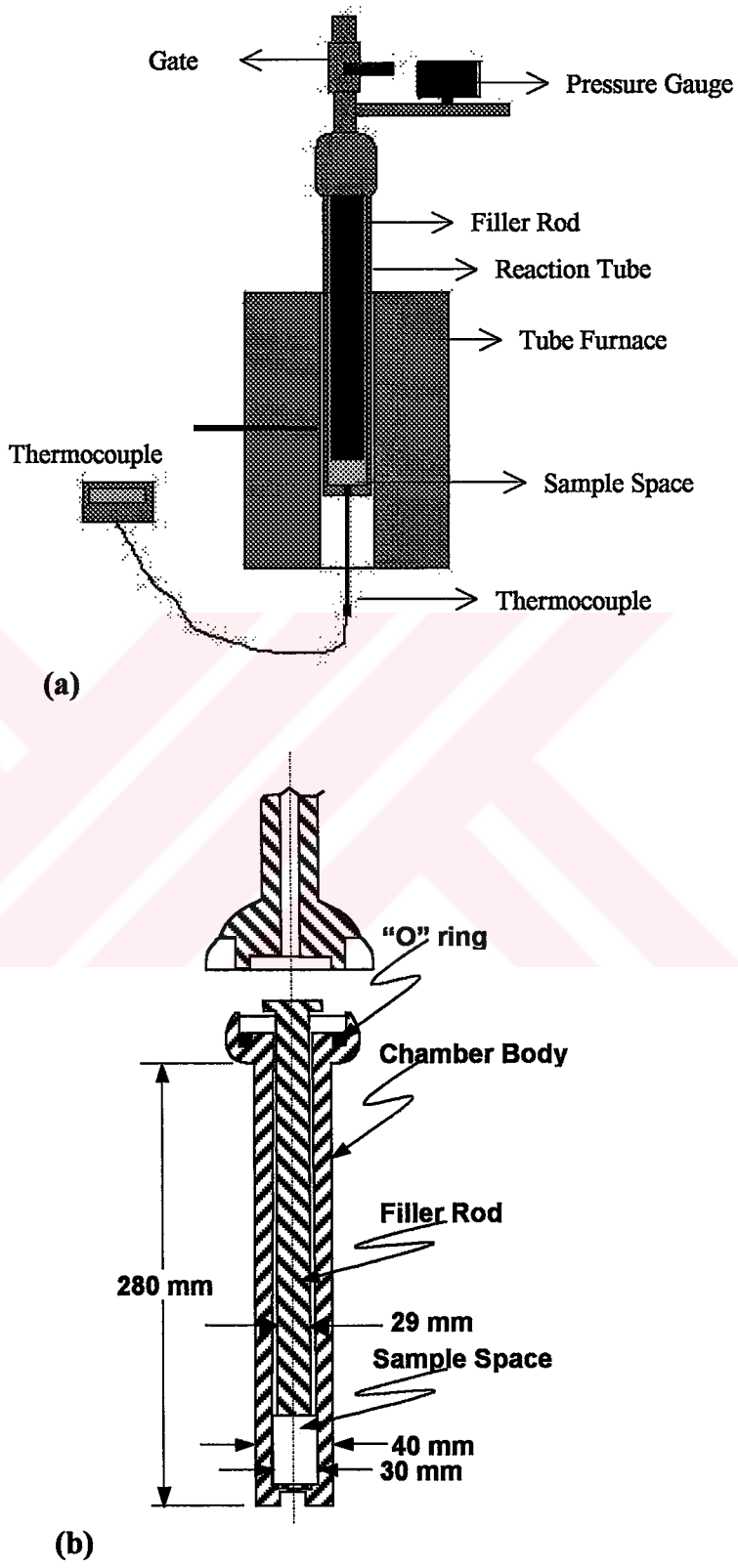

Fig. 3.6. Schematic diagram of (a) the measurement system, (b) reaction tube.

High purity gases (hydrogen; 99.995% and argon; 99.998%) are used in the experiments. Maximum outputs of the regulators (Lincoln) are 10 atmospheres and 3 atmospheres for hydrogen and argon respectively.

Hydrogen gas detector (HD-11, Macurco Inc.) working in conjunction with an alarm and an exhaust fan has been placed near ceiling above the reaction tube. Hydrogen gas detector actuates both alarm and exhaust fan when hydrogen concentration reaches 10% of lower explosive level.

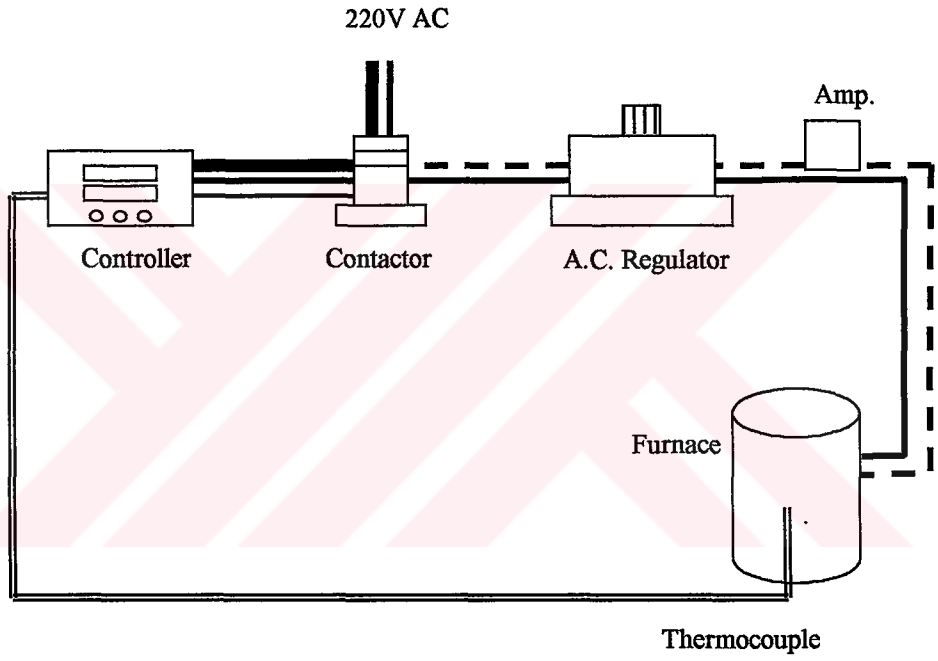

Figure 3.7. Temperature controller system.

3.5.1. Activation Treatment

Before starting sorption experiments, samples are activated. Activation involves several cycles of hydriding and dehydriding. For this purpose, milled powders are transferred into the reaction tube. Filler rod is inserted in place and the reaction tube is connected to the system. Furnace is then brought and fixed in position.

Vacuum valve; V, control valves; C1 and C2, and gate are opened, and air in the system is evacuated by the vacuum pump (see Figure 3.5).

For dehydriding, furnace is set to the desired temperature (e.g. 673K). After stabilization of temperature, dehydriding is carried out for 2 hours, i.e. the system is maintained under vacuum.

For hydriding, furnace is set to hydriding temperature (e.g. 623K). After stabilization of temperature vacuum valve V was closed and vacuum pump is isolated from the system. Hydrogen gas of desired pressure (e.g. 10atm) is introduced into the reaction tube. Hydrogen valve H was opened. The steel pipe in between release valve R^+ to separation valve S (i.e. valves C1 and C2, and gate is open) is used as hydrogen reservoir to maintain the applied pressure. After 2 hours of hydriding valve H and gate are closed, and valve R^+ is opened to release the hydrogen from the reservoir. Vacuum valve V is then closed and gate is opened. The system is taken under vacuum. The valve V is closed, and the gate is opened. This cycle is repeated until the hydrogen pressure in the system is reduced to atmospheric pressure.

This dehydriding and hydriding cycle is repeated a number of times (typically three) to activate the sample.

3.5.2. Measurement of P-C-T Diagram

Measurement of the P-C-T diagram is similar to the activation treatment except that reaction tube is isolated from the system i.e. gate is kept closed during measurement. In this experiment, different levels of hydrogen pressure were applied during hydriding. Pressure levels studied varied from 1 to 10atm at an interval of 1atm. At a given pressure, change in pressure is monitored. The experiment for that pressure is continued as long as pressure changes.

The experiment is terminated when no change in pressure occurs for a waiting time of 5 minutes. The gate is opened to set the pressure to the same value the measurement is repeated. This cycle is repeated number of times when no pressure drop is observed within 5 minutes. The reaction at the pressure is then complete. Drops in pressure are added together to find the total absorption. When reaction is complete the pressure is adjusted to a new value by opening the gate. PCT diagram is determined for hydriding only.

3.5.3. Measurement of Absorption Kinetics

Measurement of absorption kinetics is similar to the measurement of P-C-T diagram except that pressure is adjusted at the beginning and is not changed during the experiment (gate is always kept closed during experiment). In this experiment, desired hydriding pressure is applied i.e. 10atm. Pressure drop is monitored as a function of time. Reaction is considered to be complete when no drop in pressure occurs for a waiting time of 30 minutes.

3.5.4. Measurement of Desorption Kinetics

Sample is hydrided as in activation treatment. Hydrogen with a pressure of 10atm is applied to the sample and the gate is closed. The furnace is then set to dehydriding temperature. The part of the tube that is used as reservoir is released to atmosphere by opening the release valve R^+. Then valve R^+ is closed and vacuum valve V is opened and the system is taken under vacuum. After stabilization of the temperature, pressure inside the reaction tube is reduced carefully controlling the gate, until the pressure drops to 1atm at which point gate is closed. The gate is kept closed during the experiment. At that condition pressure increase is recorded as a function of time. Reaction is considered to be complete when no increase in pressure occurs for a waiting time of 30 minutes.

3.6. CALIBRATION

Sorption measurements in this work were carried out under constant temperature (desorption or absorption temperature) and constant volume (volume of reaction tube). Hydrogen sorption is reflected either by a pressure drop or a pressure increase. Pressure change (ΔP) indicates the amount of gas absorbed or desorbed by the sample, from which mole change of the gas (Δn) inside the reaction tube can be calculated by using ideal gas law.

$$P\,V = n\,R\,T \tag{3.1}$$

$$\Delta P\,V = \Delta n\,R\,T \tag{3.2}$$

The amount of hydrogen (Δn) absorbed or desorbed by the sample can therefore be easily calculated. This value can be converted into a desired form (i.e. wt.% H) if the weight of the sample is known.

Hydrogen sorption reaction takes place at the bottom of the tube in reaction chamber whereas pressure gauge is placed far above near the gate; see Figure 3.6. Temperature distribution is non-uniform in the reaction tube from bottom to top. In order to be able to find the mole change of the gas inside the reaction tube a correction factor, c, was introduced in Equation (3.2).

$$\Delta P\,V = c(T)\,\Delta n\,R\,T \tag{3.3}$$

This factor is dependent on the temperature of the experiments.

Schematic drawings of the apparatus used for determining the correction factor is given in Figure 3.8. Apparatus consists of a glass bowl, which was filled with water, and a graduated cylinder. Graduated cylinder is filled with water and turned upside down in the glass bowl. Graduated cylinder is then fixed above the glass bowl. A hose is placed just under the mouth of the graduated cylinder such that gas

evolved from the hose accumulates into the graduated cylinder and connected to release valve (R^+).

To determine the correction factor the reaction tube is set to a selected temperature. Argon is applied to the system at a pressure of 2.5atm. The gate is closed and release valve R^- is opened to release argon from the reservoir (C3 is opened while G is kept closed).

The release valve R^+ is opened. The gate is carefully controlled until the gas released from the hose fills the graduated cylinder. The gate is closed as soon as the water level inside the graduated cylinder is the same as that in the surrounding bowl. This ensures that gas inside the cylinder is under atmospheric pressure. The pressure drop in the reaction tube is then recorded.

To determine the amount of gas collected in the graduated cylinder for that pressure drop; volume of the gas is read from the cylinder. Collected gas inside the graduated cylinder is unavoidably a wet gas due to the water vapor. By using Dalton's Law of Partial Pressures

$$P_{total} = P_{gas} + P_{water} \tag{3.4}$$

Pressure of dry gas is determined by rearrangement of the Equation 3.4; $P_{gas} = P_{total} + P_{water}$, i.e. P_{total} was assumed to be equal to 1atm, P_{water} is taken as 31.26×10^{-3} atmospheres (for water temperature of 298K).

Therefore, volume as well as pressure of collected gas is known. Data collected for this purpose are given in Table 3.2. In the table V_{gas} is the volume of the collected gas in the cylinder, ΔP is the measured pressure change at various reaction tube temperatures, T_{rt}. n_{gas} denotes the calculated mole of the gas.

The correction factors for the three temperatures are given in Table 3.3. The factors are determined for condition where P is measured in atmospheres; V is 94×10^{-3} L; R is 0.082 L.atm.mol^{-1}.K^{-1}; T is in K.

Table 3.2. Calibration data and results for three sorption measurement temperatures.

T_{rt} (K)	V_{gas} (Liter) $\times10^{-3}$	ΔP (Atm) $\times10^{-3}$	n_{gas} (Mole) $\times10^{-3}$
573	96	15.15	3.560
623	95	15.15	3.760
673	101	16.16	3.999

Table 3.3. Correction factors c(t) for the three selected temperatures, T.

T (K)	c(T) $\times10^{-3}$
573	13.25
623	11.88
673	10.78

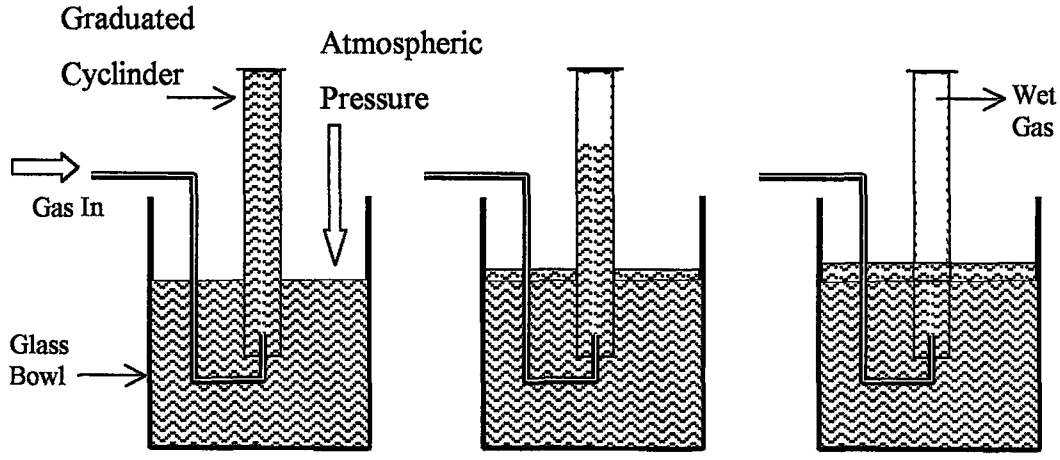

Figure 3.8. Calibration apparatus (a), gas flow over water (b) and wet gas collected in the graduated cylinder having a pressure equal to atmospheric pressure (c).

3.7. CHARACTERIZATION OF POWDERS

X-ray diffraction (XRD) and scanning electron microscopy (SEM) were used for characterization purposes.

Microstructures of powders were examined by scanning electron microscopy, JSM 6400 SEM (JEOL). Double sided adhesive, conductive carbon discs (Structure Probe, Inc.), 9 mm dia., powder sample holders were used in SEM examinations.

Diffraction experiments were carried out with a Philips Diffractometer PW 1352/20, using filtered Co Kα radiation (30kV. 7-10mA).

3.7.1. Determination of Crystallite Size

Structural refinement after mechanical milling and after sorption measurements was examined with X-ray line broadening analysis. Scherrer method was used to calculate crystallite size (Warren, 1969).

For this purpose samples were scanned in steps of 1/8 degree (2θ) per minute from 63° to 66° to determine the breadth of {211} reflection of MgH_2. In this step scanning procedure Co Kα radiation (35kV and 18mA) was used. Broadening (in radians) was measured from the width of the {211} reflection at an intensity equal to half maximum.

Unavoidably, calculated overall broadening (B_t) includes instrumental broadening, B_i, as well as structural broadening, B_s. In order to calculate crystallite size, the broadening due to instrumental errors should be eliminated. For this purpose, a reference sample was prepared by using bulk Mg; annealed for 2 hours at 250°C.

Broadening obtained for the closest peak of {211} reflection of MgH_2 from the reference sample (112) gives instrumental broadening, B_a; by using

$$(B_s)^2 = (B_t)^2 - (B_a)^2 \quad (3.5)$$

structural broadening, B_s, was calculated. Calculated structural broadening was then used to find the crystallite size, t,

$$t = (0.9\lambda) / (B_s \cos\theta_B) \quad (3.6)$$

where λ, is the wavelength of the X-ray beam; θ_B, is the Bragg's angle of the selected peak.

This approach is not precise (Warren, 1969), but considered sufficient for the current work.

CHAPTER IV

RESULTS AND DISCUSSIONS

4.1. X-RAY STUDIES

X-ray diffraction patterns for MgH_2 milled for 3 hours with additives; V and graphite (G) are given in Figure 4.1. Diffraction profiles for unmilled and milled MgH_2 are also included in the figure. All patterns are obtained with Co Kα radiation in 20° to 100° range.

MgH_2 powders used in the experiments composed of β-MgH_2 and Mg phases, Figure 4.1. After 3 hrs of milling there is a formation of γ-MgH_2 and appearance of MgO in all samples.

No alloy is formed upon 3 hrs of milling of MgH_2 with V as vanadium being hardly miscible in Mg. However, a small peak of $VH_{0.81}$ phase appeared both in MgH_2-5%V and MgH_2-10%V.

There is a small graphite peak that corresponds to (200) diffraction observed in x-ray pattern of MgH_2-5%G and MgH_2-5%V-5%G after 3 hrs of milling. This indicates that graphite structure is not completely destroyed with milling. The graphite peak is more intense in MgH_2-5%V-5%G, in which 5%G is added last 15 minutes of the milling.

The above observations are consistent with the results reported in the literature. For instance, Huot et al (1999) reported the formation of γ-MgH_2 and MgO after

three hours of milling of MgH_2. Formation of $VH_{0.81}$ phase is reported by Schulz et al (2001) and Liang et al (1999a, 2000b) after 5 hrs of milling of MgH_2 with V.

4.2. STRUCTURAL REFINEMENT: MILLED SYSTEMS

4.2.1. Structural Observation

The average particle size of the initial materials, MgH_2, V and Al_2O_3 are 15, 20 and 7 microns, respectively. Graphite has its own flaky form with an average particle size of 60 microns. Macrostructures of MgH_2 and graphite are given in Figure 4.2.

Macrostructures of MgH_2 milled with additives are given in Figure 4.3. In milled MgH_2 the structure consists of micron and sub-micron particles, Figure 4.3 (a). But there are also relatively large particles (7-8 microns) distributed randomly in the structure. Particles are circular in shape, and seem to be in the form of agglomerates, Figure 4.4.

It can be seen from the Figure 4.3 (b) that the structure of the MgH_2-5%V is composed of relatively fine particles and the particles are irregular in shape as compared to milled MgH_2. The agglomeration observed in milled MgH_2 is not observed for this system.

The structure in MgH_2-5%G (Figure 4.3 (c)) is finer. Of the systems investigated in this work finest particle size is achieved in MgH_2-5%V-5%G, Figure 4.3 (d).

As a result, the highest degree of refinement is observed in MgH_2-5%V-5%G. It is followed by MgH_2-5%G, MgH_2-5%V and MgH_2-10%V. The refinement is lower in MgH_2-5%Al_2O_3 and milled MgH_2.

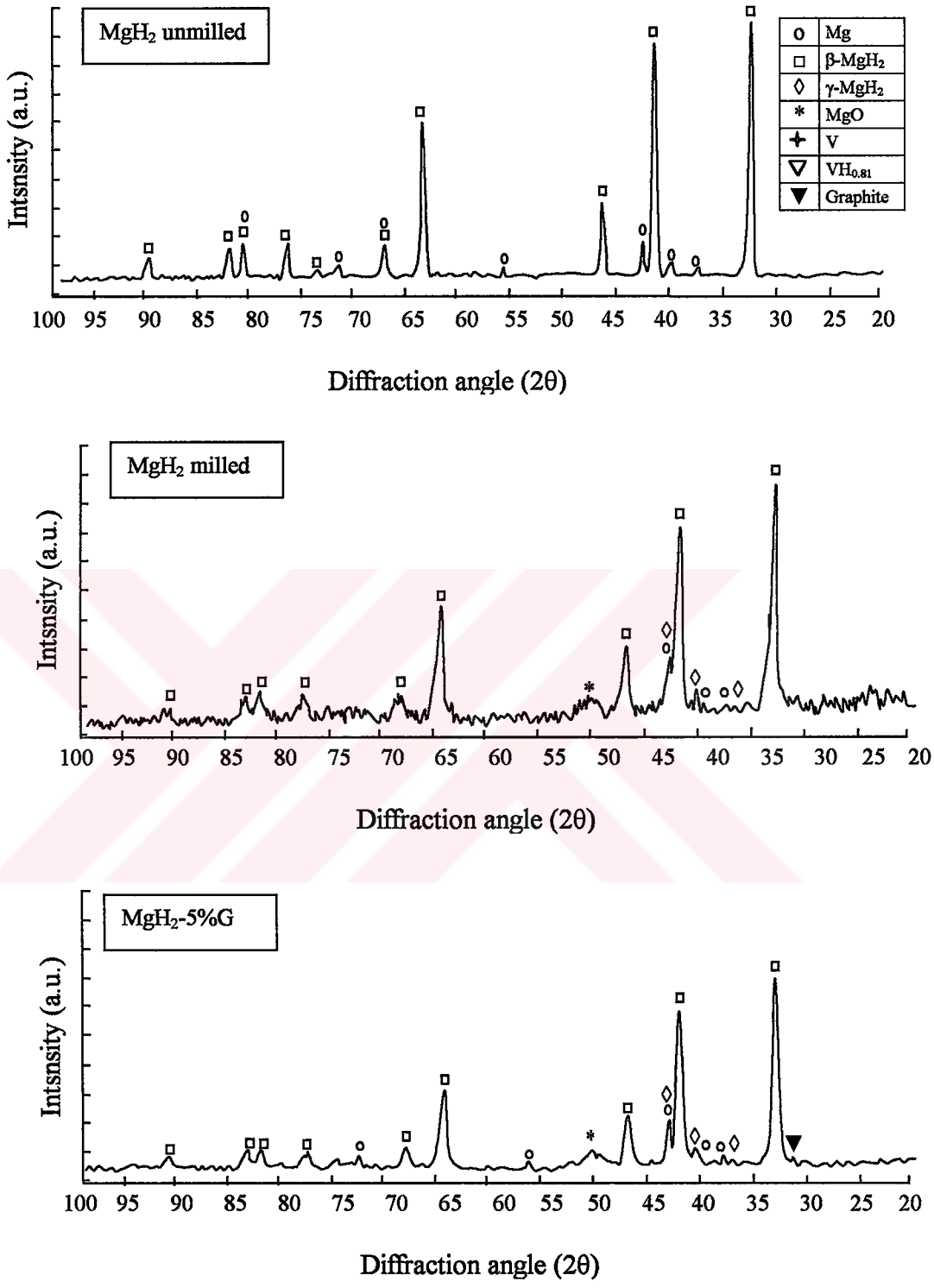

Figure 4.1. X-ray diffraction patterns of the milled systems. Unmilled MgH_2 is also included in the figure.

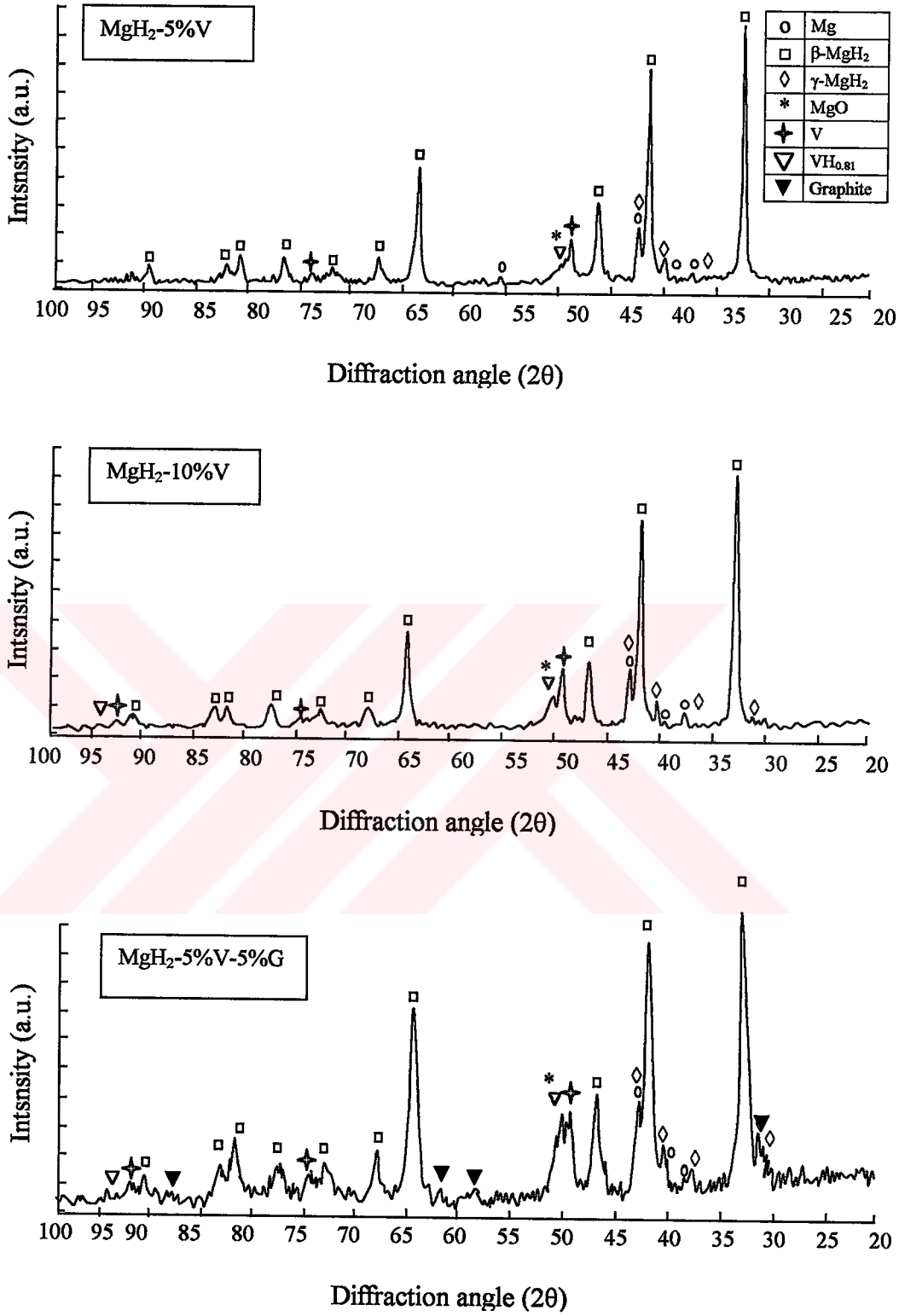

"Figure 4.1 (continued)"

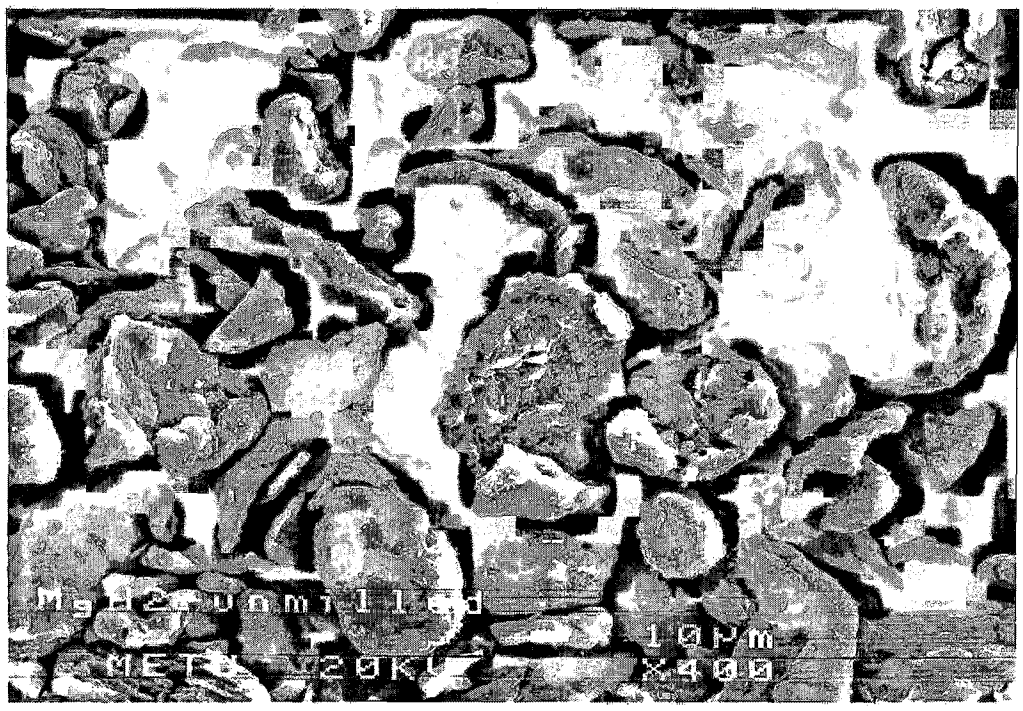

(a)

(b)

Figure 4.2 Macrostructures of initial powders; (a) MgH_2, (b) graphite.

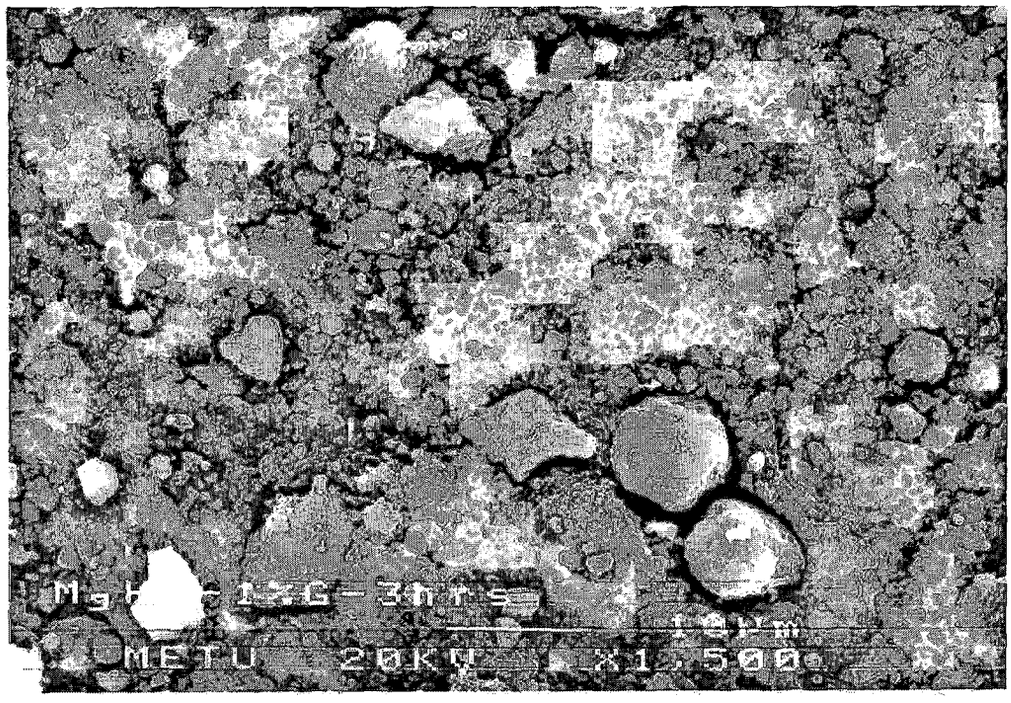

(a)

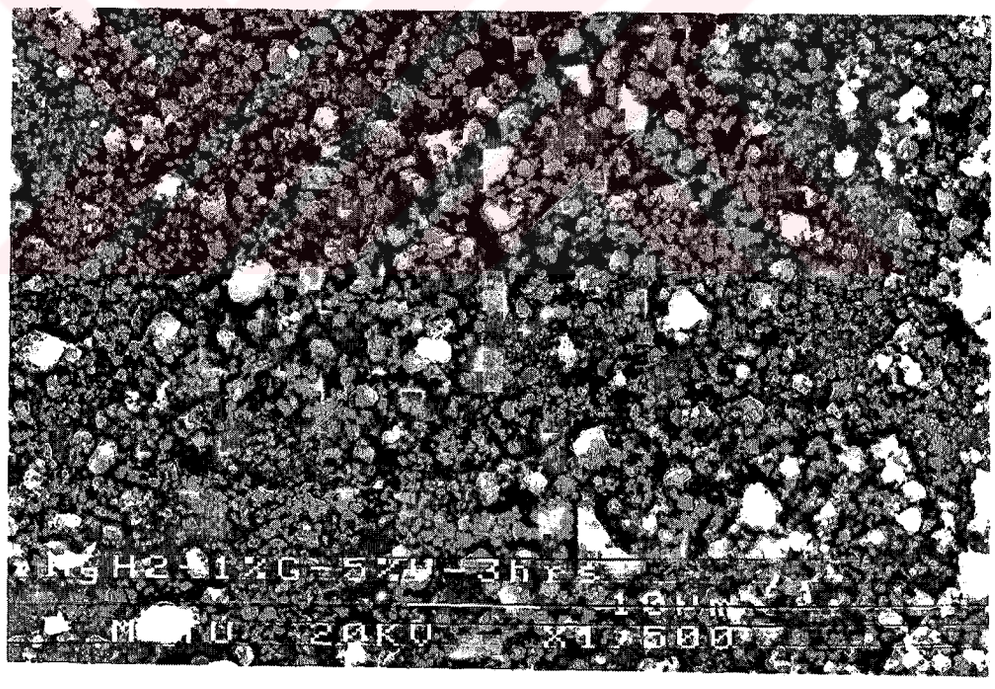

(b)

Figure 4.3. Macrostructures of MgH_2; milled with and without additives; (a) MgH_2, (b) MgH_2-5%V, (c) MgH_2-5%G, (d) MgH_2-5%V-5%G, (e) MgH_2-10%V, (f) MgH_2-5%Al_2O_3.

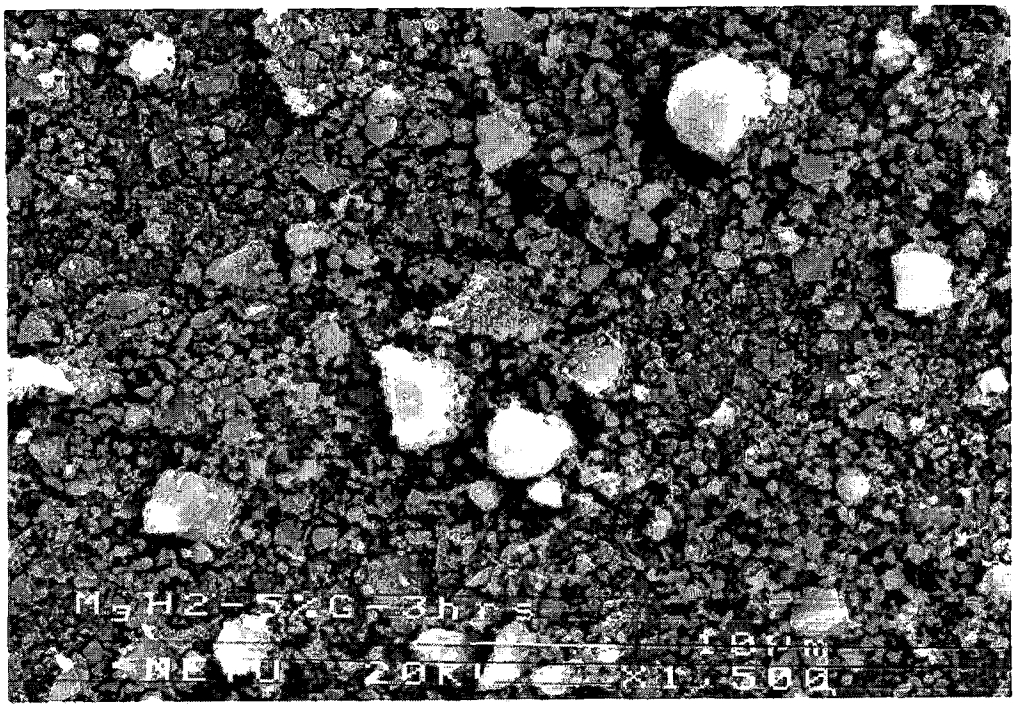

(c)

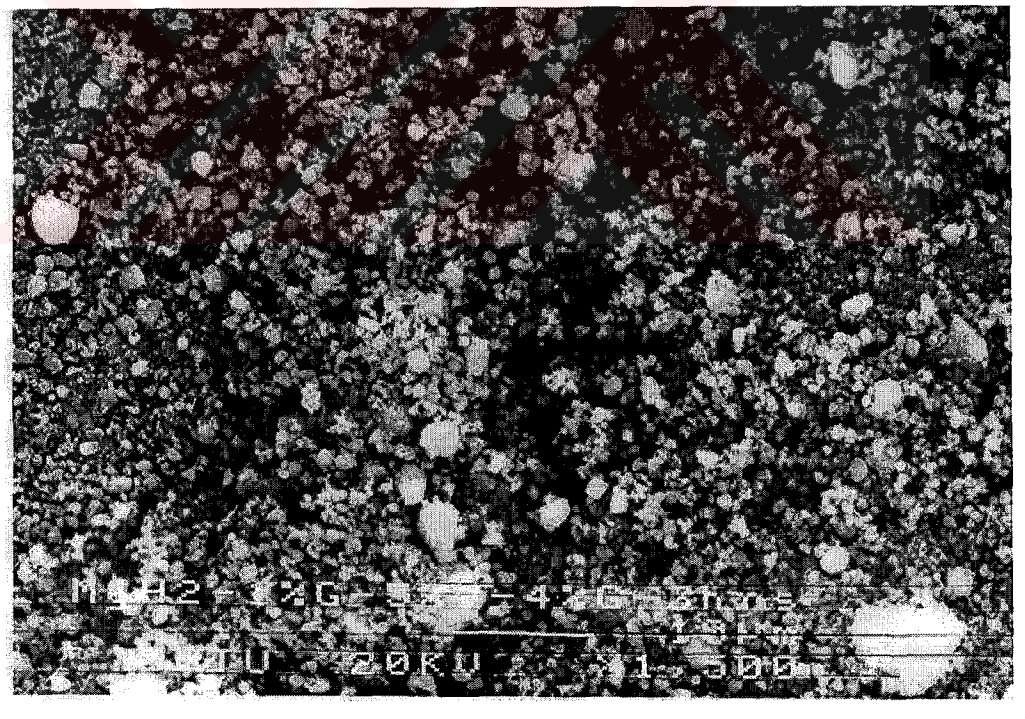

(d)

"Figure 4.3 (continued)"

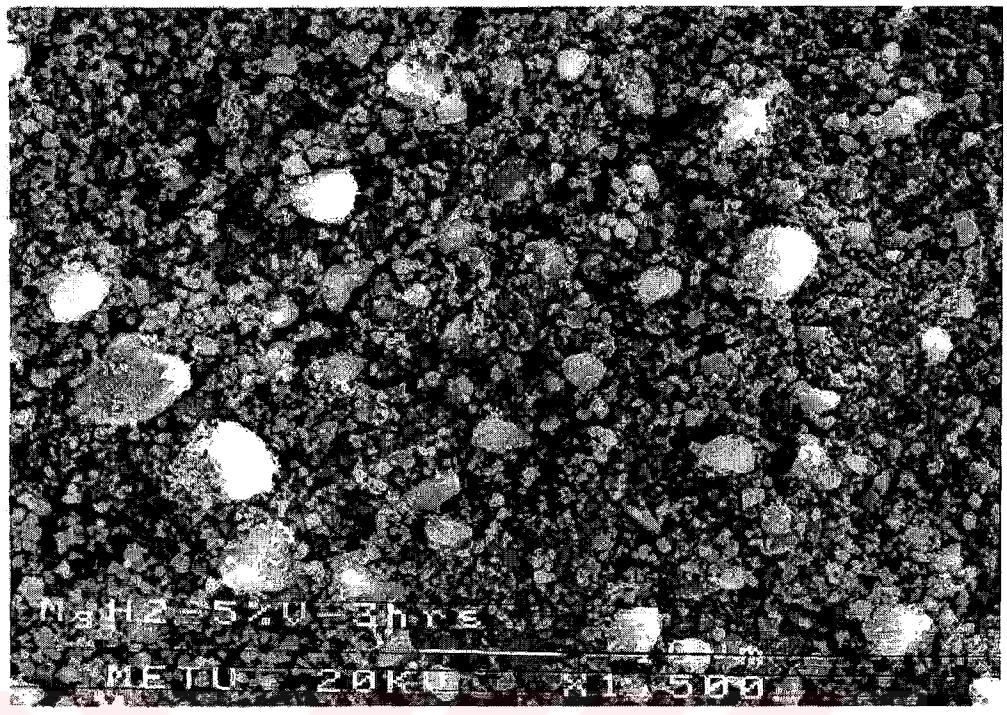

(e)

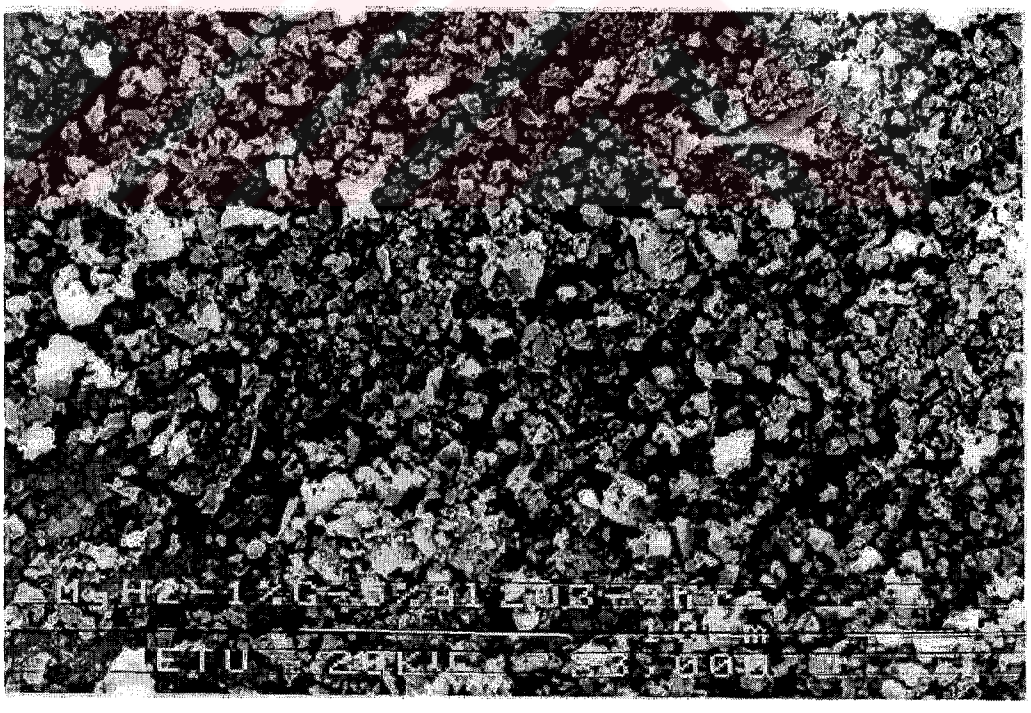

(f)

"Figure 4.3 (continued)"

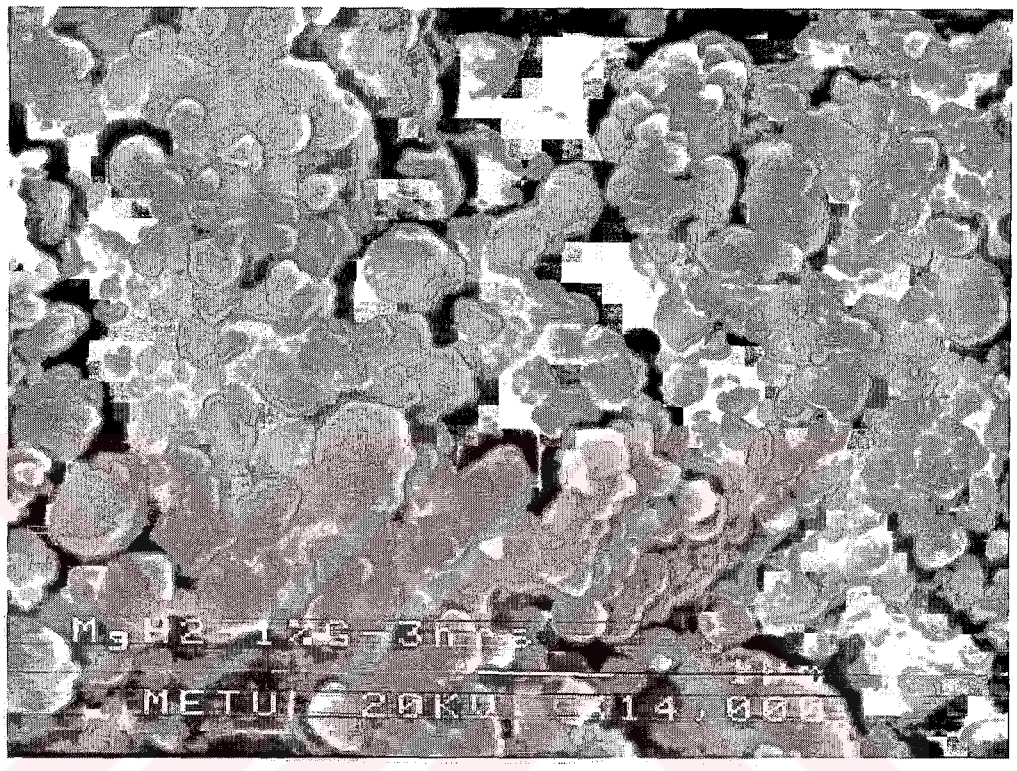

Figure 4.4. Macrostructure of the MgH_2 milled without additive.

4.2.2. X-Ray Line Broadening

X-ray line-broadening profiles of milled systems are given in Figure 4.5. Unmilled MgH_2 is also included in the figure. These profiles refer to the (211) reflections of MgH_2. All peaks are moved and superimposed on their half maximum intensity.

It can be seen from the Figure 4.5 that the largest broadening is achieved with MgH_2-5%V-5%G. It is followed by MgH_2-5%G, MgH_2-5%V and MgH_2-10%V respectively. Of the milled systems MgH_2-5%Al_2O_3 shows the smallest broadening. The observed broadenings are consistent with the macrostructural observations.

It is possible to calculate the structural size from the measured broadening by using Scherrer formula as described in Chapter III. In order to calculate the structural sizes the broadening obtained from the (102) diffraction of heat-treated bulk magnesium, which is the closest diffraction to the (211) diffraction of MgH_2, is used as a reference. The instrumental broadening based on this reference sample is found to be 0.00872 radians.

Calculated structural sizes are given in Table 4.1.

From Table 4.1 MgH_2-5%V-5%G and MgH_2-5%G have the lowest structural sizes of 15.7 and 26.1 nm respectively. MgH_2-5% V and MgH_2-10% V, i.e. 26.1 and 26.5 nm, follow these systems. For MgH_2-5%Al_2O_3 and milled MgH_2 the values are relatively large: 31.2 and 31.9 nm respectively.

The calculated structural sizes compare well with those reported in the literature. For instance, Schulz et al (2001) reported a particle size of 17.1 nm for MgH_2 after 20 hrs of milling.

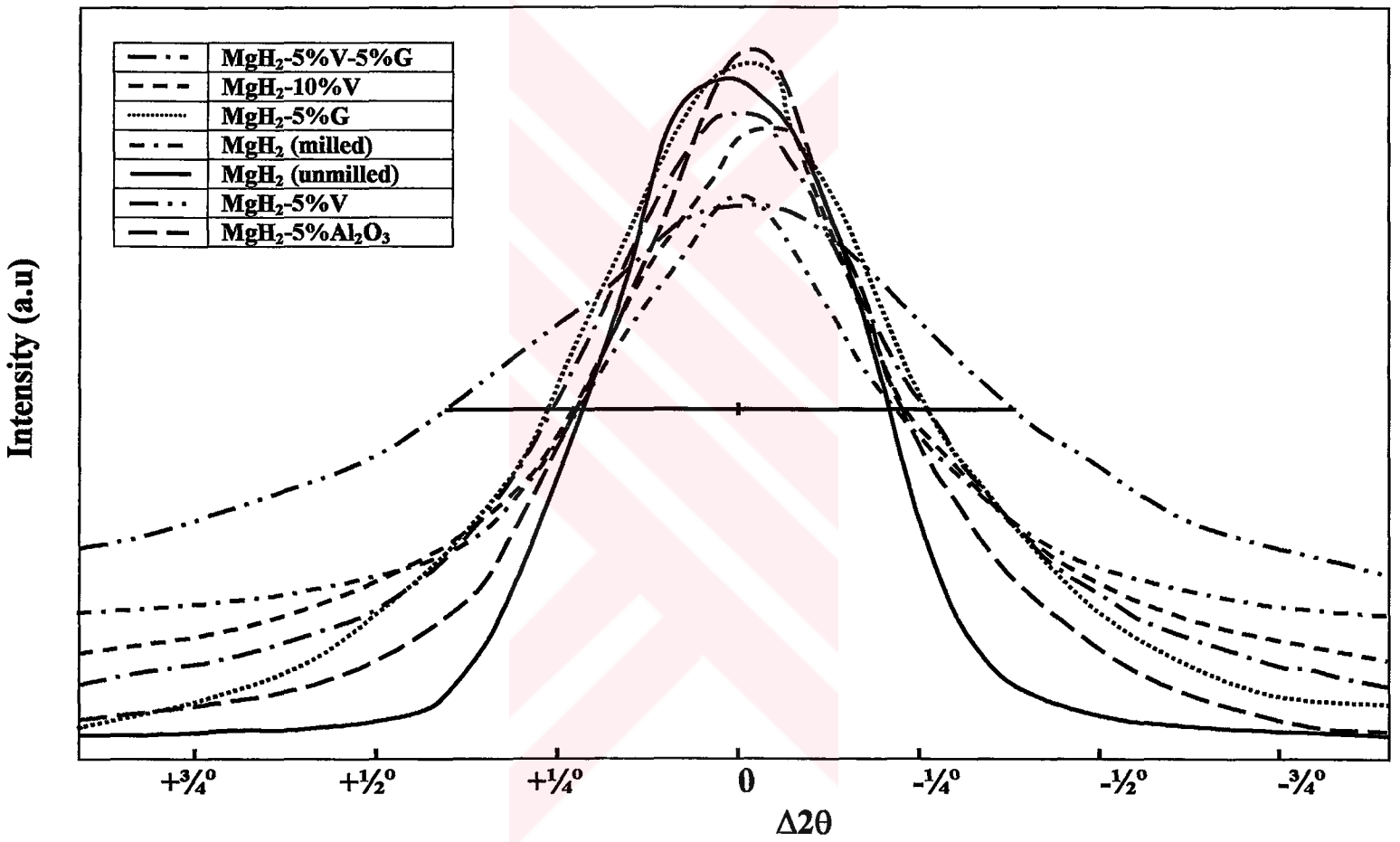

Figure 4.5. X-ray line broadening profiles that refers to (211) diffraction of MgH_2 of the milled systems. The peaks are moved and superimposed on their half maximum intensity. Unmilled MgH_2 is also included in the figure.

Table 4.1. Broadening and structural size obtained from (211) reflection of MgH_2 for all systems after milling. Diffraction angles (2θ) and lattice parameters ($d_{(211)}$) are also included in the table.

System	Broadening (Radians)	Structural Size (nm)	2θ (Degree)	$d_{(211)}$ (Angstrom)
MgH_2-5%V-5%G	0.023743	**15.7**	**23.1**	**1.680**
MgH_2-5%G	0.017580	**26.1**	**21.3**	**1.682**
MgH_2-5%V	0.014347	**26.5**	**21.3**	**1.682**
MgH_2-10%V	0.014091	**31.2**	**22.1**	**1.681**
MgH_2-5%Al_2O_3	0.011447	**31.9**	**23.5**	**1.679**
MgH_2	0.011991	**32.7**	**25.8**	**1.676**
MgH_2 *Unmilled	0.011720*	**35.2***	**19.8**	**1.684**

4.3. STRUCTURAL REFINEMENT: SORBED SYSTEMS

The above observations are for powders in "as-milled" state. However, in hydrogen sorption studies particles are subjected to relatively high temperatures (400°C) and pressures (10 atm). In order to investigate the macrostructures of the systems after sorption, sorbed systems were also examined with SEM and X-ray analysis. All systems were hydrided after sorption experiments.

4.3.1. Structural Observation

Macrostructures of the milled systems after sorption are given in Figure 4.6. Unmilled MgH_2 is also included in the figure.

In unmilled MgH_2 (Figure 4.6 (a)) the particles seem to be fragmented after sorption as compared to milled state (Figure 4.3 (a)).

Similarly, for MgH_2-5%V (Figure 4.6 (c)) the larger particles in milled state (Figure 4.5 (b)) seem to be fragmented, and this fragmented particle are in the form of agglomerates.

The case is similar in milled MgH_2 after sorption (Figure 4.6 (b)). Relatively larger particles in milled state disappear after sorption. But the particles seem to be in the form of agglomerates.

Thus, it can be concluded that after sorption agglomerated structure, which may be due to in situ fragmentation of particles, is observed in all systems except in unmilled MgH_2.

4.3.2. X-Ray Line Broadening

X-ray diffraction profiles after sorption is given in Figure 4.7 and Figure 4.8. Figure 4.7 refers the hydrided state whereas the latter denoted the dehydrided state of MgH_2-V system* and unmilled MgH_2**.

It can be seen from the Figure 4.7 that after sorption the peaks become sharpened and narrower as compared the milled state. This may be due to the structural recovery and relieve of stress in the structure. For all system sharp β-MgH_2 peaks and a small MgO peak is observed in the diffractograms. For MgH_2-V system there appears an additional small peak of $VH_{0.81}$. Mg peaks are observed in the diffraction pattern of unmilled MgH_2. This may be due to the presence of excess Mg that does not react with hydrogen.

---

*It can be seeen from Figure 4.8 that the vanadium hydride phase, $VH_{0.81}$, disappears after dehydriding.

**For unmilled MgH_2, MgH_2 peaks are observed after dehydriding which indicates the presence of unreacted MgH_2 in the structure.

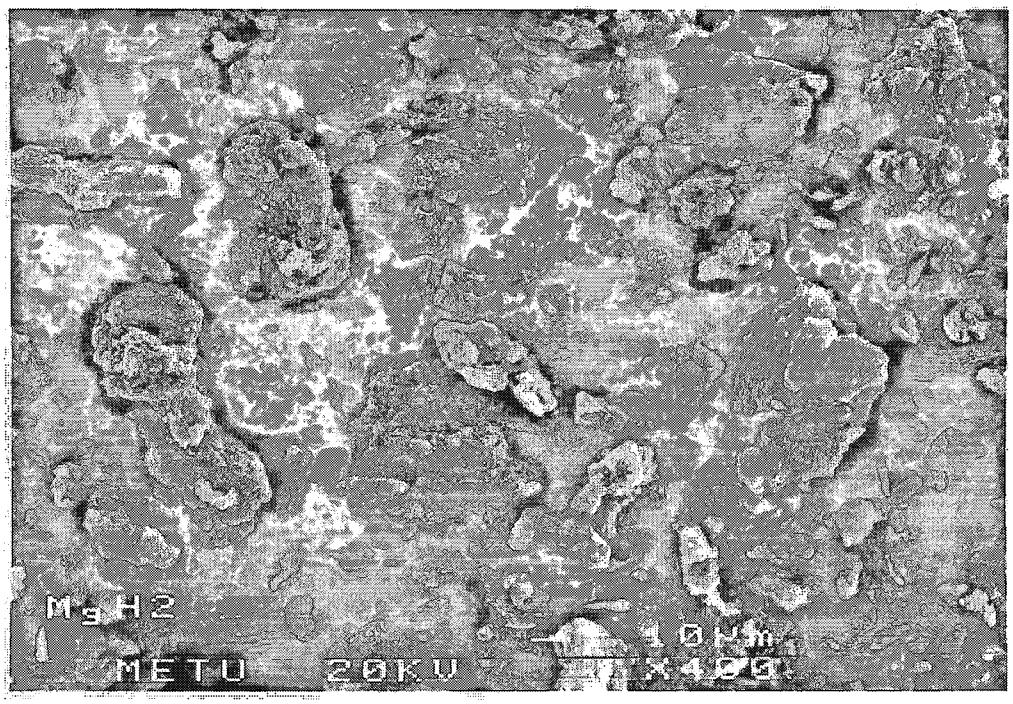

(a)

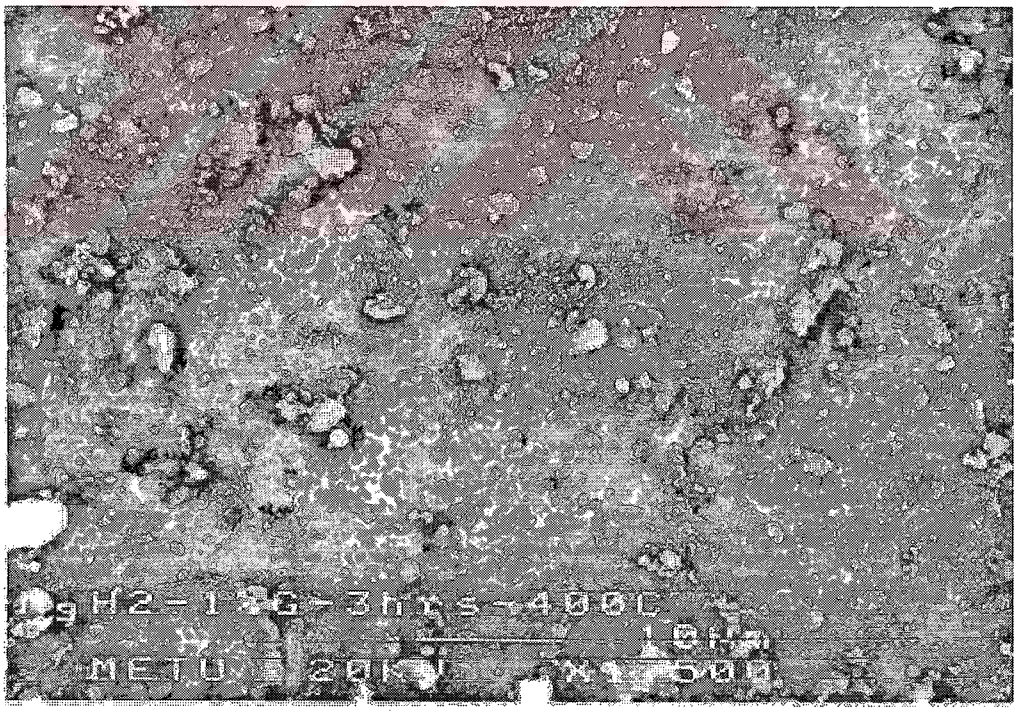

(b)

Figure 4.6. Macrostructures of the powders after sorption; (a) unmilled MgH_2, (b) milled MgH_2, (c) MgH_2-5%V, (d) MgH_2-5%G, (e) MgH_2-5%V-5%G

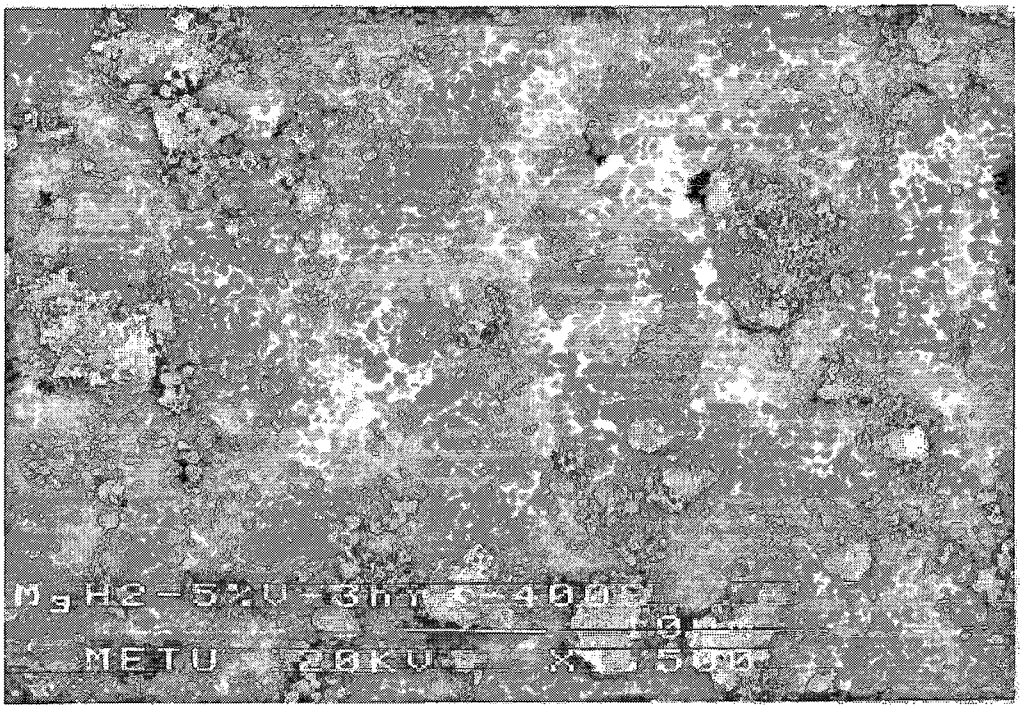

(c)

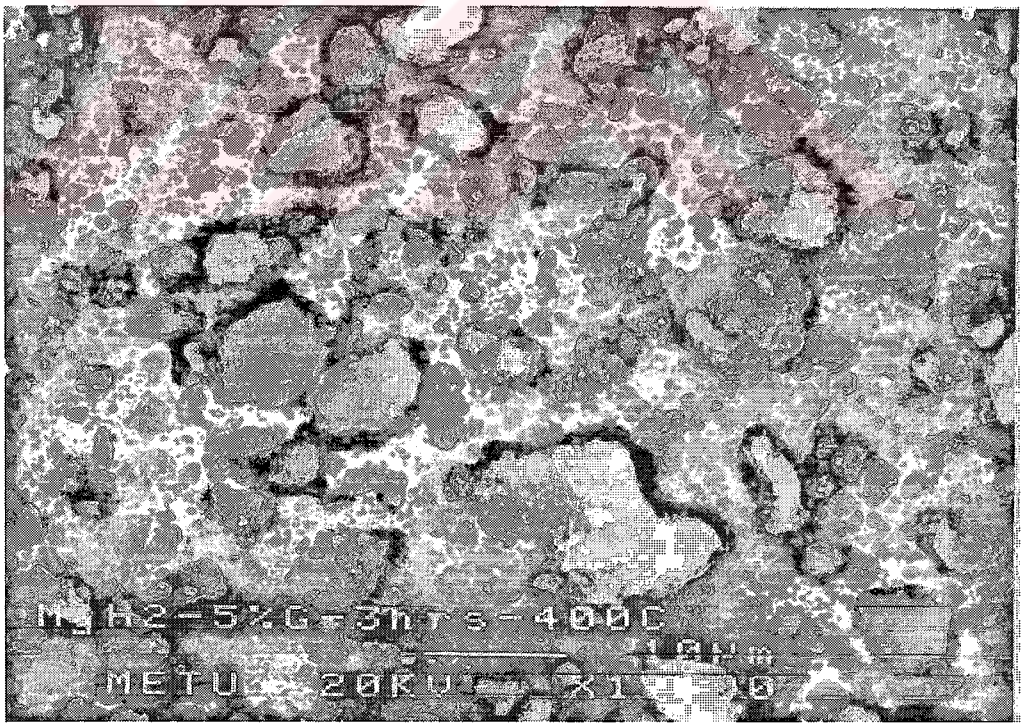

(d)

"Figure 4.6. (continued)"

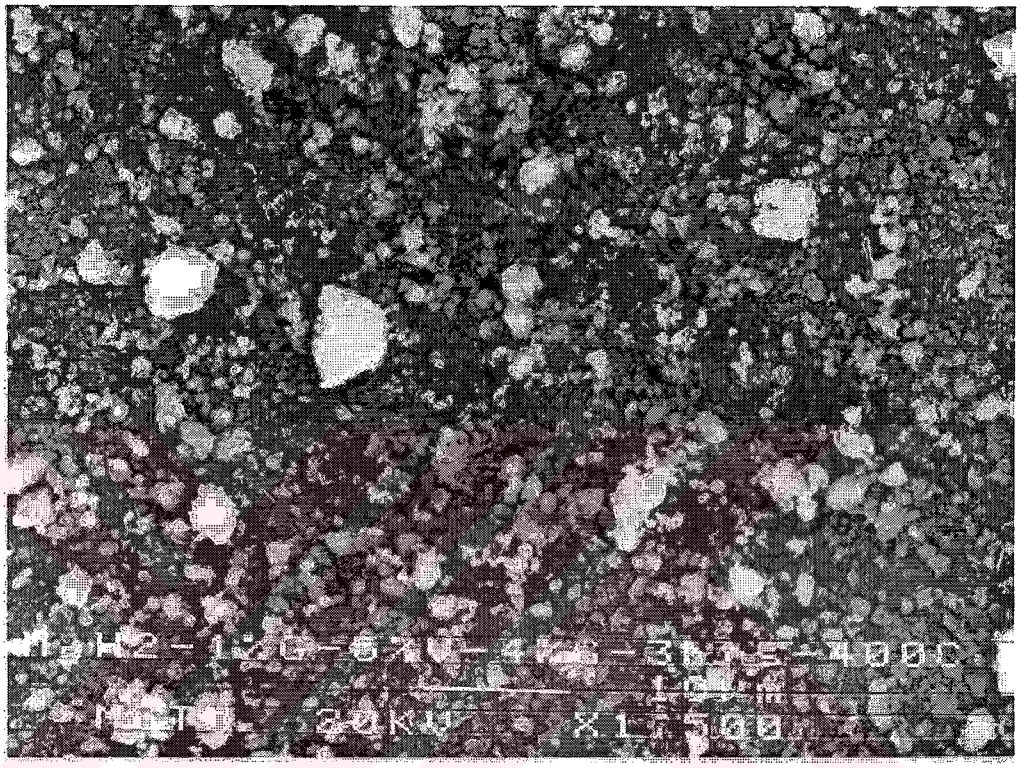

(e)

"Figure 4.6. (continued)"

X-ray line-broadening profiles for (211) reflection of MgH_2 after sorption for all samples are given in Figure 4.9, and separately in Figure 4.10.

It can be seen from the Figure 4.9 that the largest broadening is observed in MgH_2. It is followed by MgH_2-5%Al_2O_3, MgH_2-10%V, MgH_2-5%V-5%G, MgH_2-5%G and MgH_2-5%V respectively. Thus, the observed broadening sequence for milled systems is changed after sorption. (For the milled state the order is MgH_2-5%V-5%G, MgH_2-5%G, MgH_2-5%V, MgH_2-10%V, MgH_2-5%Al_2O_3 and MgH_2, see Section 4.2.2.)

The calculated structural sizes are given in Table 4.2.

Table 4.2. Broadening and structural size obtained from (211) reflection of MgH_2 for all systems after sorption. Diffraction angles (2θ) and lattice parameters ($d_{(211)}$) are also included in the table.

Systems	Broadening (radians)	Structural Size (nm)	2θ (Degree)	$d_{(211)}$ (Angstrom)
MgH_2-5%V-5%G	0.006542	**57.1**	**23.1**	**1.678**
MgH_2-5%G	0.008855	**57.1**	**20.4**	**1.683**
MgH_2-5%V	0.006542	**60.6**	**20.4**	**1.683**
MgH_2-10%V	0.006171	**57.1**	**22.1**	**1.681**
MgH_2-5%Al_2O_3	0.008231	**45.4**	**20.8**	**1.683**
MgH_2	0.006542	**45.4**	**19.1**	**1.685**
MgH_2 Unmilled	0.008231	**40.8**	**21.5**	**1.682**

The smallest structural size is obtained for MgH_2-5%Al_2O_3 and milled MgH_2, i.e. 45 nm. For MgH_2-10%V, MgH_2-5%V-5%G and MgH_2-5%G structural size is relatively higher, 57.1 nm. Of the sorbed systems the largest structural size is 60.6 nm for MgH_2-5%V.

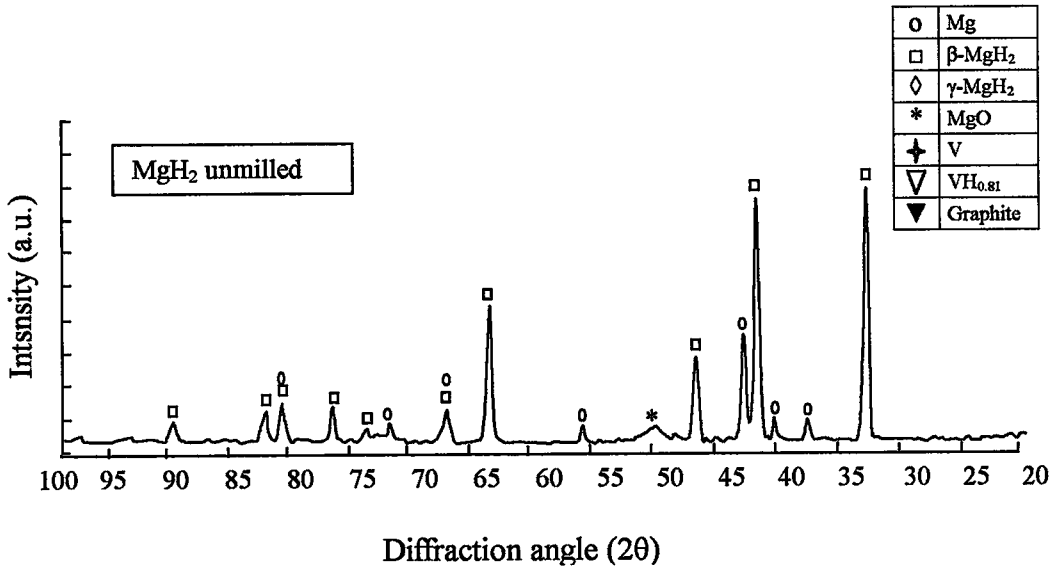

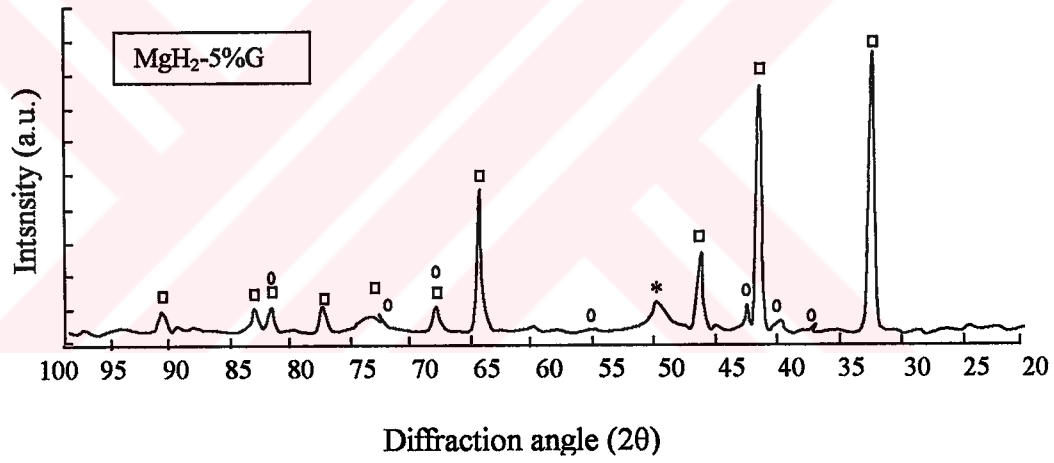

Figure 4.7. X-ray diffraction profiles of the milled systems after sorption in hydrided state. Unmilled MgH_2 is also included in the figure.

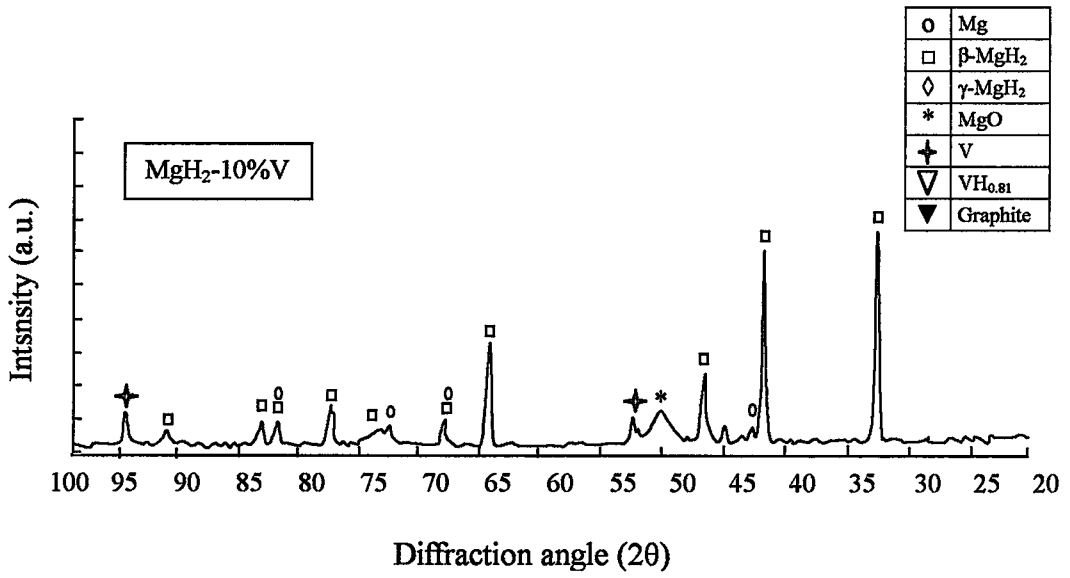

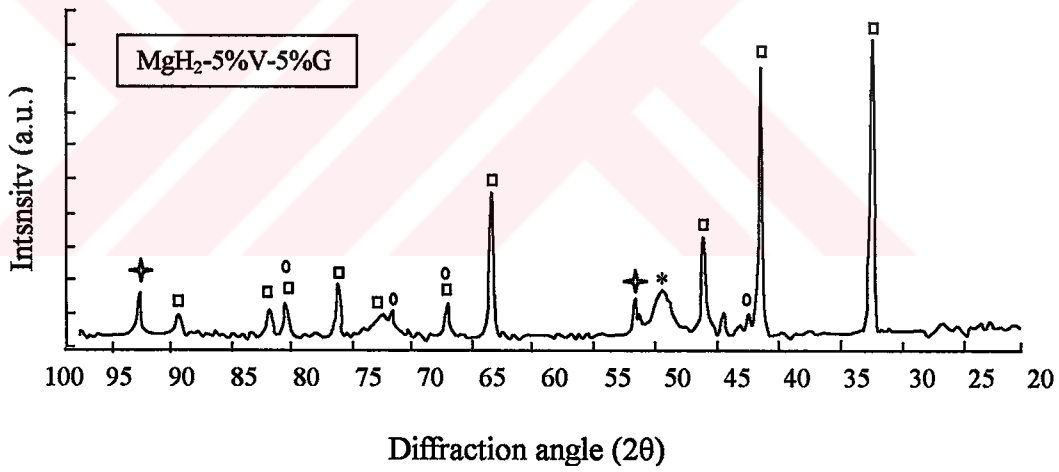

"Figure 4.7. (continued)"

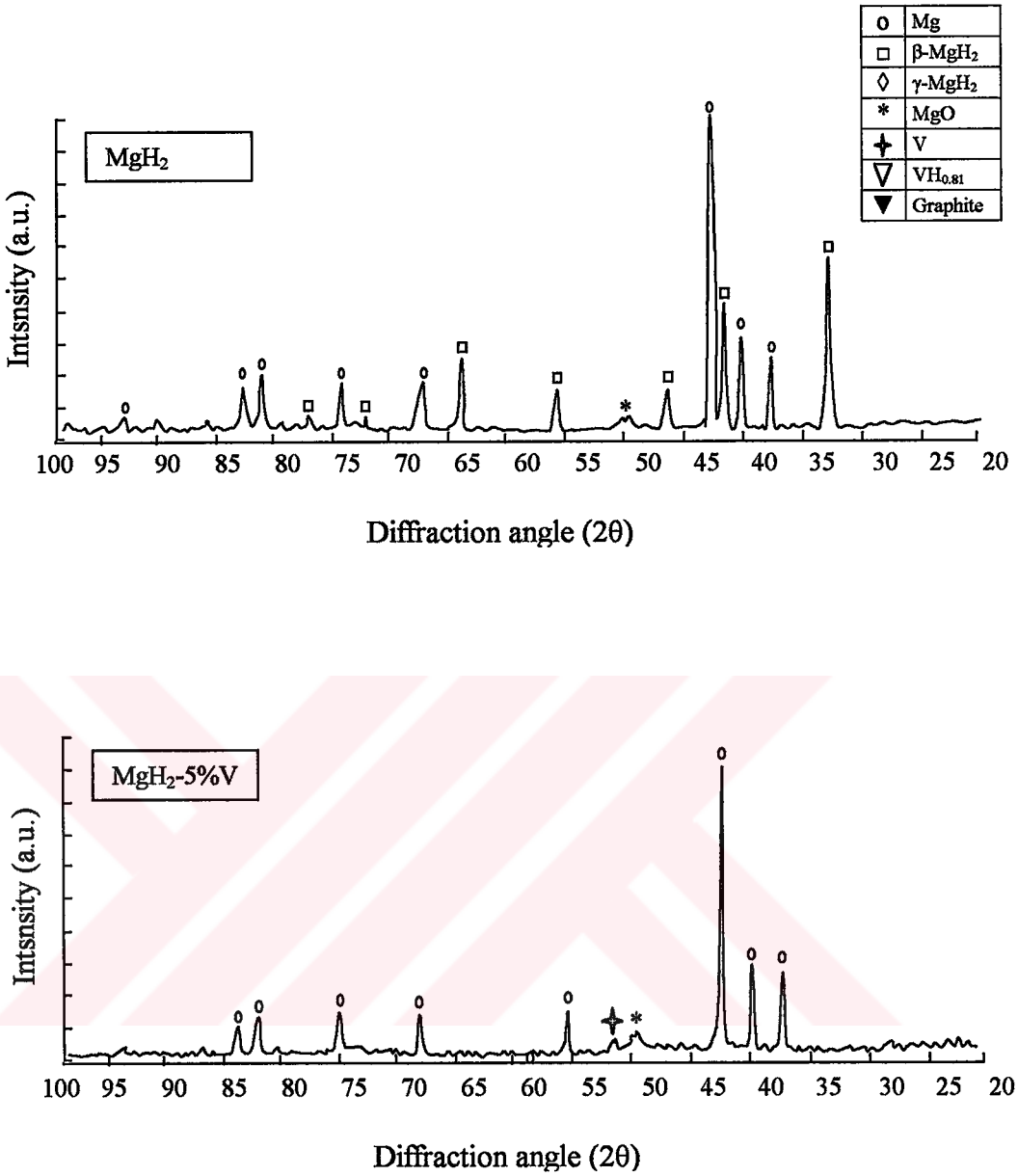

Figure 4.8. X-ray diffraction profiles of MgH_2-5%V and unmilled MgH_2 after sorption in dehydrided state.

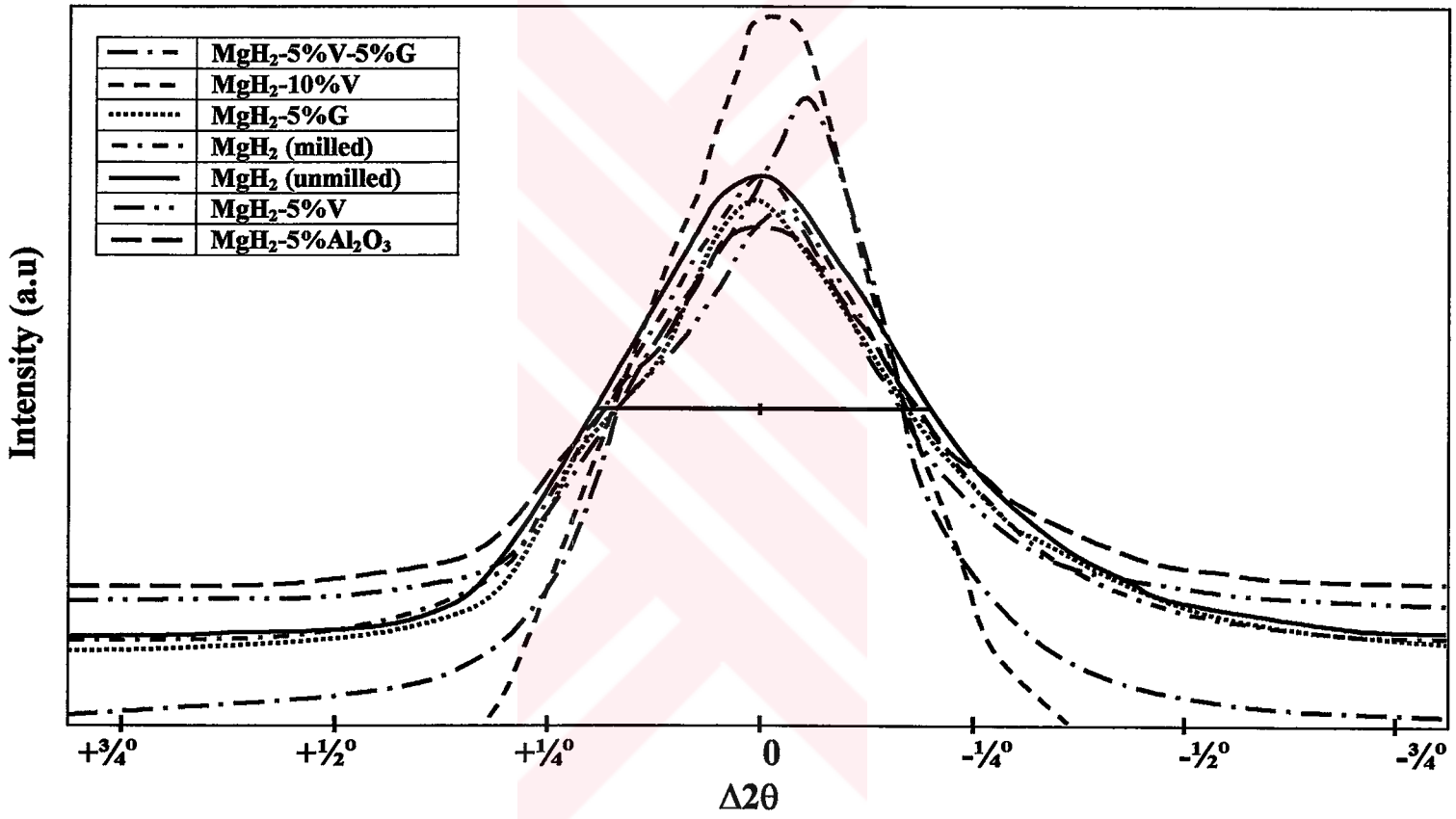

Figure 4.9. X-ray line broadening profiles of all milled systems that refers to (211) diffraction of MgH_2 after sorption. The peaks are moved and superimposed on their half maximum intensity. Unmilled MgH_2 is also included in the figure.

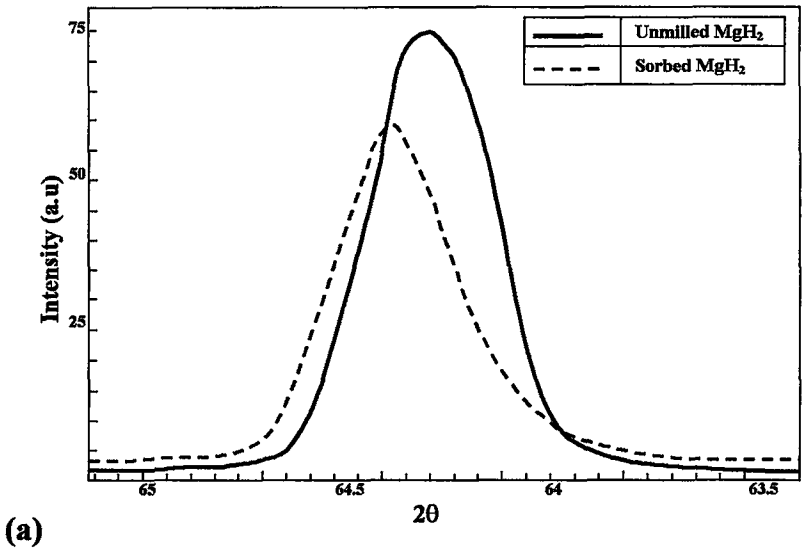

(a)

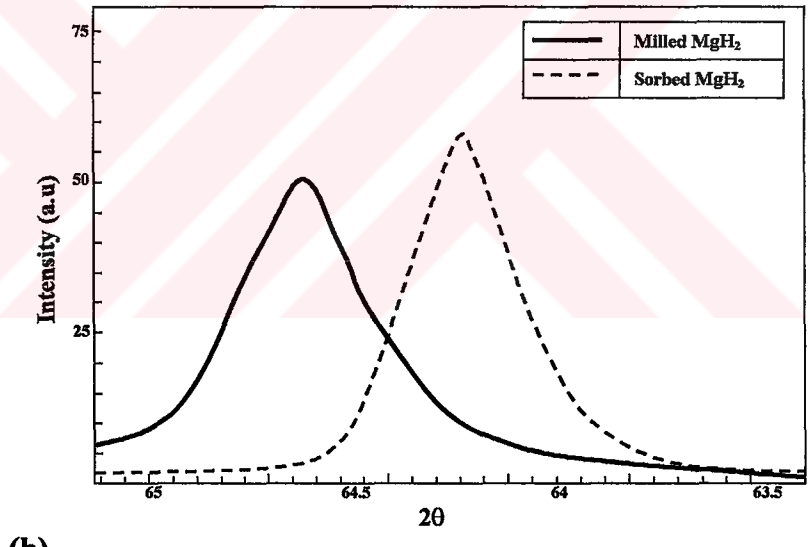

(b)

Figure 4.10. X-ray line broadenings of (211) diffraction of MgH_2 as milled and sorbed state together for each system; (a) unmilled MgH_2, (b) milled MgH_2, (c) MgH_2-5%V, (d) MgH_2-5%V-5%G, (e) MgH_2-5%G, (f) MgH_2-5%Al_2O_3, and (g) MgH_2-10%V.

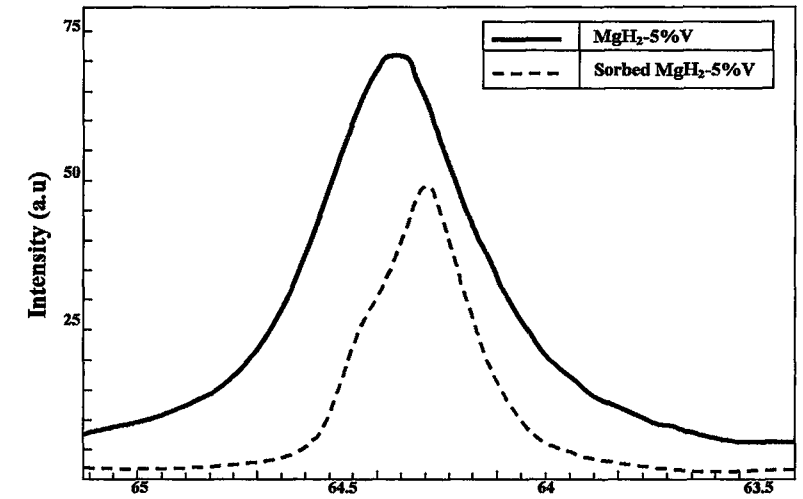

(c)

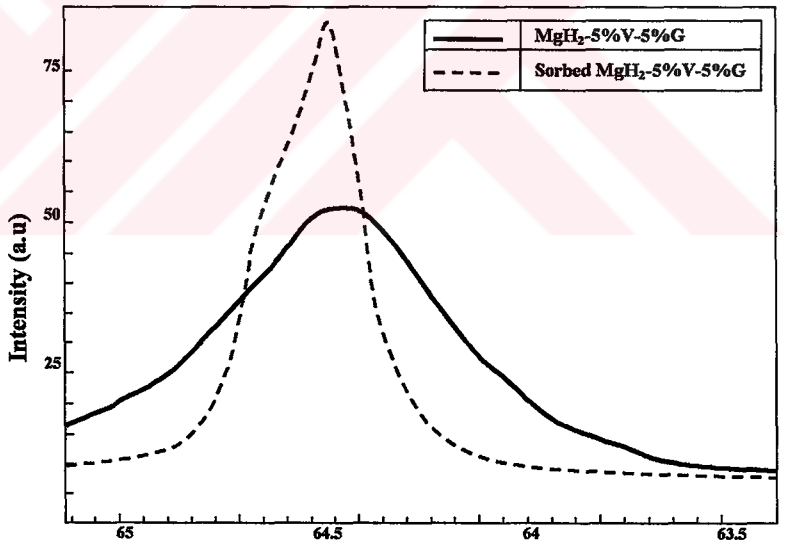

(d)

"Figure 4.10 (continued)"

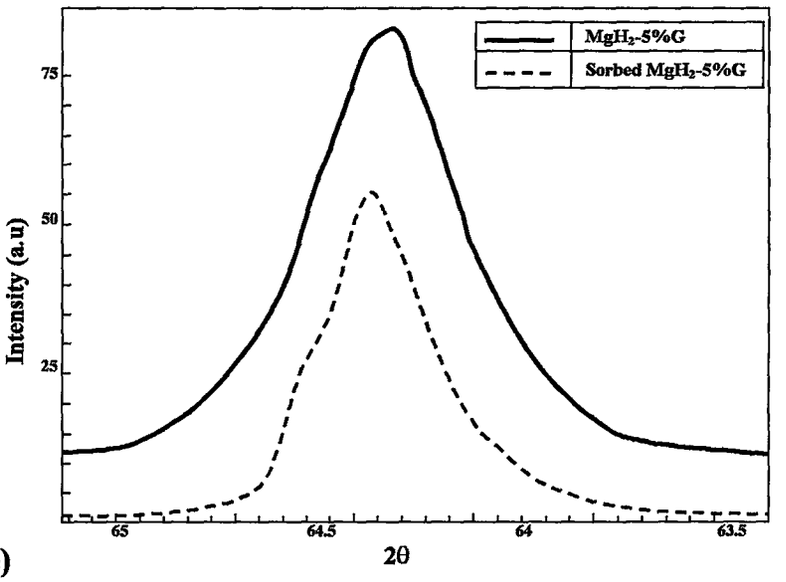

(e)

"Figure 4.10. (continued)"

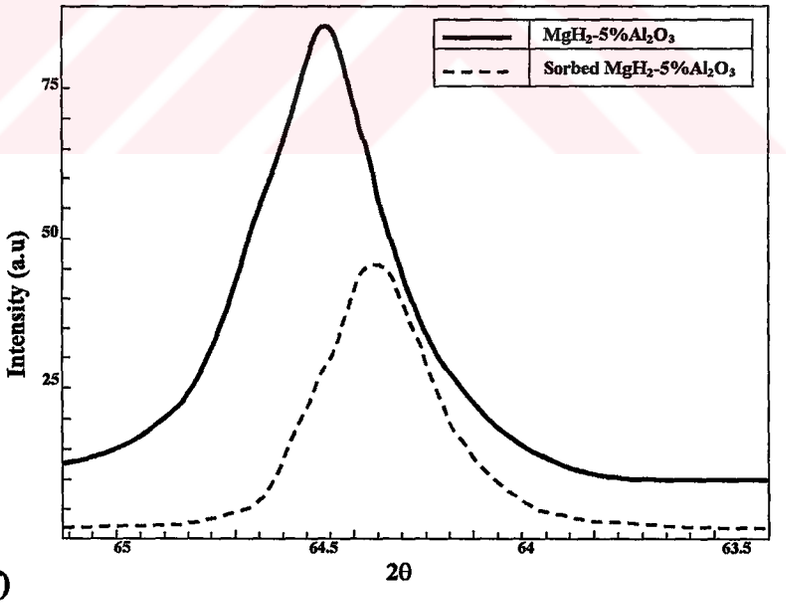

(f)

"Figure 4.10 (continued)"

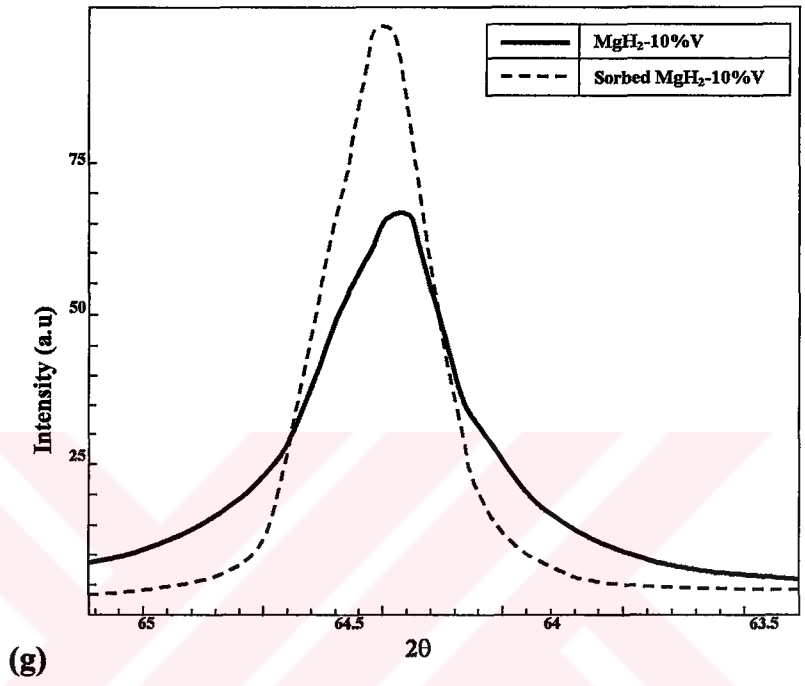

"Figure 4.10 (continued)"

It can be seen from the figures that the structural refinements obtained after milling is recovered to certain extend after sorption. This may be due to structural recovery after sorption. The highest recovery is observed in MgH_2-5%V-5%G, which has the lowest structural size after milling. It is followed by MgH_2-5%V, MgH_2-5%G and MgH_2-10%V respectively. The recovery is smallest for milled MgH_2 and MgH_2-5%Al_2O_3, which have the largest structural size after milling.

From these results it can be concluded that finer structure in milled state recovers more in sorption so that after sorption the structural size of the systems become closer to each other.

4.4. PRESSURE-COMPOSITION ISOTHERMS

Pressure-composition isotherms measured at 350°C (673°K) of MgH_2 milled with additives of graphite and V are given in Figure 4.11. Isotherms of MgH_2 before and after milling are also included in the figure. It is seen that isotherms have a pressure "plateau" with a slight slope.

Plateau pressures and hydrogen capacities of the system obtained from Figure 4.11 are reported in Table 4.3. The plateau pressures (P_p) reported in this table are obtained as average value since the plateau is not perfectly flat. The hydrogen capacity (C_t) refers to amount of hydrogen absorbed by the system at the end of the plateau. C_p refers to hydrogen capacity at P_p, i.e. average plateau pressure.

It can be seen from Table 4.3 that hydrogen storage capacity decreases with milling. The reason for this is not known but may be attributed to a partial oxidation of particles during milling.

Of the milled samples, MgH_2-5%G has the largest hydrogen capacity, 6.5 wt.% H. This is followed by MgH_2 milled without additive. The capacity is low with V addition.

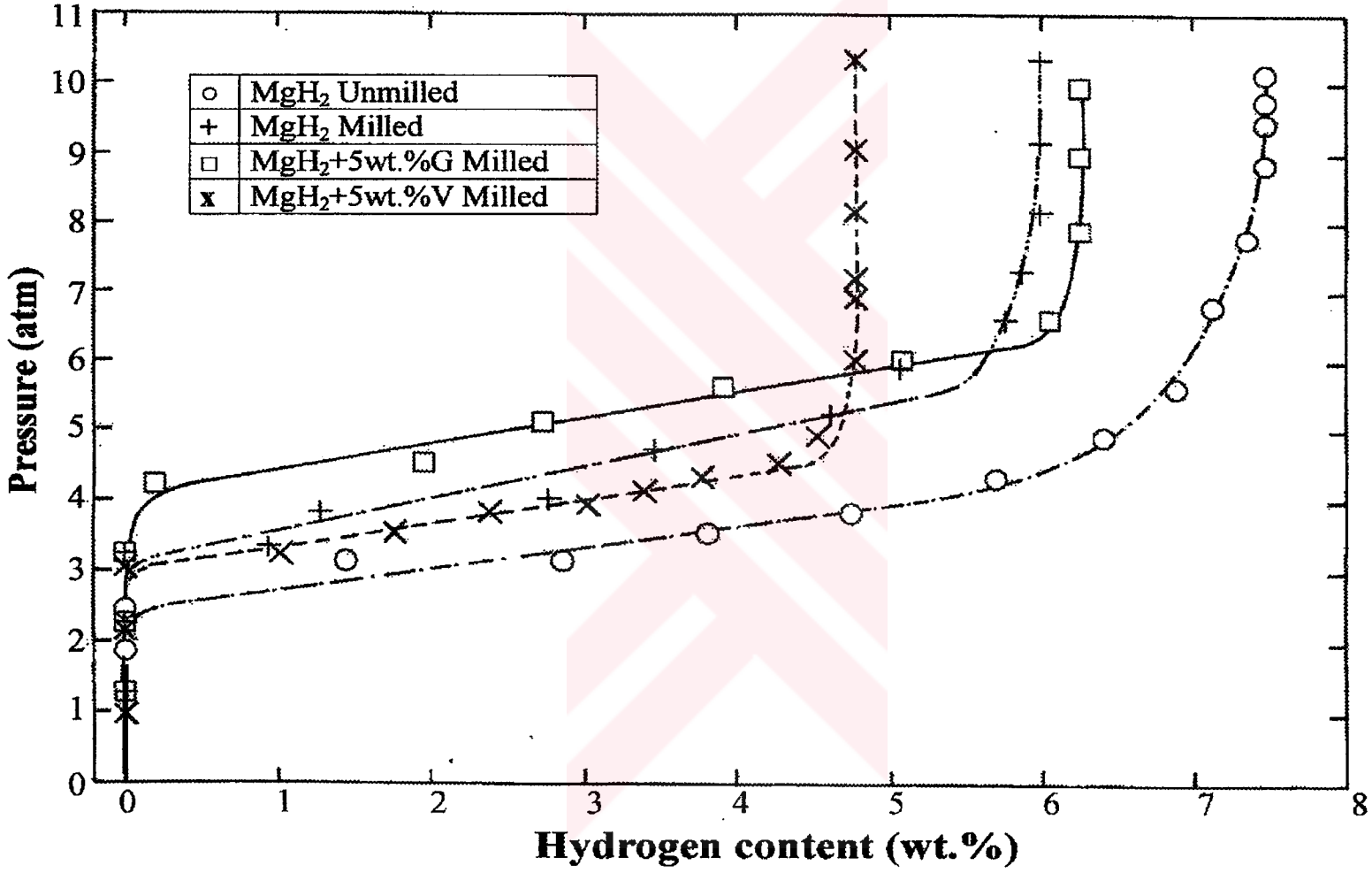

Figure 4.11 Pressure-composition isotherms (absorption at 350 °C) of unmilled and milled MgH_2.

Table 4.3. Plateau pressures (P_p) and hydrogen capacities (Ct, Cp) for MgH_2 with and without additives.

System	Ct (Wt%* H)	P_p (atm.)	C_p (Wt%* H)
Unmilled MgH_2	6.90	3.850	3.85
MgH_2 (without additive)	6.00	5.103	4.50
MgH_2+5%G	6.25	6.287	4.78
MgH_2+5%V	4.75	4.321	4.00
MgH_2+10%V	3.90	4.775	2.47

* Wt% is based on MgH_2 only, i.e. the additive is not taken into account.

Unmilled MgH_2 has a plateau pressure of 3.8 atm. There is an increase in plateau pressure in milled systems. For example, milled MgH_2 has a plateau pressure of 5.1 atm. The highest plateau pressure is measured for MgH_2-5%G system, i.e. 6.3 atm. With V addition the plateau pressure is less but still higher than unmilled magnesium.

P-C isotherms reported above are obtained at 350°C. In order to investigate the effect of temperature, the isotherms were also measured at 300°C (623°K) for milled MgH_2, MgH_2-5%V, MgH_2-10%V. An example is given in Figure 4.12, which refer to milled MgH_2.

From the isothermal graph it is possible to obtain the equilibrium pressure as a function of temperature. In fact, according to Van't Hoff equation.

$$\ln P_p = \Delta H/RT - \Delta S/R \qquad \textbf{(4.1)}$$

where P_p is the plateau pressure in atmospheres, ΔH is the enthalpy change, ΔS is the entropy change, R is the gas constant and T is the absolute temperature in °K. Thus in Van't Hoff plot there is a linear relationship between ln P with 1/T. Van't Hoff plot for milled MgH_2 is given in Figure 4.13.

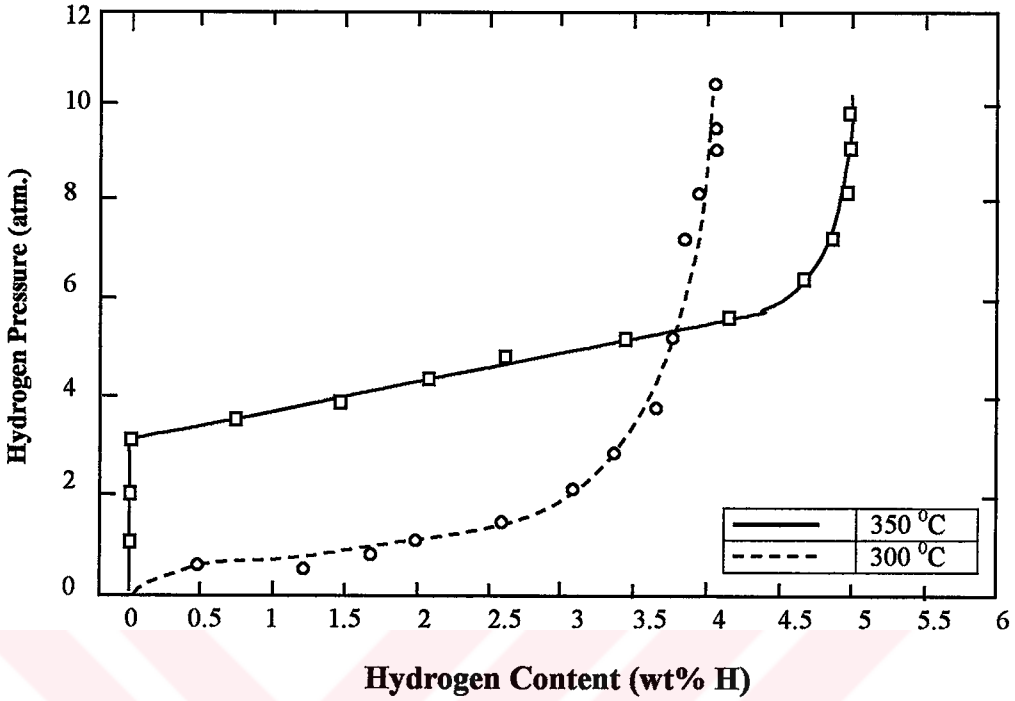

Figure 4.12 Pressure-composition isotherms (absorption) for milled MgH_2.

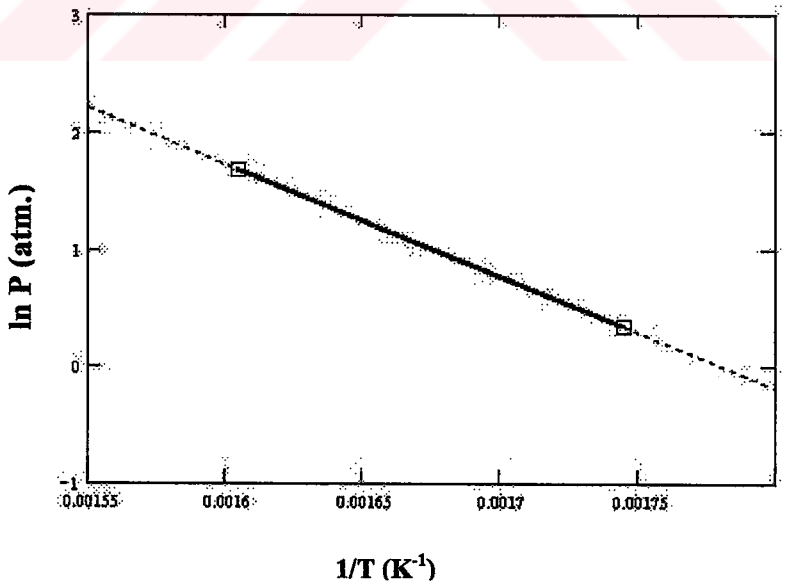

Figure 4.13. Van't Hoff plot for milled MgH_2.

Thermodynamic data calculated from such plots are given in Table 4.4.

Table 4.4. Thermodynamic data obtained from Van't Hoff Plot. Data from literature are also included in the table.

System	Equation	ΔH kcal mol^{-1}	ΔS cal $mol^{-1} K^{-1}$
MgH_2 (without additive)	ln P = 9614/T - 17.12	-19.1	-34.0
MgH_2+5%V	ln P = 9900/T - 17.24	-19.6	-34.2
MgH_2+10%V	ln P = 9671/T - 17.13	-19.2	-34.0
MgH_2 (Mueller et al., 1968) (400 °C)		-17.4±1.0	-31±2
MgH_2 (Douglas et al.,1983) (400 °C)		-18.7±1.0	-
MgH_2 (Bogdanovic et al, 1999) (300-450 °C)		-17.8	-32.2

Data reported in Table 4.4 are consistent with those reported in the literature for MgH_2 (Mueller et al, 1968; Douglas et al, 1983; Bogdanovic et al, 1999).

Using Van't Hoff equation it is possible to calculate plateau pressures for different temperatures. Values predicted for MgH_2 are given in Table 4.5.

Table 4.5. Calculated plateau pressures (P) of milled MgH_2 for different temperatures.

T (^{0}C)	T (K)	P (atm)
20	293	$1.53x10^{-7}$
50	323	$3.22x10^{-6}$
100	373	$1.74x10^{-4}$
150	423	$3.67x10^{-3}$
200	473	$4.05x10^{-2}$
250	523	$2.83x10^{-1}$ (0.41*)
300	573	1,41 (1.83*)
350	623	5,41 (6.4*)
400	673	17,02

* Values reported in hydride database, hydparc.ca.sandia.gov.

4.4.1. Effect of Cycling

Isotherms recorded for the initial cycles are somewhat different than those reported above. The isotherms at initial cycles for MgH_2-5%G are given in Figure 4.14.a. There is a significant drop in absorbed hydrogen content and a slight increase in plateau pressure in the first three cycles. However, p-c isotherm at fourth cycle is the same as the third. The case for MgH_2-5%V is the same, i.e. isotherms are nearly the same after third cycle, Figure 4.14.b, for which measurements were carried out only for forth, fifth and sixth cycles. Therefore, it can be concluded that pressure-composition isotherms are stabilized after the third cycle.

4.5. SORPTION KINETICS

Initial cycles for absorption and desorption is given in Figure 4.15 (a) and (b). It can be seen from the curves that initial absorption and desorption rate change with cycling, and are not therefore reproducible. For this reason kinetic data were measured after three absorption-desorption cycles.

Absorption and desorption curves for MgH_2 milled with additives of Al_2O_3, V and Graphite, are reported in Figure 4.16 (a) and (b). The curves of unmilled and milled MgH_2 are also included in the figure. Absorption curves were obtained at 350°C (623°K) and under initial hydrogen pressure of 10atm. Desorption measurements were carried out under initial hydrogen pressure of 1atm and temperature of 400°C (673°K).

All milled systems give similar absorption and desorption curves. Hydrogen capacities and time needed to reach these capacities are given in Table 4.6 and 4.7, for absorption and desorption, respectively. C_a and C_d values reported in the tables refer to the half values of the amount of hydrogen absorbed and desorbed respectively within 7200 seconds. Time values t_{Ca} and t_{Cb} are also included in the tables (time needed to reach the C_a and C_b, respectively).

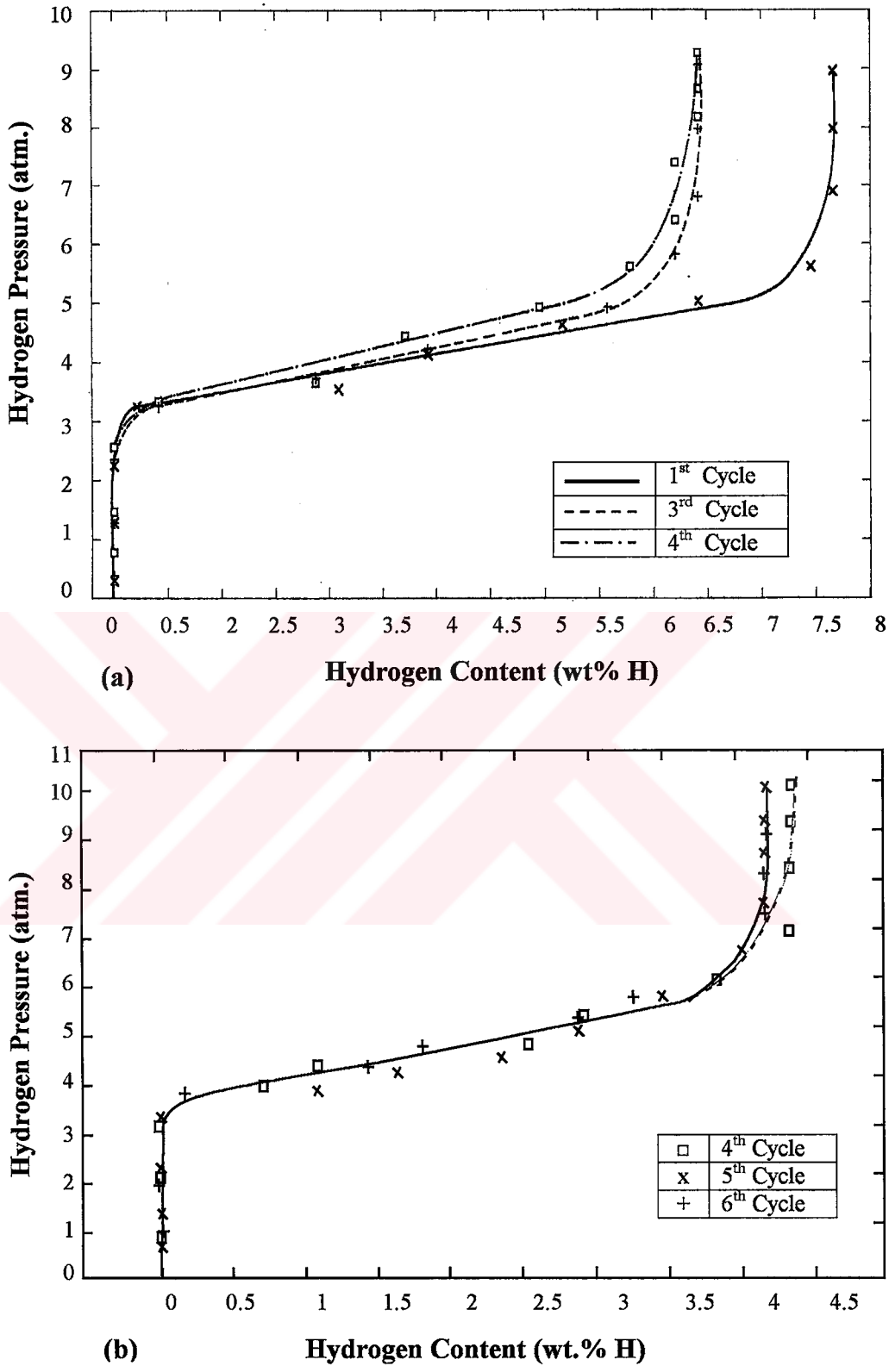

Figure 4.14 Pressure-composition isotherms of MgH_2-5%G; (a) for the first four cycles, (b) for the fourth to sixth cycles.

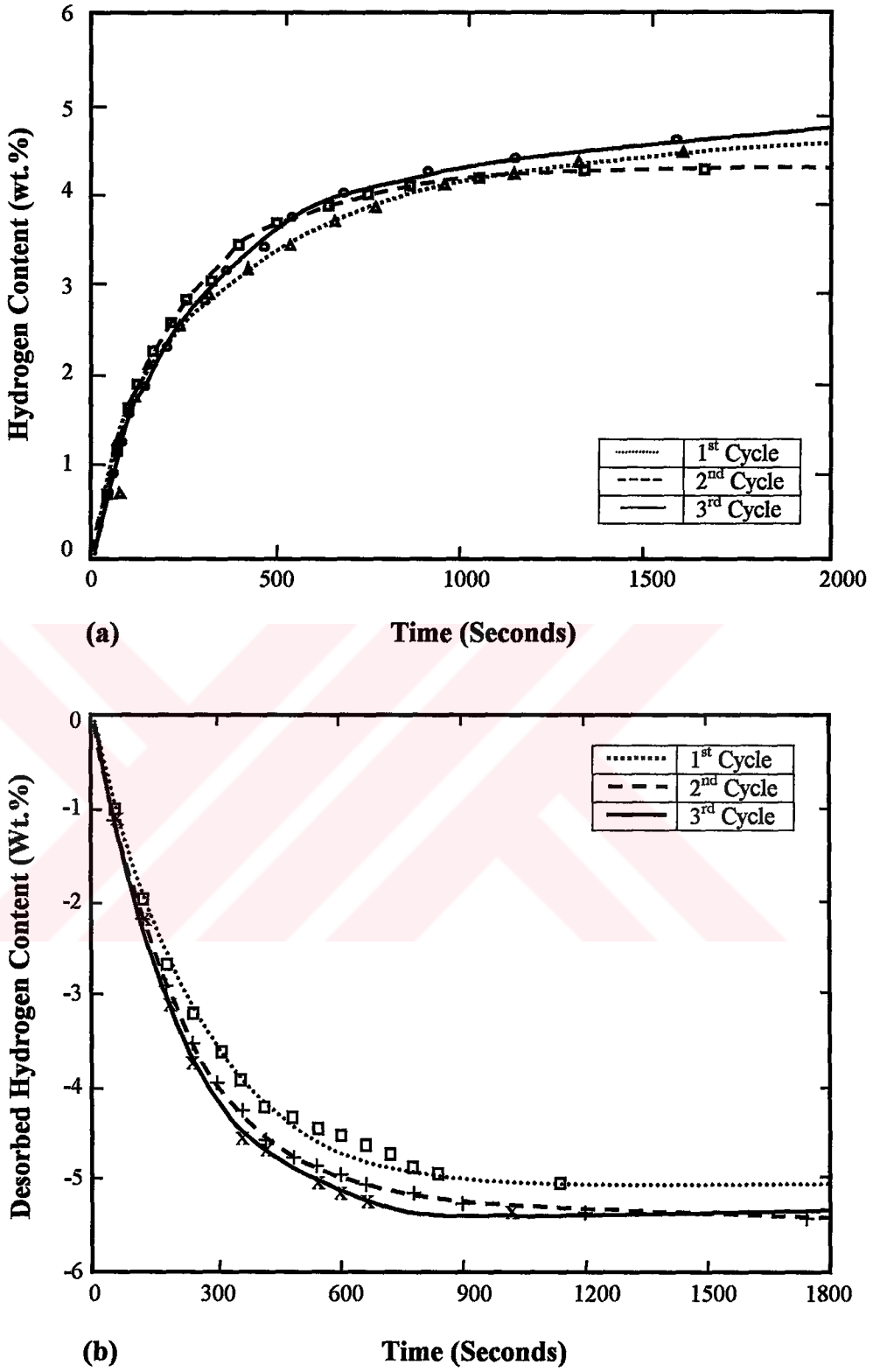

Figure 4.15. Initial sorption curves; (a) absorption of MgH_2-5%G, and (b) desorption of MgH_2-5%V.

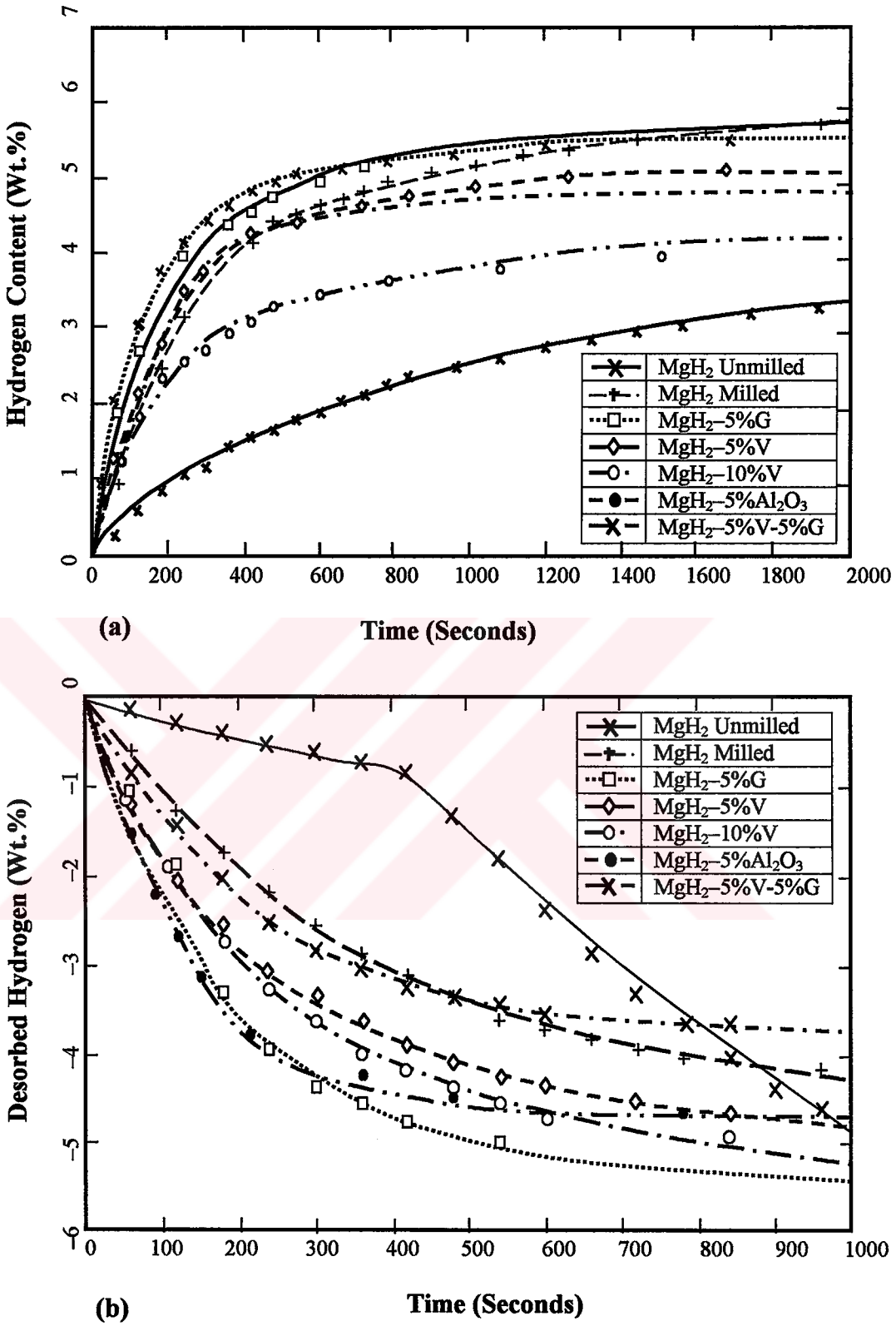

Figure 4.16 Absorption (a), and desorption (b) curves. Absorption curve is obtained at 350 °C under 10-atm initial hydrogen pressure. Desorption curve is obtained 400 °C under initial hydrogen pressure of 1-atm.

t_{Cm} values reported in the tables are based on theoretical capacity of MgH_2, i.e. 7.6 wt% H. They refer to the time needed to charge or discharge the half capacity, i.e. 3.8 wt% H.

Table 4.6. Hydrogen absorption content (C_a), absorption times t_{Ca} and t_{Cm} for MgH_2 with and without additives.

System	C_a (Wt.%* H)	t_{Ca} (Seconds)	t_{Cm} (Seconds)
Unmilled MgH_2	2.45	323	2700
Milled MgH_2	3.05	254	331
MgH_2+5%G	2.90	128	181
MgH_2+5%V	2.80	181	305
MgH_2+10%V	2.10	150	1000
MgH_2+5%V+5%G	2.85	106	181
MgH_2+5%Al_2O_3	2.45	134	335

Wt.%* is based on MgH_2 only, i.e. the amount of additive is not taken into account.

Table 4.7. Hydrogen desorption content (C_d), desorption times t_{Cd} and t_{Cm} for MgH_2 with and without additives.

System	C_d (wt% H)	t_{Cd} (Seconds)	t_{Cm} (Seconds)
Unmilled MgH_2	2.85	664	818
Milled MgH_2	2.25	257	672
MgH_2+5%G	2.5	150	236
MgH_2+5%V	2.39	169	418
MgH_2+10%V	2.46	162	336
MgH_2+5%V+5%V	1.82	162	-
MgH_2+5%Al_2O_3	2.32	94	218

Wt.%* is based on MgH_2 only, i.e. the amount of additive is not taken into account.

Data in Table 4.6 shows that in terms of absorption, MgH_2-5%G has the fastest rate (MgH_2-5%V-5%G is also as fast). This system absorbs 2.90 wt.% H within 128 seconds. It is followed by MgH_2-5%V. The absorption rate is slowest in MgH_2-5%Al_2O_3 and MgH_2-10%V. The case is similar when t_{Cm} values are used as basis.

Of the milled systems, desorption rates of MgH_2-5%Al_2O_3 and MgH_2-5%G is the highest, Table 4.7. The values are 2.32 wt% H within 94 seconds and 2.5 wt% H within 150 seconds for MgH_2-5% Al_2O_3 and MgH_2-5%G respectively. They are followed by MgH_2-V systems.

Therefore, it can be concluded that of the systems investigated in this work graphite is most influential when absorption and desorption rates are considered together.

Absorption and desorption curves reported above are obtained at 350°C and 400°C respectively. In order to see the effect of temperature, these measurements were also performed at a lower temperature. Therefore, the experiments were repeated at 300°C and 350°C for absorption and desorption, respectively. An example is given in Figure 4.17 for milled MgH_2. As can be seen from the figures, the rate of absorption and desorption changes with temperature.

4.6 ANALYSIS OF SORPTION KINETICS

The analysis of sorption kinetics are complicated since it depends on various steps including physisorption and chemisorption, surface penetration and diffusion of hydrogen atoms and hydride formation and decomposition as given in Chapter II for absorption and desorption separately. Of these steps the slowest one is the rate-determining step.

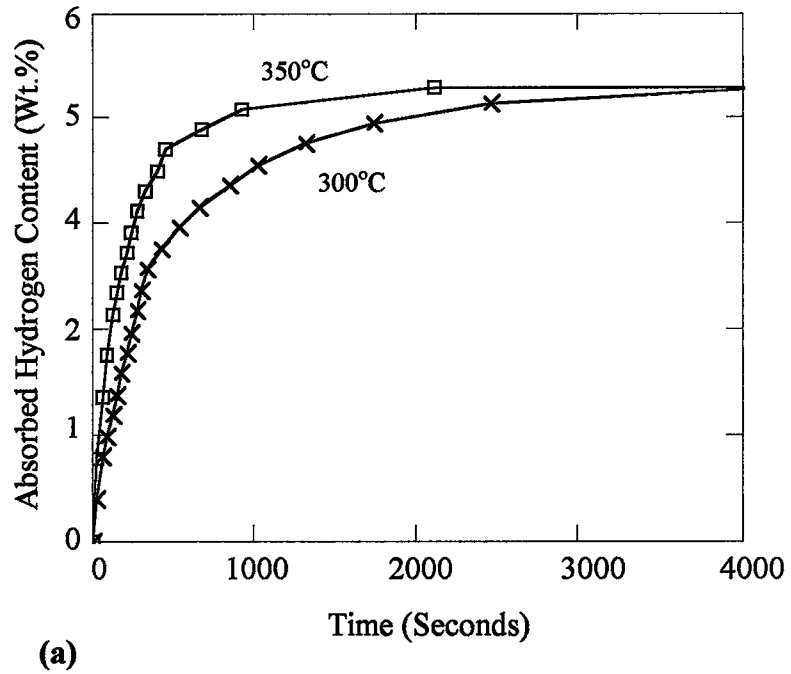

(a)

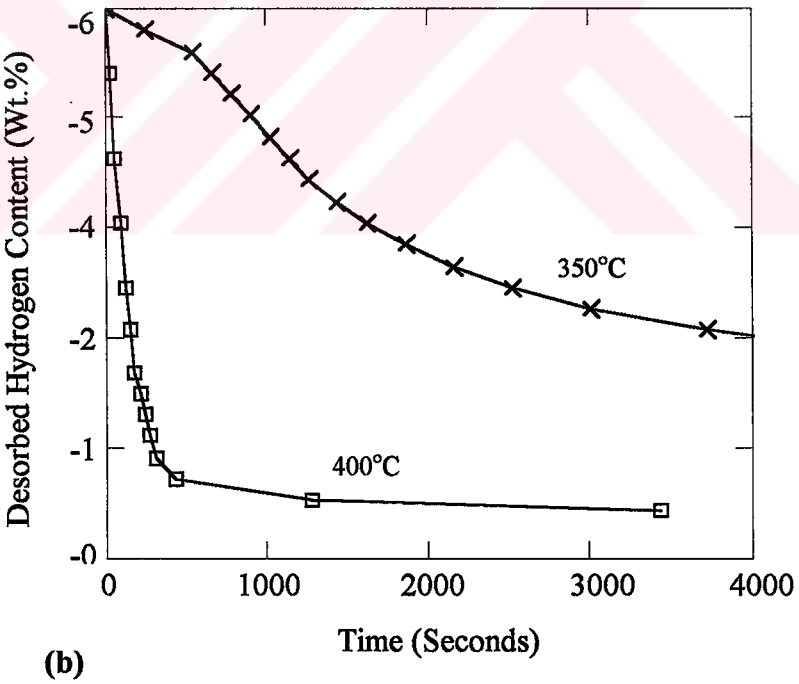

(b)

Figure 4.17. (a) Absorption and **(b)** desorption curves at two different temperatures for milled MgH_2.

In this study simplified macro analysis are carried out based on i) nucleation and growth model (Christian, 1975; Rudman, 1983; Huot et al., 1999), and ii) shrinking core model (Sharp, 1966; Hancock, 1972; Stander, 1977, Osovizki et al., 1996; Martin et al., 1996).

According to nucleation and growth model, i.e. Johnson-Mehl-Avrami equation (Christian, 1975), transformed fraction, α, is given by

$$\alpha = 1 - \exp(-K_{ng}.t)^n \qquad \textbf{4.2}$$

where K_{ng} is the rate constant, t is the time in seconds, and n is the reaction rate order.

According to shrinking core model (Osovizky et al., 1996) transformed fraction, α, is given by

$$*\alpha = 1 - (1 - ut/r)^3 \qquad \textbf{4.3}$$

where u is the constant velocity of shrinkage, and r is the radius of the spherical particle. In this equation u/r designates the reaction rate constant for shrinking core model, K_{sc}.

The Equations 4.2 and 4.3 can be rearranged into the following forms,

$$\ln(-\ln(1-\alpha)) = n \ln K_{ng} + n \ln t \qquad \textbf{4.4}$$

$$\ln(1 - (1-\alpha)^{1/3}) = \ln K_{sc} + \ln t \qquad \textbf{4.5}$$

---

* The original equation for reacted fraction $\alpha(t)$ for a parallelepiped of dimensions a, b, c, shrinking at a constant velocity u is given by (Sharp et al., 1966, Hancock et al., 1972)

$\alpha(t) = 2ut(1/a + 1/b + 1/c) - 4(ut)^2 (1/ab + 1/bc + 1/ac) + 8(ut)^3 / abc$

This equation can be rearranged to Equation 4.3 for a spherical particle of radius r, where a=b=c≡2r (Bronfman et al., 1991)

Thus, from these equations rate constants can easily be determined.

Temperature dependence of rate constant K, whether in the form of K_{ng} or K_{sc}, follows Arrhenius equation (Christian, 1975):

$$K = K_o \exp(-Q/RT) \qquad \textbf{4.6}$$

where Q is the activation energy, R is the rate constant, T is the temperature in °K. Thus,

$$\ln K = \ln K_o - Q/R\ 1/T \qquad \textbf{4.7}$$

Data for desorption for milled MgH_2 arranged according to Equation 4.2 and 4.3 are given in Figure 4.18, i.e. fraction transformed versus time plot. In order to determine reaction rate constants, Equation 4.4 and 4.5 are plotted and lines were fitted with least square analysis. An example of such plots is also reported in Figure 4.19 (a) and (b) for milled MgH_2. Measured rate constants are given in Table 4.8 for desorption.

In order to determine desorption activation energies, K values derived from Equation 4.7 are plotted against 1/T. An example for such plots is given for milled MgH_2 in Figure 4.19 (c) and (d).

Activation energies calculated for desorption are given in Table 4.8. For nucleation and growth model, "n" values measured from the line fitting are also included in the table.

From Table 4.8, MgH_2-5%Al_2O_3 has the lowest desorption activation energy, 99.3 kJ/mole. This is followed by vanadium and graphite systems. These results are consistent with the observed desorption rates (Table 4.7).

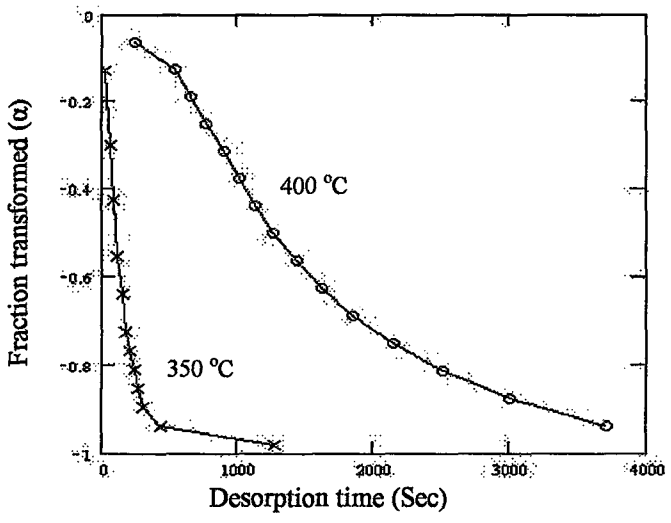

Figure 4.18. Fraction transformed versus time plots for milled MgH_2 at temperatures of 400 °C and 350 °C.

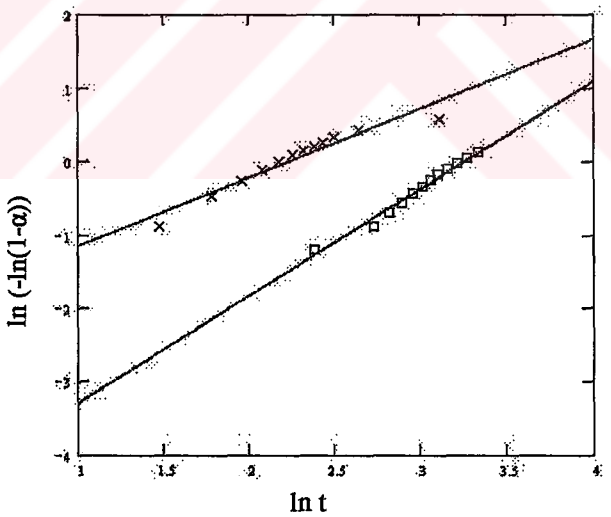

(a)

Figure 4.19. Plots of nucleation and growth (a), and shrinking core (b) equations. Least square fitting of Arrhenius equation by using calculated reaction rates; (c) for nucleation and growth, and (d) for shrinking core model.

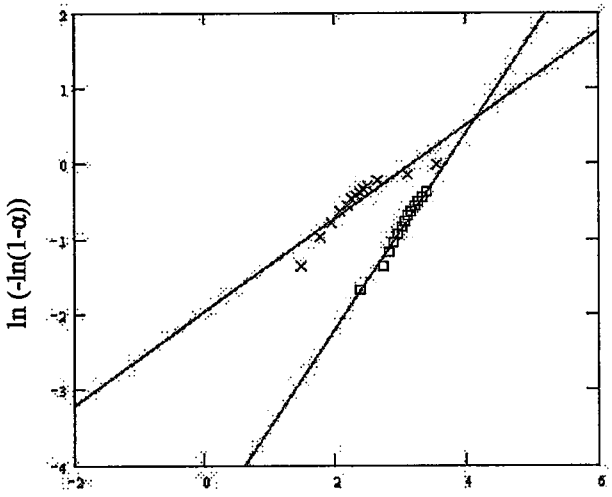

(b)

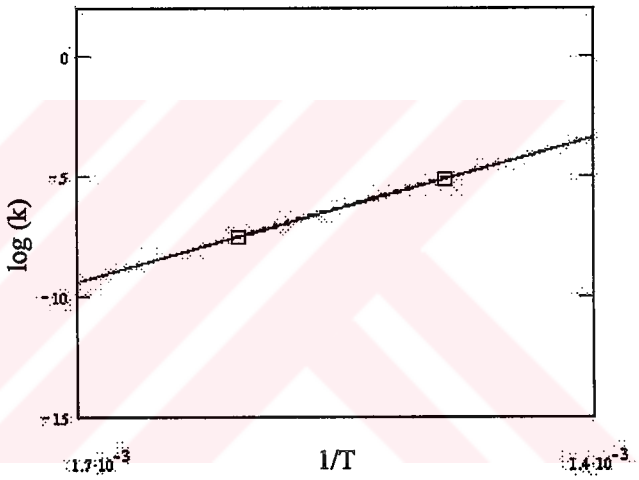

(c)

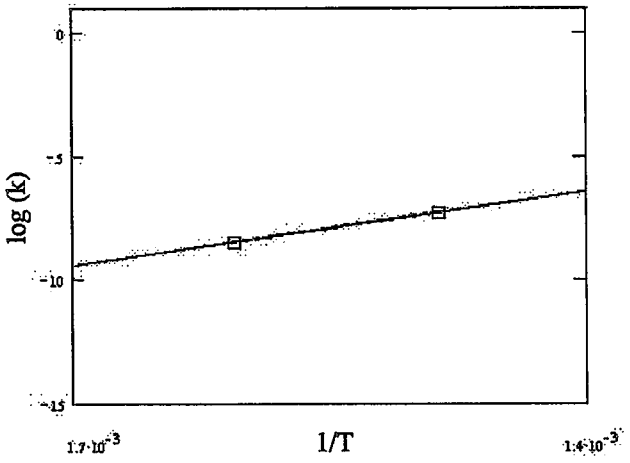

(d)

"Figure 4.19. (continued)"

Table 4.8. Kinetics data for desorption. "Q" refer to the calculated activation energies, the subscripts "ng" and "sc" denotes nucleation and growth and shrinking core models respectively. "n" refers the measured reaction rate order in nucleation and growth model for desorption curves of selected systems.

System	n	Q_{ng} (kJ/mole)	Q_{sc} (kJ/mole)
MgH_2	1.20	164.9	139.3
MgH_2-5% Al_2O_3	1.16	137.3	99.3
MgH_2-5% V	1.35	150.5	95.4
MgH_2-5% G	1.23	164.6	166.0

Similar values have also been reported in the literature. For instance, for milled MgH_2 Schulz et al., (1999) reported activation energy of 120 $KJ.mol^{-1}$ (at 623K). For MgH_2-10%V Liang et al., (2000a, b) found that the activation energy for desorption is 98.7 $kJ.mol^{-1}$.

Similar evaluations were also carried out for absorption. Results of analysis are reported in Table 4.9.

Table 4.9. Kinetics data for absorption. "Q" refer to the calculated activation energies, the subscripts "ng" and "sc" denotes nucleation and growth and shrinking core models respectively. "n" refers the measured reaction rate order in nucleation and growth model for desorption curves of selected systems.

System	n	Q_{ng} (kJ/mole)	Q_{sc} (kJ/mole)
MgH_2	0.79	51.9	-
MgH_2-5% Al_2O_3	0.83	35.1	46.0
MgH_2-5% V	0.77	33.6	14.9
MgH_2-5% G	0.77	33.3	-

Of the milled systems graphite system seem to have lower absorption activation energy, Table 4.9. It is followed by MgH_2-5%V. These results are consistent with the observed absorption rates (Table 4.6).

For nucleation and growth model the average reaction rate orders, n, measured for desorption and absorption are 1.24 and 0.79 respectively. The value for desorption may be interpreted as the growth of Mg particles into MgH_2 that have an appreciable initial volume. For absorption this may be interpreted as an early stage precipitation of hydrogen atoms on dislocations in diffusion controlled growth of hydride phase. (Christian, 1975)

Comparisons of data in Table 4.8 and 4.9 shows that desorption activation energies are greater than that of absorption. This is also the case in the literature. For instance, the absorption activation energy of pure Mg and desorption activation energy of pure MgH_2 is given as 231.0 kJ/mol (Selvam et al., 1986) and 289±5 kJ/mol (Selvam et al., 1988) respectively.

This result seems to be confusing as hydrogen diffusivities in β-MgH_2 and α-Mg are compared. San-Martin and Manchester (1988) reported that hydrogen diffusion through β phase is slower ($2.5x10^{-13}$ at 350°C) than that of α-Mg ($1.5x10^{-5}$ at 400°C). Therefore, it can be expected that in absorption once the hydride phase is formed and covers the Mg particles, hydrogen diffusion through hydride phase would be difficult. However, in desorption MgH_2 particles are covered with Mg and diffusion through Mg is easier as compared to absorption. This may be interpreted as early nucleation and growth in desorption. While in absorption the nucleation and growth of Mg is low.

4.7. CONCLUDING REMARKS

The results reported above show that the highest hydrogen storage capacity is achieved with graphite addition, 6.25 wt.% H. With graphite addition magnesium can absorb and desorb 4.2 wt.% hydrogen within 300 seconds.

This may be related to the highest structural refinement achieved with graphite addition after milling. But it has to be considered that during sorption powders are exposed to high temperatures up to 400°C, thus the "as-milled" structural refinement is not preserved. The results show that after sorption the structure of the systems recovers in a way that highest recovery is obtained in finest structure after milling. After sorption the systems approach one another in terms of structural size.

Although graphite system has lost the advantage of finest structure after milling it has the fast sorption kinetics and capacity as given above. This indicates that the degree of structural refinement after sorption is not the only criteria for fast kinetics.

It should be pointed out that if the sorption temperatures could be decreased the structural recovery might be minimized, so that better sorption kinetics may be obtained.

In all measurements sorption characteristics show deviations for the initial cycles. It can be due to the structural changes such as structural recovery and stress relaxation during initial cycles. It is shown that for all systems the deviations are minimized after third cycle. This may be due to the stabilization of structural changes.

CHAPTER V

CONCLUSION

In this study it is aimed to improve hydriding/dehydriding characteristics of magnesium. For this purpose magnesium is mechanically milled with several additives, namely Al_2O_3, V and graphite, under argon atmosphere. The structural study shows that:

1) The most efficient refinement is achieved with graphite addition, MgH_2-5%V-5%G and MgH_2-5%G. It is followed by MgH_2-5%V, MgH_2-10%V and. MgH_2-5%Al_2O_3

2) The sequence of refinement in "as-milled" state changes after sorption. This can be attributed to the structural recovery due to exposure to relatively high temperatures during sorption. In as-sorbed state finest structure is obtained in MgH_2-5%Al_2O_3. It is followed by MgH_2-10%V, MgH_2-5%G and MgH_2-5%V-5%G.

Measurement of sorption properties of the systems within a temperature range of 300-400°C show that

1) A capacity of 6.25 wt.% H is reached in MgH_2-5%G, which is the highest capacity observed in the systems. This corresponds to a hydrogen storage capacity of 450 L hydrogen per kg of powder at STP.

2) The plateau pressures of the systems are in the range of 3-6 atm.

Measurements on sorption kinetics indicates that:

1) The highest sorption rate is achieved in MgH_2-5%G. It can absorb and desorbs 4.2 wt.% H within 300 seconds respectively. This corresponds to a sorbing rate of 70 L/min per kg of powder at STP.

The storage capacity and sorption rate reported above are quite acceptable for practical applications. However, temperatures within which these values are obtained are rather high. Therefore, further work is necessary so as to reduce the working temperature while maintaining the storage capacity as well as the fast sorption rate.

REFERENCES

Akiyama T., Isogai H., Yagi J., 1997, J. Alloys and Compounds, **252**, L1-L4.

Awasthi K., Kamalakaran R., Singh A.K., Srivastava O.N., 2002, Int. J. Hydrogen Energy, **27**, 425-432.

Bastide J.P., Bonnetot B., Letoffe J.M., Claudy P., 1980, Mat. Res. Bull., **15**, 1215-1224.

Baybörü E., Master Thesis-METU, 2001.

Bernhardt B., Bohmhammel K., 2002, Thermochimica Acta, **382**, 249-254.

Bobet J.L., Akiba E., Darriet B., 2001, Int. J. Hydrogen Energy, **26**, 493-501.

Bobet J-L., Akiba E., Nakamura Y., Darriet B., 2000, Int. J. Hydrogen Energy, **25**, 987-996.

Bogdanovic B., Ritter A., Spliethoff B., Strassburger K., 1995, Int. J. Hydrogen Energy, **20**, 811-822.

Bognanovic B., Bohmhammel K., Christ B., Reiser A., Schlichte K., Vehlen R., Wolf U., 1999, J. Alloys and Comp, **282**, 84-92.

Bohmhammel K., Wolf U., Wolf G., Königsberger E., 1999, Thermochicmica Acta, **337**, 195-199.

Bohmhammel K., Christ B., Wolf U., 1998, Thermochicmica Acta, **310**, 167-171.

Bolcich J.C., Yawny A.A., Corso H.L., Peretti H.A., Ayala C.O., 1994, Int. J. Hydrogen Energy, **19**, 605-609.

Bouaricha S., Huot J., Guay D., Schulz R., 2002, Int. J. Hydrogen Energy, **27**, 909-913.

Bouaricha S., Dodelet J.P., Guay D., Huot J., Schulz R., 2001a, J. Alloys and Compounds, **325**, 245-251.

Bouaricha S., Dodelet J.P., Guay D., Huot J., Schulz R., 2001b, J. Materials Research **16 (10)**, 2893-2905.

Boureau G., Kleppa O.J., Antoniu P.D., 1979, J. Solid St. Chem., **28**, 223.

Bronfman N., Bloch J., Mintz M.H., Sarussi D., Jacob I., 1991, J. Alloys and Compounds, **177**, 183.

Cao P., Lu L., Lai M.O., 2001, Materials Research Bulletin, **36**, 981-988.

Choi W-K., Tanaka T., Morikawa T., Inoue H., Iwakura C., 2000, Int. J. Alloys and Compounds, **302**, 82-86.

Cui N., Luo J.L., Chuang K.T., 2000, J. Alloys and Compounds, **302**, 218-226.

Cui N., He P., Luo J.L., 1999, Acta Metallurgica, **47-14**, 3737-3743.

Dantzer P., 1997, Topics in Applied Physics, **73**, 279-340.

Dehouche Z., Klassen T., Oelerich W., Goyette J., Bose T.K., Schulz R., 2002, J. Alloys and Compounds, **347**, 319-323.

Dehouche Z., Djaozandry, Huot J., Boily S., Goyette J., Bose T.K., Schulz R., 2000, J. Alloys and Compounds, **305**, 264-271.

Douglas G.I., Derek O.N., 1983, J. Materials Science, **18**, 321-347.

Douglass D.L., 1975, Metall. Trans., **6A**, 2179.

Fernandez J.F., Sanchez C.R., 2002, J Alloys and Compounds, **340**, 189-198.

Flanagan T.B., Bowerman B.S., Biehl G.E., 1980, Scripta Metallurgica, **14**, 443-447.

Flangan T.B., 1978, "Hydride s for Energy Storage", (Pergamon Press, Oxford), **43**, 135.S

Gennari F.C., Castro F.J., Urretavizcaya, 2001, J. Alloys and Compounds, **321**, 46-53.

Genossar J., Rudman P.S., 1979, Phys. Chem., **116**, 215.

Groll M., Isselhorst A., Wierse M., 1994, Int. J. Hydrogen Energy, **19**, 507-515.

Gross K.J., Thomas G.J., Jensen C.M., 2002, J. Alloys and Compounds, **330-332**, 683-690.

Hancock J.D., Sharp J.H., 1972, J. Am. Ceram. Soc., **55**, 74.

Hjort P., Krozer A., Kasemo B., 1996, J. Alloys and Compounds, **237**, 74-80.

Huot J., Pelletier J.F., Liang G., Sutton M., Schulz R., 2002, J. Alloys and Compounds, **330-332**, 727-731.

Huot J., Liang G., Boily S., Schulz R., Van Neste A., Schulz R., 1999, J. Alloys and Compounds, **293-295**, 495-500.

Huot J., Boily S., Akiba E., Schulz R., 1998a, J. Alloys and Compounds, **280**, 306-309.

Huot J., Bouaricha S., Boily S., Dodelet J.P., Guay D., Schulz R., 1998b, J. Alloys and Compounds, **266**, 307-310.

Huot J., Akiba E., Takada T., 1995, J. Alloys and Compounds, **231**, 815-819.

Imamura H., Tabata S., Shigetomi N., Takesue Y., Sakata Y., 2002, **330-332**, 579-583.

Imamura H., Takesue Y., Akimoto T., Tabata S., 1999, J. Alloys and Compounds, **293-295**, 564-568.

Imamura H., Sakasaki N., Kajii Y., 1996, J Alloys and Compounds, **232**, 218-223.

Imamura H., Sakasaki N., 1995, J Alloys and Compounds, **231**, 810-814.

Inui H., Yamamoto T., Hirota M., Yamaguchi M., 2002, J. Alloys and Compounds, **330-332**, 117-124.

Ivey D.G., Northwood D.O., 1983, J. Materials Science, **18**, 321.

Jacobson N., Tegner B., Schröder E., Hyldgaard P., Lundqvist B.I., 2002, 24, 273-277.

Jain I.P., Vijav Y.K., 1987, Progress in Hydrogen Energy, 111-122.

Kadir K., Tanaka H., Sakai T., Uehara I., 2000, J. Alloys and Compounds, **302**, 112-117.

Kadir K., Tanaka H., Sakai T., Uehara I., 1999, J. Alloys and Compounds, **289**, 66-70.

Kapischke J., Hapke J., 1998, Exp. Thermal and Fluid Science, **18**, 70-81.

Karty A., Grunzweig-Genossar J., Rudman P.S., 1979, J. Appl. Phys., **50**(11), 7200-7209.

Khrussanova M.,Grigorova E., Mitov I., Radev D., Peshev P., 2001, J. Alloys and Compounds, **327**, 230-234.

Khrussanova M., Bobet J-L., Terzieva M., Chevalier B., Radev D., Peshev P.,

Darriet B., 2000, J. Alloys and Compounds, **307**, 283-289.

Kuijpers F.A., Van Mal H.H., 1971, J. Phys. Chem., **23**, 395.

Larsen J.W., Livesay B.R., 1980, J. Less-Common Metals, **73**, 79-88.

Liang G., Huot J., Boily S., Schulz R., 2000a, J. Alloys and Compounds, **305**, 239-245.

Liang G., Huot J., Boily S., Van Neste A., Schulz R., 2000b, J. Alloys and Compounds, **297**, 261-265.

Liang G., Huot J., Boily S., Van Neste A., Schulz R., 1999a, J. Alloys and Compounds, **291**, 295-299.

Liang G., Huot J., Boily S., Van Neste A., Schulz R., 1999b, J. Alloys and Compounds, **292**, 247-252.

Liang G., Huot J., Boily S., Van Neste A., Schulz R., 1999c, J. Alloys and Compounds, **282**, 286-290.

Liang G., Wang E., Fang S., 1995, J. Alloys and Compounds, **223**, 111-114.

Libowitz G.G., Hayes H.F., Gibb T.R.P., 1957, Inorg. Chem., **62**, 76.

Liu W., Wu H., Lei Y., Wang Q., Wu J., 1997, J. Alloys and Compounds, **261**, 289-294.

Lundin C.E., Lynch F.E., 1977, "Hydrides for Energy Storage", (Pergamon Press, Elmsford, New York)

Luz Z., Senossar J., Rudman P.S., 1980, J. Less-Common Metals, **73**, 427.

Mandal P., Srivasta O.N., 1994, J. Alloys and Compounds, **205**, 111-118.

Martin M., Gommel C., Borkhart C., Fromm E., 1996, J. Alloys and Compounds, **238**, 193-201.

Mintz M.H., Bloch J., 1985, Progr. Solid. State Chem., **16**, 163.

Mintz M.H., Gavra Z., Kimmel G., 1980, J. Less Common Metals, **74**, 263-270.

Mueller W.M., Blackedge J.P., Libowitz G.G., 1968, "Metal Hydrides", (Academy Press, Inc., London).

Nohara S., Inoue H., Fukumoto Y., Iwakura C., 1997, J. Alloys and Compounds, 259, 183-185.

Oelerich W., Klassen T., Borman R., 2001a, J. Alloys and Compounds, **315**, 237-242.

Oelerich W., Klassen T., Borman R., 2001b, J. Alloys and Compounds, **322**, L5-L9.

Okamoto H., 1988, "Phase Diagrams of Binary Mg-Alloys", (ASM Int., Metals Park, Ohio 44073).

Osovizky A., Bloch J., Mintz M.H., Jacob I., 1996, J. Alloys and Compounds, **245**, 168-178.

Ramakrishna K., Singh S.K., Singh A.K., Srivastava O.N., 1987, Progress in Hydrogen Energy, 81-110.

Raymor G.V., 1959, "Physical Metallurgy of Magnesium and its Alloys", (Pergamon Press, New York).

Reiser A., Bogdanovic B., Schlichte K., 2000, Int. J. Hydrogen Energy, **25**, 425-430.

Renner J., Grabke H.J., 1972, Z. Metallkd., **H5**, 63.

Reule H., Hirscher M., Weisshardt A., Kronmüller, 2000, J. Alloys and Compounds, **305**, 246-252.

Rudman P.S., 1983, J. Less-Common Materials, **89**, 93-110.

San-Martin A., Manchester F.D., 1988, "Phase Diagrams of Binary Mg-Alloys", (ASM Int., Metals Park, Ohio 44073).

Sandrock G., 1999, J. Alloys ans Compounds, **293-295**, 887-888.

Schlapbach L., 1980, J. Less-Common Metals, **73**, 79.

Schulz R., Liang G., Huot J., 2001, Proc. 22nd Rise Int. Symposium on Materials Science, Denmark.

Schulz R., Huot J., Liang G., Boily S., Lalanda G., Denis M.C., Dodelet J.P., 1999, Mat. Sci and Eng., **A267**, 240-245.

Selvam P., Viswanathan B., Swamy C.S., Srinivasan V., 1988, Int. J. Hydrogen Energy, **13**(2), 87-94.

Selvam P., Viswanathan B., Swamy C.S., Srinivasan V., 1986, Int. J. Hydrogen Energy, **11**(3), 169-192.

Sharp J.H., Brindley G.W., Naharari Achar B.N.,1966, J. Am. Ceram. Soc., **49**, 379.

Skol'skaya L.I.,1961, "Gasses in Light Metals", (Pergamon Press, London).

Song MY. Bobet J-L., Darriet B., 2002, J. Alloys and Compounds, **340**, 256,262.

Spassov T., Köster U., 1999, J. Alloys and Compounds, **287**, 243-250.

Stander C.M., 1977a, Z. Phy. Chem., **104**, 229.

Stander C.M., 1977b, J. Inorg. Nucl. Chem., **39**, 221.

Suda S., Kobayashi N., 1980, J. Less-Common Metals, **73**, 119-126.

Tessier P., Akiba E., 2000, J. Alloys and Compounds, **302**, 215-217.

Tessier P., Akiba E., 1999, J. Alloys and Compounds, **293-295**, 400-402.

Tessier P., Enoki M., Bououdina M., Akiba E., 1998, J. Alloys and Compounds, **268**, 285-289.

Uchida H., Uchida H., 1984, J. Less-Common Metals, **101**, 459-468.

Vigeholm B., Jensen K., Larsen B., Pedersen A.S., 1987, J. Less Common Metals, **131**, 133.

Vigeholm B., Kjoller J., Larsen B., Pedersen A.S., 1983, J. Less-Common Metals, **89**, 135-144.

Wang P., Wang A.M., Ding B.Z., Hu Z.Q., 2002, J. Alloys and Compounds, **334**, 243-248.

Wang P., Wang A.M., Zhang H.F., Ding B.Z., Hu Z.Q., 2000a, J. Alloys and Compounds, **313**, 218-223.

Wang P., Zhang H.F., Ding B.Z., Hu Z.Q., 2000b, J. Alloys and Compounds, **313**, 209-213.

Wang P., Wang A.M., Zhang H.F., Ding B.Z., Hu Z.Q., 2000c, J. Alloys and Compounds, **297**, 240-245.

Warren B.E., 1969, "X-Ray Diffraction", (Addison-Wesley Publishing Co., Inc.)

Wu M-S., Wu H-R., WangY-Y, Wan C-C., 2000, J. Alloys and Compounds, **302**, 248-257.

Zaluska A., Zaluski L., Ström-Olsen J.O., 1999, J. Alloys and Compounds, **289**, 197-206.

Zaluski L., Zaluska A., Ström-Olsen J.O., 1997, J. Alloys and Compounds, **253-254**, 70-79.

Zeng K., Klassen T., Oelerich W., Bormann R., 1999a, J. Alloys and Compounds, **283**, 213-224.

Zeng K., Klassen T., Oelerich W., Bormann R., 1999b, Int. J. Hydrogen Energy, **24**, 989-1004.

APPENDIX A

HİDROJEN DEPOLAMA AMACIYLA MAGNEZYUM TOZLARININ ÖĞÜTÜLMESİNDE KATKI MADDELERİNİN ETKİSİ*

Murat GÜVENDİREN, H. Emrah ÜNALAN ve Tayfur ÖZTÜRK
Orta Doğu Teknik Üniversitesi , Metalurji ve Malzeme Mühendisliği Bölümü,
06531, Ankara, e-posta guvendir@metu.edu.tr, ozturk@metu.edu.tr

ÖZET

Hidrojenin metal tozlarda hidrürler olarak depolanmasında mekanik alaşımlandırma yaygınca kullanılmaktadır. Özellikle magnezyumda mekanik alaşımlandırmanın amacı hidrojenin emilme ve serbest bırakılma hızının pratik uygulamalara cevap verebilecek hızlılığa kavuşturulmasıdır. Bu çalışmada magnezyuma değişik kakı maddeleri eklenmiş ve bu maddelerin atritörle yapılan öğütme sonrası oluşan "mekanik alaşımlandırma" 'daki etkinliği incelenmiştir. Etkinlik yapısal incelme olarak ele alınmış ve öğütme sonrası incelme gerek metalografik gerekse X-ışınları kırınım yöntemleri ile tesbit edilmiştir. Bu amaçla sisteme sabit hacim oranında (%5) farklı sertlik değerlerinde SiC, Al_2O_3, V, Grafit ilaveleri yapılmıştır. Yapılan çalışma yapısal incelmede katkı maddesinin sertliğinin tek başına belirleyici olmadığını, katkı maddesinin öğütme sırasında büyüklüğünü muhafazasının daha etkin olduğunu göstermiştir. Bu açıdan yapılan ilaveler içerisinde en etkininin grafit ve Al_2O_3 olduğu gözlenmiştir.

Anahtar Kelimeler: Mekanik Alaşımlandırma, Atritörle Öğütme, X-Işınları Profil Analizi, Magnezyum Hidrür, Hidrojen Depolama

HYDROGEN STORAGE IN MECHANICALLY ALLOYED MAGNESIUM POWDERS: EFFECTS OF ADDITIVES ON MILLING

**Presented and published, 3th International Powder Metallurgy Conference Proceedings, Editor: Süleyman Sarıtaş, Gazi University, Ankara, TURKEY, September 4-7, 2002, pp.876-885.*

ABSTRACT

Mechanical alloying is becoming quite common as a method of improving the hydrogen storage properties of metal powders. This is particularly important in magnesium where the sorption, i.e. absorption and desorption rate is quite sluggish. So to imrove the rate to values suitable for practical applications, an efficient method of structural refinement is necessary. In this study various additives are used to aid milling of magnesium powders. Milling is carried out with an attritor, addtives are on a constant volume basis, (5vol.%). Additives investigated in this work , namely SiC, Al_2O_3, V, graphite are chosen so as to cover a wide hardness range. Structural refinement after milling are studied both metallographically and in terms of X-ray profile analysis. It is concluded that for effiecient structural refinement the additive should be chosen not on the basis of its hardness, but rather whether or not it is preserved with an acceptable size during milling. Thus of the addtives investigated in this work graphite and Al_2O_3 are found to be most effective.

Keywords: Mechanical Alloying, Attritor Milling, X-ray Profile Analysis, Magnesium Hidride, Hydrogen Storage.

1- GİRİŞ

Son yıllarda temiz enerji kaynaklarına hızlı bir yönelim gerçekleşmiştir. Bu amaçla yapılan çalışmaların büyük çoğunluğu hidrojeni esas almakta ve hidrojenin üretimi depolanması ve değişik amaçlar için kullanımı ana çalışma konularını oluşturmaktadır [1,2]. Hidrojenin yakın gelecekte beklenen yaygınlıkta kullanılabilmesi için hidrojenin etkin tarzda depolanması çözüm bekleyen sorunlar arasındadır [2]. Hidrojenin metal hidrür olarak depolanabileceği, depolanan bu hidrojenin basınç/sıcaklık değişilikleri ile arzu edildiğinde serbest bırakılabileceği bilinen bir hususutur. Bu tür sistemlerde amaç birim hacimde olabildiğince yüksek miktarda hidrojeni gene olabildiğince düşük malzeme yoğunluklarında elde edebilmektir. Bu açıdan magnezyum özellikle dikkat çekicidir. Nitekim magnezyum metal hidrür olarak sıvılaştırılmış hidrojene kıyasla hidrojeni daha etkin depolayabilmektedir (sıvı hidrojenin 1.59 katı) [3]. Ayrıca magnezyum düşük yoğunluğu nedeni ile de diğer metal hidrürler arasında ön plana çıkmaktadır.

Hidrojen depolamada, çözüm bekleyen sorunlardan biri sorplama (depolama-serbest bırakma) hızıdır. Pratik uygulamalarda hidrojenin hızla depolanabilmesi ve depolanmış olan bu hidrojenin gene hızla sistemden alınabilmesi gerekmektedir. Son yıllarda yapılan çalışmalar (örneğin, [4]), özellikle sorplama kinetiğinin iyileştirilmesi üzerine yoğunlaşmış ve bu amaçla magnezyum çeşitli katkı maddeleri ile mekanik olarak alaşımlandırılmıştır.

Magnezyumun mekanik alaşımlandırılmasında metalik ilaveler yapılmış, örneğin Ni, V vb ve bu tür ilavelerin sorplama kinteğini iyileştirmesi kimyasal faktörlere

bağlanmıştır [5, 6]. Ancak yapılan son çalışmalarda sisteme oksit ilavesi yapılarak mekanik alaşımlandırma yapılmış ve bu ilavelerin de kineteği iyileştirdiği tespit edilmiştir [7, 8]. Sonuç olarak magnezyumun mekanik alaşımlandırılması ile elde edilen yapılarda katkı maddelerin sorplama kinetiğini ne şekilde ve nasıl etkilediği konusunda tereddütler oluşmuştur. Bu etki kimyasal olabileceği gibi, sırf yapısal incelmeden kaynaklanan fiziksel bir etki sonucu da olabilir.

Bu çalışmada yukarıda belirtilen etki fiziksel temelli olarak ele alınmış ve bu amaçla magnezyuma faklı özelliklerde çeşitli ilaveler yapılmıştır. Aynı koşullarda yapılan mekanik alaşımlandırma sonrası elde edilen yapısal incelme nicel yöntemlerle ölçülmüştür. Çalışmanın amacı en iyi yapısal incelmeyi mümkün kılan ilavenin tespiti ve bu şekilde hidrojen sorplama kinteğini en iyi kılacak işlem koşullarının tespitidir.

2- MALZEME VE YÖNTEM

Bu çalışmada mekanik alaşımlandırma bir atritör yardımı ile gerçekleştirilmiştir. Yapılan deneylerde 6.5 mm çapında paslanmaz çelik bilyeler kullanılmış, toz/bilye oranı ağırlıkça 1/10 olarak seçilmiştir. Oksitlenmeyi önlemek amacıyla hazne bilye seviyesinin üstüne kadar alkolle doldurulmuştur (20 mL). Atritör 515 devir/dakika hızda çalıştırılmıştır. Öğütmeler 3 saat süreyle gerçekleştirilmiştir.

Çalışmada magnezyum hidrüre Al_2O_3, SiC, V ve Grafit ilaveleri yapılmıştır. Bu amaçla %5'lik sabit hacim oranı verecek tarzda karışımlar hazırlanmıştır. Bu karışımlara ve kullanılan tozlara ilişkin bilgiler Çilzege 1 'de verilmektedir.

Çizelge 1. Deneysel çalışmada kullanılan sistemler.

Sistem	Ort. Parçacık Büyüklüğü (ilavenin)	ilave % hacim	ilave % ağırlık
MgH_2- SiC	≈5 μm	5	10
MgH_2- Al_2O_3	≈5 μm	5	13
MgH_2 -V	≈13 μm	5	18
MgH_2- G(Grafit)	≈60 μm	5	8
MgH_2	≈15μm		

Öğütme sonrası magnezyumda oluşan incelme X-ışınları Scherrer yöntemi [9] ile ölçülmüştür. Bu amaçla Co K_α radyasyonu kullanılmış ve MgH_2 {112} kırınımı 63°-66° (2θ) aralığında 1/8 derece/dakika hızında hassas bir şekilde kaydedilmiştir. Elde edilen kırınımda kırınım genişliği, B_t, yarı yükseklikte radyan cinsinden ölçülmüştür. Cihazdan kaynaklanan genişlemeyi ölçmek amacıyla saf MgH_2 tozlarından ayrıca bir numune hazırlanmıştır. Sıkıştırma sonrası numune 350 ^{0}C'de 24 saat süreyle tavlanarak yapı olabildiğince irileşitirilmiştir. Bu numuneden elde edilen genişleme, B_c, benzer şekilde ölçülmüş ve bu değer cihaz kökenli genişleme

olarak kabul edilmiştir. Öğütme sonucu numunelerde oluşan gerçek yapısal genişleme,

$$(B_y)^2 = (B_t)^2 - (B_c)^2 \quad (1)$$

olarak hesaplanmıştır.

"Parçaçık" boyutu, t, yapısal genişleme arasındaki ilişki Scherrer bağıntısı yardımı ile

$$t = (0.9\ \lambda) / (B_y \cos\theta_B) \quad (2)$$

hesaplanmıştır. Bu bağıntıda, λ, x-ışını dalga boyunu; θ_B, Bragg açısını; B_y, ölçülen yapısal genişlemeyi göstermektedir.

3- BULGULAR ve TARTIŞMA

MgH_2'nin katkı maddesi kullanılmaksızın öğütme öncesi ve sonrası yapısı sırası ile Şekil 1 a ve b 'de verilmektedir. Görüldüğü gibi öğütme sonrası tozda yer yer 2-3 mikron boyutunda nispeten iri parçacıklar yer almakta ancak yapının büyük çoğunluğu mikron veya mikronaltı parçaçıklardan oluşmaktadır.

Katkı maddeleri ile öğütülen numunelerde gözlenen temel fark yapı içerisinde gözlenen nispeten iri paçacıkların azlığıdır. Buna bir örnek Şekil 2 'de MgH_2-V için verilmektedir. Öğütme sonrası V, SiC ve Grafit ilavelerinde elde edilen yapılarda belirgin bir fark gözlenmemiş her üç numuneninde nispeten daha homojen olduğu tespit edilmiştir. Al_2O_3 ilavesinde elde edilen yapı Şekil 3 'te verilmektedir. Bu yapı diğerlerine nispeten daha ince ve homojen bir görünüm sergilemektedir.

Çizelge 2. Atritörle öğütülmüş numunelerde MgH_2 'nin (211) kırınımında ölçülen genişleme ve bu genişlemeye göre tespit edilen yapısal boyut.

Sistem	$d_{(211)}$ (Angström)	Yarı Şiddette Genişlik(rad)	Yapısal Boyut (Angström)
MgH_2+5%Al_2O_3 (3 saat öğütme)	1,683	0,02028	≈204
MgH_2+5%G (3 saat öğütme)	1,682	0,01941	≈216
MgH_2+5%SiC (3 saat öğütme)	1,683	0,01810	≈236
MgH_2 (3 saat öğütme)	1,675	0,01483	≈312
MgH_2+5%V (3 saat öğütme)	1,679	0,01483	≈312
MgH_2 (öğütme öncesi)	1,679	0,01374	≈352

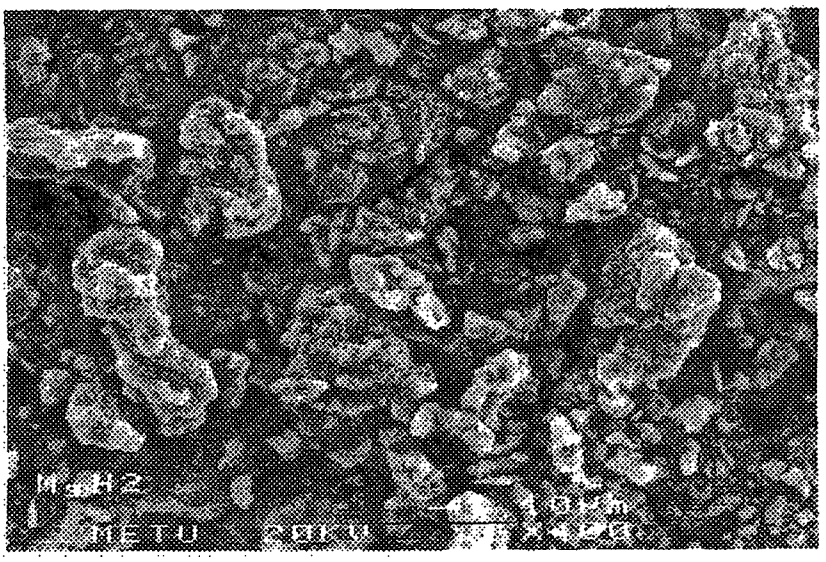

(a)

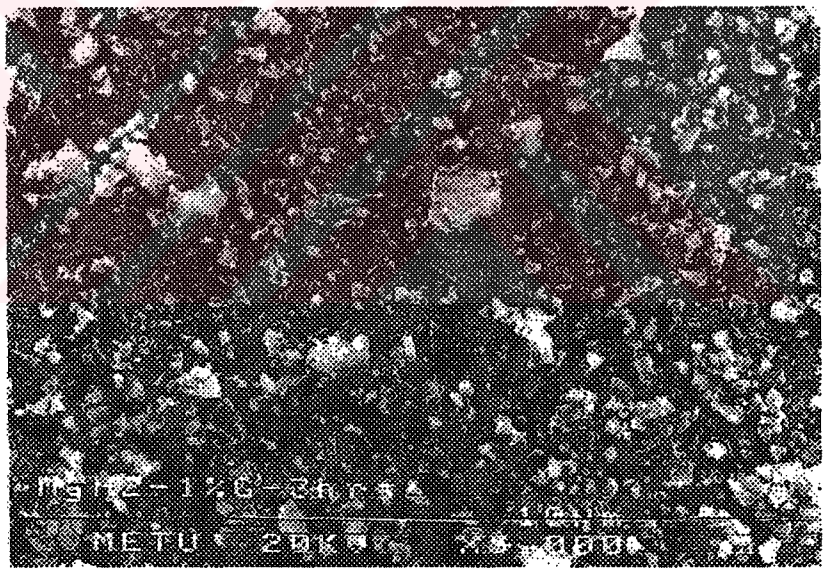

(b)

Şekil 1. MgH_2 tozlarının atritörle öğütme öncesi **(a)** ve sonrası **(b)** yapısı.

Yapılan X-ışını ölçüm sonuçları Şekil 4 ve Çizelge II'de verilmektedir. Şekil 4 numunelerde tespit edilen (211) kırınım profillerini üstüste göstermektedir. Bu verilere göre numuneler için hesaplanan "yapısal boyut" değerleri Çilzege II de gösterilmiştir.

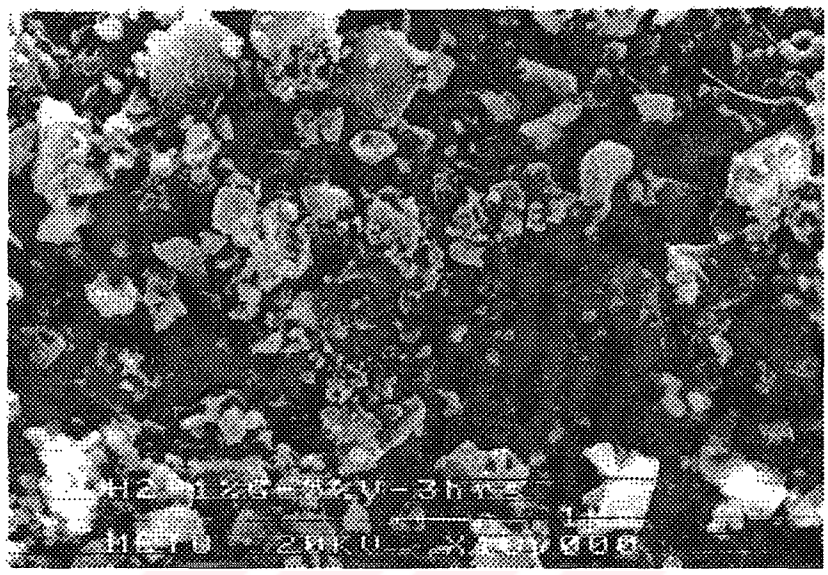

Şekil 2. MgH_2+ %5 V tozlarının atritörle öğütme sonrası yapısı.

Şekil 3. MgH_2+ %5 Al_2O_3 tozlarının atritörle öğütme sonrası yapısı.

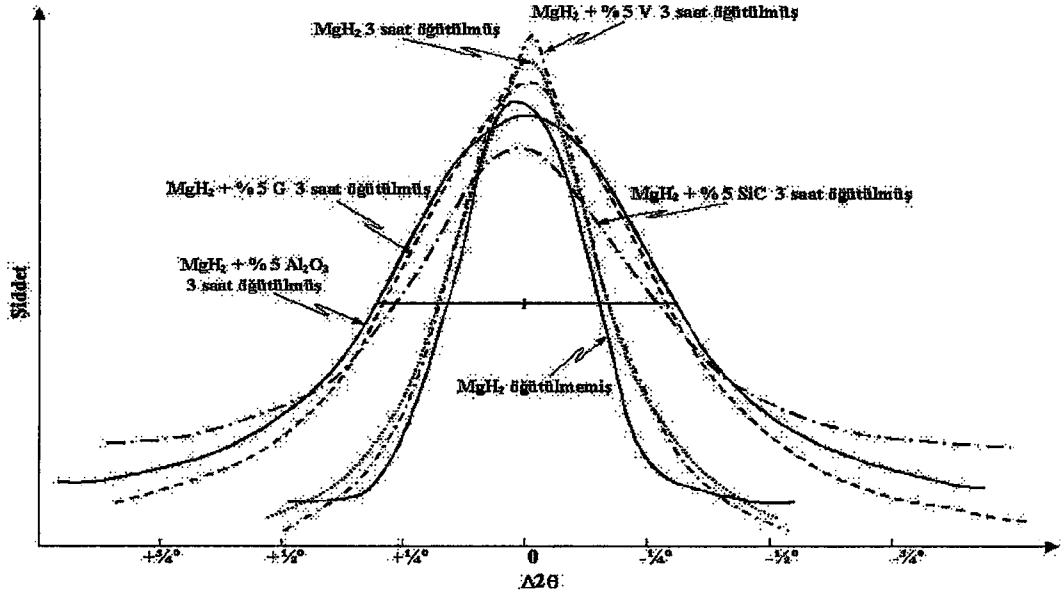

Şekil 4. MgH_2'de katkı maddelerinin ilavesi ile 3 saat öğütme sonrası Co Kα radyasyonu ile tespit edilen (211) profilleri. Kırınımlarda kayma olduğundan profiller açısal olarak kaydırılmış ve yarı şiddetlerinde çakıştırılmıştır, bakınız Çizelge II.

Yapısal boyut değerleri kıyaslandığında V ilavesi yapısal incelmede saf öğütmeye oranla belirgin bir iyileştirme oluşturmamakta, bunun dışındaki diğer katkı maddelerinin tümü daha ince bir yapıya işaretetmektedir. Bu açıdan en iyi incelme Al_2O_3 ve grafitçe gerçekleştirilmektedir. 3 Saat öğütme sonunda ortalama parçacık büyüklüğü sırası ile yaklaşık olarak 204 ve 216 angstromdur.

Bu çalışmada hazırlanan tüm numuneler aynı hacim oranında hazırlanmış ve bu şekilde katkı maddelerinin kendi özellikleri dışındaki diğer değişkenlerin sabit tutulması hedeflenmiştir. Bu durum katkı maddelerinin hepsinin aynı parçacık büyüklüğünde olması durumunda öğütülen toz başına aynı oranda katkı parçacığının sistemde mevcut olması anlamındadır. Yapılan deneylerde Al_2O_3 ve SiC katkıları aynı parçacık büyüklüğünde seçilmiştir (5 mikron). Vanadyum ilavesinde ise paraçaçıklar nispeten daha iridir (13 mikron), Grafitte ise yapısı gereği yaklaşık 60 mikron boyutunda levhalar şeklindedir. Bu koşullarda Al_2O_3 ve SiC katkılı numenelerin aynı geometrik koşullarda öğütüldüğü söylenebilir.

Koşulların aynı olması durumunda sert parçacıkların öğütmeye yardımcı olacağı ve daha iyi bir incelmeye yol açmasını beklemek doğaldır. Ancak yapılan deneyde bunu tam tersi gözlenmiştir. SiC ilavesi yüksek sertliği ile daha ince bir yapı vermesi gerekirken, elde edilen yapı bu düzeyde sert olmayan alumina (yaklaşık SiC'ün 2/3'ü sertlikte) ilavesi ile elde edilen yapıdan daha iri kalmıştır.

Grafit ilavesinin alumina ilavesi ile kıyaslanabilecek düzeyde bir incemeye yol açmış olması şasırtıcı bulunmuştur. Bilindiği gibi grafit Al_2O_3 ve SiC'den farklı olarak yapıda sert bir faz görünümünden daha çok grafit levaların birbiri üstünde kolaylıkla kaymasından kaynaklanan yağlayıcı bir etkiye sahiptir. Bu etkinin sert paraçacıklarla kıyaslanabilir düzeyde bir incelmeye yol açmış olması mekanik alaşımlandırmada yapısal oluşumun ne denli karmaşık faktörleri içerdiğinin bir göstergesidir.

Yapısal incelmede oluşan bu karmaşıklığa açıklık getirmek amacıyla öğütme sonrası katkı maddelerinde oluşan yapısal boyut değişiklikleri de X-ışınları ile incelenmiştir. Elde edilen sonuçlar Şekil 5'te verilmektedir. Yarı yükseklikteki kırınım genişlikleri kıyaslandığında öğütme sonucu en az etki grafit ve Al_2O_3 te oluşmakta ve bunları takiben V ve en fazla etki de SiC gözlenmektedir. Öğütme sonrası SiC nerdeyse yapısal boyut olarak nano/amorf düzeyine yaklaşmıştır. Bu değerler grafit ve Al_2O_3'un çok fazla etkilenmeden öğütme sırasında sistemde kaldıklarını ancak V ve özellikle de SiC'un öğütücü olarak katılmalarına rağmen kendilerinin öğütüldüğünü göstermektedir.

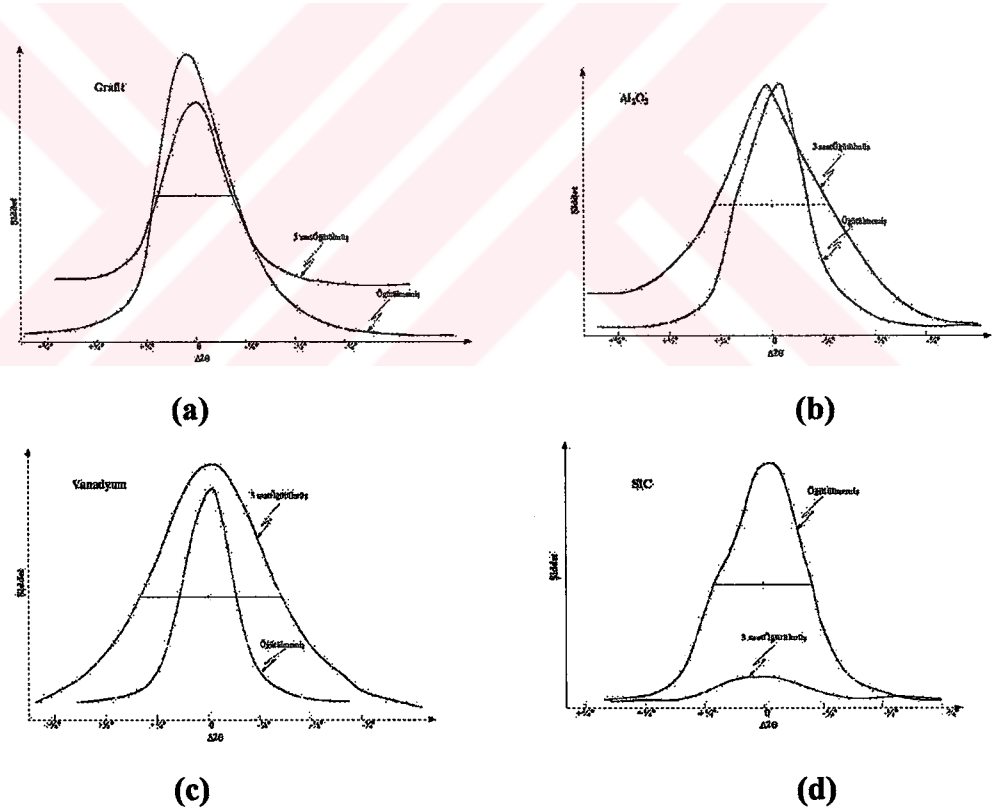

Şekil 5. MgH_2 'nin 3 saat öğütülmesi sonunda katkı madde ilavelerinde tespit edilen X-Işını Kırınım Profilleri. Bu profiller katkı maddelerine kıyaslamalı olarak çizilmiştir.
a) Grafit; (002) b)Al_2O_3; (116) c) Vanadyum; (110) d) SiC; (110)

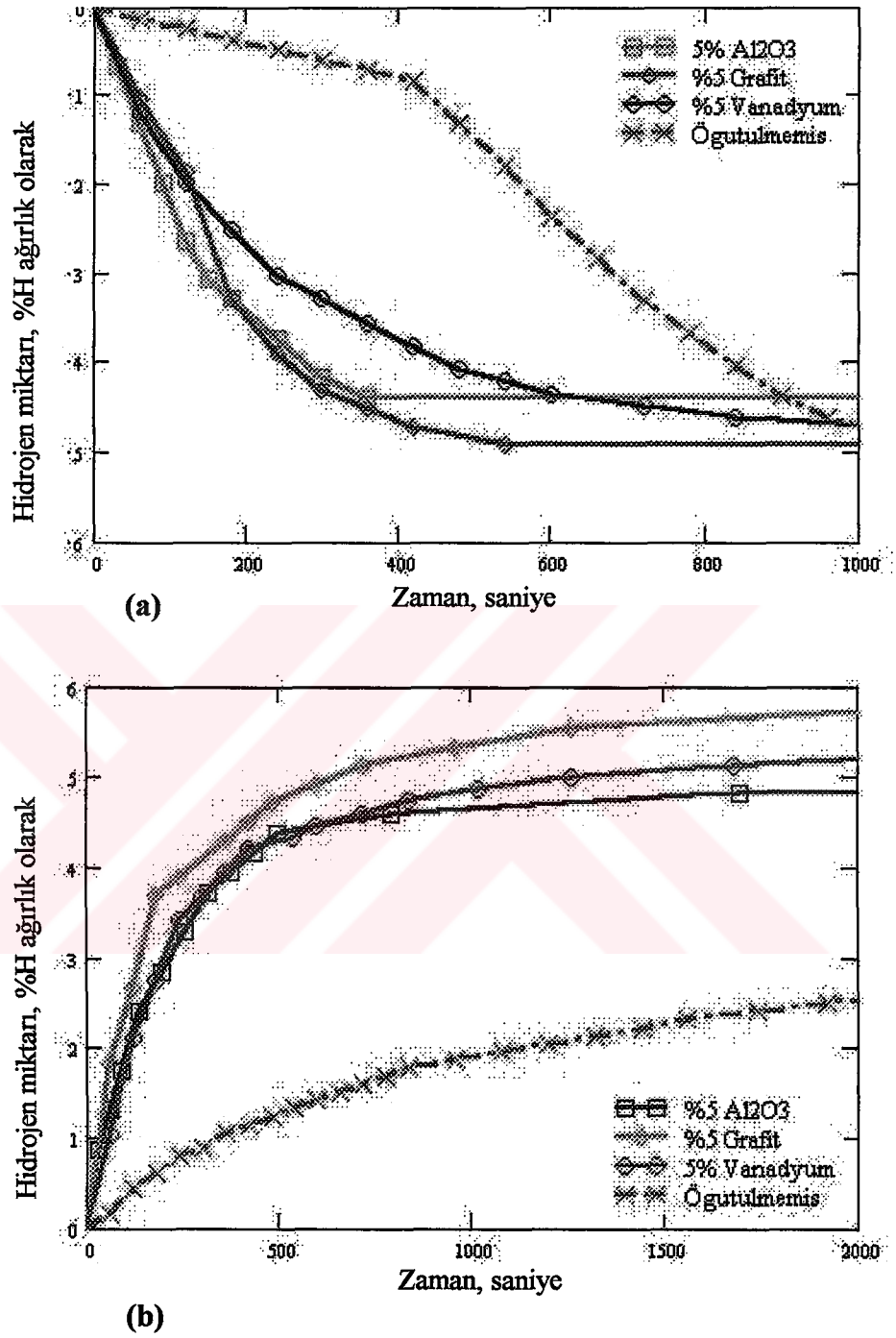

Şekil 6. Mekanik alaşımlandırılmış ve saf MgH_2'de sorplama; geribırakım (a), emilim (b) hızı karşılaştırması.

SiC'ün yüksek sertliğine rağmen öğütmede Al_2O_3 kadar başarılı olmayışı büyük bir ihtimalle öğütme sırasında etkin büyüklüğünü muhafaza edememesinden kaynaklanmaktadır. Büyüklüğü muhafaza etmenin önemi grafitçede doğrulanmaktadır. Grafit nispeten yumuşak yapısına rağmen etkin büyüklüğünü öğütme sırasında birşekilde korumuş ve öğütmeyi kolaylaştırıcı katkı maddesi olarak işlevini yerine getirebilmiştir.

Bu çalışmada elde edilen tozlar için tespit edilen emilme ve serbest bırakma eğrileri Şekil 6 'da verilmektedir. Şekillerde görüleceği üzere öğütülmüş tüm tozlarda öğütülmemiş MgH_2 'ye kıyasla belirgin bir hızlanma mevcuttur. Hızlanma açısından en iyi sonucu veren ilaveler Al_2O_3 ve grafittir.

4. SONUÇ

Hidrojen depolama özelliklerini geliştirmek amacıyla magnezyum hidrür değişik ilavelerle atritörle öğütülmüş ve ilavelerin yapısal incelmeye etkisi değerlendirilmiştir. Yapılan çalışma hidrojenin emilim ve geri bırakım hızının magnezyumun öğütülmesi ile iyileştiğini doğrulamıştır. İlavelerin yapılması ile öğütmenin etkinliği metallografi ve X-ışınları profil analizi ile tespit edilmiştir. Bu tespitler;

i. İnceltmede, ilave sertliğinin tek başına belirleyici olmadığını,

ii. Etkin incelme için öğütme sırasında ilave büyüklüğünün muhafazasının daha önemli olduğunu,

göstermiş ve incelenen katkı maddeleri içersinde en iyi incelmeyi grafit ve Al_2O_3 'ün oluşturduğu sonucuna varılmıştır.

Teşekkür

Bu çalışma, **ODTÜ** (AFP 2001-07-02-00-15 , BAP 2002-07-02-00-47) ve **TÜBİTAK** (MİSAG 213) tarafından desteklenmiştir.

KAYNAKLAR

1. Momirlan M., Veziroğlu T.N., "Current Status of Hydrogen Energy", **Renewable and Sustainable Energy Reviews**, Vol. 6, pp. 141-179, 2002.
2. Dantzer P, "Metal Hydride Technology: A Critical Review", **Topics in Applied Physics**, Vol. 73, pp. 273, Springer-Verlag, Berlin Heidelberg, 1997.
3. Selvam P.,Viswanathan B., Swamy C.S., Srinivasan V., "Magnesium and Magnesium Alloy Hydrides", **Int. J. Hydrogen Energy**, Vol. 11, pp. 169-192, 1986.

4. Huot J., Liang G., Boily S., Van Neste A., Shulz R.,"Structural study and hydrogen sorption kinetics of ball milled Mg hydride", **J Alloys and Compounds**, Vols. 293-295, pp. 495-500, 1999.
5. Oerlich W.,Klassen T., Bormann R.,"Metal oxides as catalysts for improved hydrogen sorption in nanocrystalline Mg-based materials", **J. Alloys and Compounds**, Vol. 315, pp 237-242, 2001.
6. Liang G., Huot J., Boily S., Van Neste A., Shulz R.,"Catalytic effect of transition metals on hydrogen sorption in nanocrystalline ball milled MgH_2-Tm systems", **J Alloys and Compounds**, Vol. 292, pp. 247-252, 1999.
7. Oerlich W., Klassen T., Bormann R.,"Comparison of the catalytic effects of V, V_2O_5, VN, and VC on the hydgrogen sorption of nanocrystalline Mg", **J. Alloys and Compounds**, Vol. 322, pp L5-L9, 2001.
8. Wang P., Wang A.M., Zhang H.F., Ding B.Z., Hu Z.Q.,"Hydrogenetion characteristics of Mg-TiO_2 composite", **J. Alloys and Compounds**, Vol. 313, pp 218-223, ,2000.
9. Warren B.E., Biscoe J., **J. Am. Ceram. Soc**. Vol.21, p. 49, 1938.

APPENDIX B

Taşınabilir Enerji Kaynağı Olarak Hidrojenin Metal Tozlarda Depolanması*

Murat GÜVENDİREN [a], Elif BAYBÖRÜ[b], Tayfur ÖZTÜRK [c]

[a] Orta Doğu Teknik Üniversitesi, Met. ve Malz. Müh. Böl., 06531,Ankara, guvendir@metu.edu.tr

[b] Orta Doğu Teknik Üniversitesi, Met. ve Malz. Müh. Böl., 06531, Ankara,

[c] Orta Doğu Teknik Üniversitesi, Met. ve Malz. Müh. Böl., 06531, Ankara, ozturk@metu.edu.tr

ÖZET

Hidrojen özellikle sahra koşullarında taşınabilir veya sabit uygulamalarda yüksek enerji yoğunluğu ile dikkat çeken alternatif bir yakıttır. Aynı zamanda hidrojen, aynı koşullarda farklı yöntemlerle üretilebilecek rüzgar/güneş vb enerjinin uygun tarzda depolanmasına olanak veren bir ortam oluşturur. Bu ve benzeri uygulamaların tamamı hidrojenin güvenilir, hafif ve yoğun tarzda depolanmasını gerekli kılmaktadır. Bu çalışmada hidrojenin magnezyum esaslı tozlarda metal hidrür olarak depolanması incelenmiştir. Etkin tarzda depolama için tozlar katkı maddeleri ile mekanik olarak alaşımlandırılmıştır. İncelenen katkı maddeleri içersinde en iyi sonuç grafit ilaveli magnezyumda elde edilmiş ve bu şekilde %5 grafitle alaşımlandırılmış tozlarda kg başına 70 litre/dakika 'lık depolama ve serbest bırakma hızı elde edilmiştir. Tozlarda depolanabilecek hidrojen miktarı ağırlıkça %6 düzeyindedir.

Anahtar Kelimeler: Sahra Koşulları, Enerji Depolama, Hidrojen, Magnezyum, Mekanik Alaşımlandırma

---

**Presented and published, Defense Industries Congress Proceedings, Editors: O. Yıldırım et al., METU, Ankara, TURKEY, 24-25 October 2002, Vol.1, pp.115-122.*

ABSTRACT

The use of hydrogen in many applications; i.e. automotive, thermodynamic devices etc, requires an efficient and reliable method of storage. In recent years there has been considerable interest in metal hidrides as a medium to store hydrogen and recover it when necessary. Those hydrides based on magnesium is highly desirable due to its low density and high storage capacity. In this work magnesium powders have been processed with attritor mill with a variety of additives so as to improve its storage characteristics. Of the additives investigated in this work it is found that garphite addition enhances the storage characterictics yielding 70 liters/min sorbing rate per kilogram of this powder. The total storage capacity of the powder with 5 % graphite addition is approximately 6 % by weight.

Keywords: Hydrogen Storage, Metal Hydrides, Magnesium, Attritor Milling.

1. GİRİŞ

Bir enerji kaynağı olarak hidrojenin en ayırt edici özelliği enerji yoğunluğudur. Birim ağırlıkta hidrojenin içerdiği enerji benzinin ve doğal gazın yaklaşık 3 katı kadardır (142 MJ/kg) [1]. Bu açıdan hidrojen gerek üretilen enerjinin depolanmasına gerekse enerjinin taşınmasına uygun bir ortam oluşturur. Hidrojenin çok farklı uygulamaları olamakla beraber (otomotiv, termodinamik - ısıtma/soğutma- gereçler) bu uygulamalar içersinde sahra koşullarında enerji gereksiniminin karşılanması büyük yer tuttar. Bu uygulamalar bir taraftan kişisel olarak taşınabilecek kompakt enerji kaynağı şeklinde olabileceği gibi, ulusal şebekeden uzak koşullarda elektrik enerjisinin üretimi şeklinde de olabilmektedir. Özellikle ikinci durumda hidrojeni yakıt pilleri ile birlikte düşünmek gerekmekte ve bu konuda yoğun araştırma çalışmaları devam etmektedir [2].

Hidrojen basınçlı tüplerde depolanabilmektedir. Ancak bu tür depolamada tüplerin ağırlıktaki payı yüksek olmakta, gerekli emniyet ancak belirli bir düzeyde sağlanabilmektedir. Bu açıdan özellikle son yıllarda hidrojenin hidrürler olarak katı tozlarda veya sıvılar içersinde depolanması önem kazanmıştır.

Bu çalışmada hidrojenin metal hidrürler olarak katı ortamda depolanması konu alınmış ve bu amaçla farklı sisemler arasından düşük yoğunluğu ve yüksek depolama kapasitesi nedeniyle magnezyum seçilmiştir. Magnezyumun ağırlıkça % 7,6 düzeyinde hidrojen depolayabildiği bilinen bir gerçektir [3]. Ancak depolama ve serbest bırakma çok yavaş olmakta, bu da yukarıda belirtilen uygulamalar için sorun teşkil etmektedir. Hemen hemen tüm uygulamalar için depolama ve serbest bırakmanın makul hızlılıkta olması ve buna ilave olarak sözkonusu işlemlerin olabildiğince düşük sıcaklık (tercihen 100-200 ^{0}C) ve gene olabildiğince düşük basınç (tercihen 1-4 atm.) aralığında gerçekleştirilmesi hedef niteliğindedir. Bu amaçla saf Mg'da 300-400 ^{0}C sıcaklık ve 5-10 atm. basınç aralığında gerçekleşen sorplamanın hedef değerlere düşürülmesi gerekmektedir.

Bu çalışma, yukarıdaki hedefler doğrultusunda magnezyumun katkı maddeleri ile mekanik alaşımlandırılmasını ve bu işlemlerin magnezyumun hidrojen depolamasındaki ekilerini konu almaktadır.

2. MALZEME VE YONTEM

Yapılan çalışmada MgH_2, V, Al_2O_3 ve Grafit (C) tozları kullanılmıştır; kullanılan tozların parça büyüklükleri sırasıyla yaklaşık olarak 20, 13, 5 ve 60 mikrondur. MgH_2 'ye V, Al_2O_3 ve Grafit (C) ilaveri yapılarak 5'er gramlık toz karışımları elde edilmiştir. Bu karışımlara ilişkin bilgiler Çizelge 1 de verilmektedir.

Çizelge 1. Deneysel çalışmada kullanılan sistemler.

Sistem	**İlave, ağırlıkça %**	**İlave, hacimce %**
MgH_2 - V	5	1,24
MgH_2 - G(Grafit)	5	3,29
MgH_2 – Al_2O_3	5	1,88

Elde edilen karışımlar, daha sonra atritör yardımıyla argon atmosferi altında mekanik olarak alaşımlandırılmıştır. Mekanik alaşımlandırmada kullanılan atritör şematik olarak Şekil 1 'de verilmiştir. Öğütme işlemi serleştirilmiş çelik hazne içinde çubuk kanatlı bir karıştırıcı yardımı ile 6,5 mm'lik paslanmaz çelik bilyelerle yapılmıştır. Ağırlıkça %1 oranında grafit öğütme sırasında yağlayıcı olarak sisteme eklenmiştir. Bilye-toz oranı 10/1 olarak seçilmiştir. Öğütme 515 devir/dakika hızda 3 saat süre ile yapılmıştır.

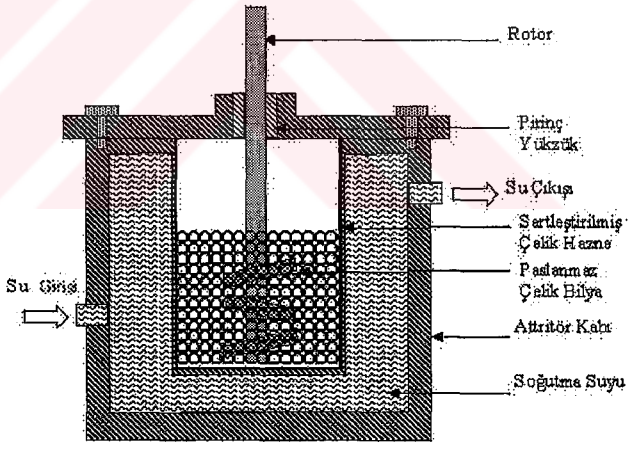

Şekil 1. Mekanik Alaşımlandırmada kullanılan atritör, şematik olarak.

Üretilen toz karışımlarındaki incelme tarama elektron mikroskopu ve X-ışınları yöntemi ile incelenmiştir [4].

Öğütme sonrasında hidrojen depolama deneyleri için 0,2-0,4 gr toz, hidrojen depolama test düzeneğine aktarılmıştır. Tüm bu işlemler argon atmosferi altında yapılmıştır.

2.2.1. Basınç-Kompozisyon Eşısıl Diyagramı Ölçümü

Hidrojen depolama test düzeneğine kaynak [5, 6] verilmektedir. Deney öncesi tozlar en az üç kez emilme-serbest bırakma döngüsünden geçirilerek "aktive" edilmiştir. Takiben yapılan basınç-kompozisyon eşısıl diyagramı ölçümüne geçilmiştir. Bu amaçla reaktörün istenilen sıcaklıkta kararlılaşması ile sisteme sabit basıçta hidrojen verilmiş ve basınçtaki düşme zamana bağlı olarak kaydedilmiştir. Emilim hızı $2,74\times10^{-4}$ mol/dakika 'nın altına düştüğünde sistem yeniden aynı basınç değerine getirilmiştir. Yeniden ayarlanan basınç değerinde emilim hızı verilen değerin altına düştüğünde o basınç için deney tamamlanmıştır. Deneyler 1-10 atmosfer aralığında 1 atmosfer aralıklarla gerçekleştirilmiştir. Bu şekilde eşısıl diyagram, ağırlıkça emilme miktarı basınç eksenlerinde gösterilmiştir.

2.2.2 Hidrojen Emilme- Serbest Bırakma Hızı Ölçümü

Hidrojen emilim hızı için reaktör seçilen sıcaklıkta (örnek olarak 350 ^{0}C) sabitlendikten sonra 10 atmosfer hidrojen verimiş ve basınç düşüşü zamana bağlı olarak kaydedilmiştir. Hidrojenin emilim hızı $4,56\times10^{-5}$ mol/dakika 'nın altına düşmesi ile deney tamamlanmıştır.

Hidrojen serbest bırakma hızı gene reaktör seçilen sıcaklıkta sabitlendikten sonra (örnek olarak 400 ^{0}C) tespit edilmiştir. Bu amaçla basınç 1 atmosferde tutulmuştur. Basınç artışı zamana göre kaydedilmiştir. Hidrojen serbest bırakma hızı $5,2\times10^{-5}$ mol/dakika 'nın altına düşmesi ile deney tamamlanmıştır.

3. BULGULAR

350 ^{0}C için elde edilen basınç-kompozisyon eşısıl diyagramları Şekil 2 'de verilmektedir. Diyagramlar sistemlerde oluşan plato basıncına ek olarak depolanabilecek toplam hidrojen miktarlarını da göstermektedir.

Şekil 2 'de görüldüğü gibi öğütme öncesi ve sonrasında gerek saf MgH_2 'de gerekse vanadyum ve grafit ilaveli öğütülmüş sistemlerde plato basıncı yaklaşık 4 atmosfer değerinde oluşmakta, ve yapılan ilavelerle plato basıncında görünür bir düşme oluşmamaktadır. Hatta grafit ilaveli sistemde plato basıncında hissedilir bir yükselme oluşmuştur.

Üretilen tozlarda toplam depolanabilen hidrojen miktarı % 6 mertebesindedir. Saf magnezyumda daha yüksek olan bu değer, yapılan kakı maddeleri ilavesi ile belirtilen % 6 'lık değere düşmüştür. Bu düşüş kısmen katkı maddelerinin ilavesi ile numunede mevcut aktif maddenin azalmasından kaynaklanmaktadır. Özellikle %5 grafit ilaveli numunede gözlenen toplam depolama miktarı tatmin edici düzeydedir.

Yapılan çalışmanın temel amacı saf magnezyumda yavaş olan sorplama hızının arttırlmasıdır. Saf magnezyum ve öğütülmüş magnezyum ve katkı maddeleri ile birlikte öğütülmüş magnezyum numunelerinde tespit edilen emilme ve serbest bırakma hızları sırası ile Şekil 3 ve Şekil 4 'de verilmektedir.

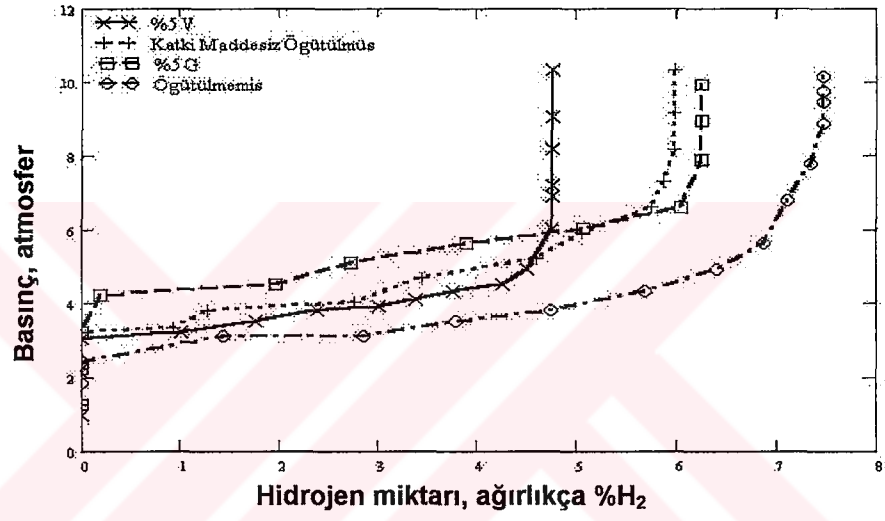

Şekil 2. 350 ^{0}C de elde edilen basınç-kompozisyon eşısıl diyagramları.

Hidrojenin emilme hızı açısından katkı maddeli olsun olmasın işlem görmüş tüm numunelerde tatmin edici bir hızlanma elde edilmiştir. Öyleki ilk 500 saniye içersinde öğütülmemiş saf MgH_2 sadece ağırlıkça %1.5 hidrojen depolayabilirken, öğütülmüş numnelerin tümünde aynı süre içersinde bunun yaklaşık 4 katı (% 5) hidrojen depolanabilmiştir. Depolamada hızlılık açısından en iyi sonuc %5 grafit katkılı sistemde elde edilmiştir. Verilen değer 1 kg'lık Mg-%5grafitte dakikada yaklaşık 70 litre (standart koşullarda) hidrojenin depolanabileceği anlamındadır.

Benzer hızlanma hidrojenin serbest bırakılmasında da gözlenmiştir. Öğütümemiş Mg ilk 500 saniyede ağırlıkça % 1.5 hidrojeni bırakırken, bu değer diğer numunelerde daha yüksektir. Ancak depolamda öğütülmüş numuneler arasında fark azken, serbest bırakmada bu fark daha belirgindir. Artan hıza göre sıralama MgH_2 (öğütülmüş), vanadyumlu, aluminalı ve grafitli sistemler şeklindedir. Burada da en iyi sonuç -500 saniyede %5- Mg-%5 grafitte elde edilmiştir. Bu değer tam kapasitesinde depolanmış 1 kg'lık Mg-5%grafit sisteminden dakikada yaklaşık 70 litre hidrojenin alınabileceğini göstermektedir.

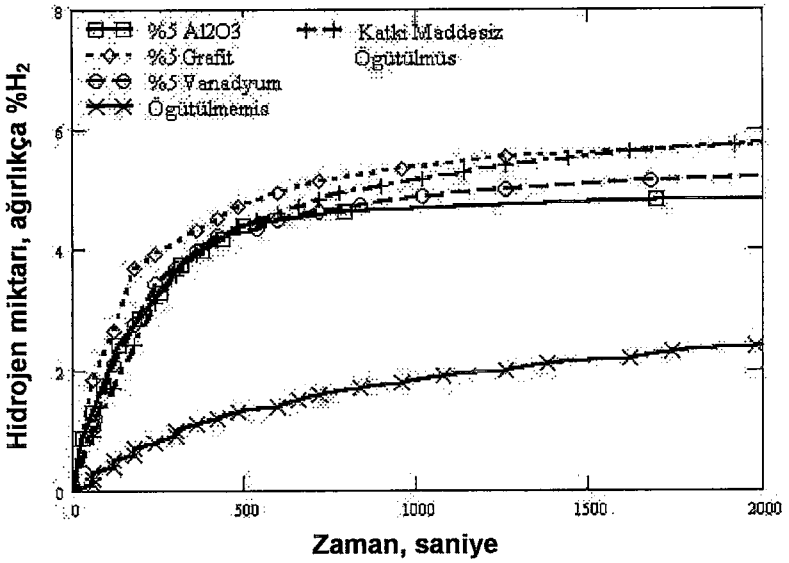

Şekil 3. Hidrojen emilim eğrileri. Eğriler 350 ^{0}C 'de 10 atmosferlik başlangıç hidrojen basıncında elde edilmiştir. Metne bakınız.

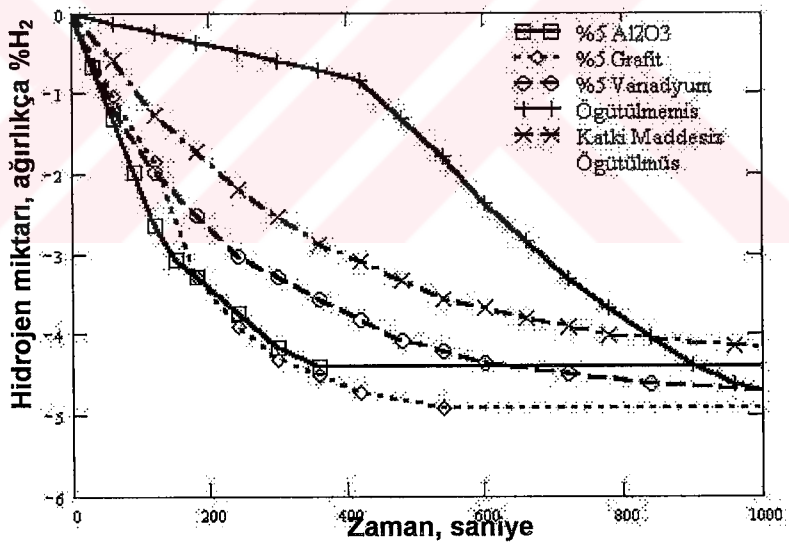

Şekil 4. Hidrojenin serbest bırakılma eğrileri. Eğriler 400 ^{0}C 'de 1 atmosferlik başlangıç hidrojen basıncında elde edilmiştir.

İncelenen sistemler içersinde öğütülmüş tüm numneler birbirlerine benzer sonuçlar vermekle beraber, bunların içerisinde özellikle emilme ve serbest bırakma hızı açısından magnezyum-5% grafit sistemi daha dikkat çekicidir. Magnezyum-%5 grafit sisteminde öğütme sonrası elde edilen yapı Şekil 5 'de verilmektedir. Kıyaslamaya olanak vermek amacıyla katkı maddesiz öğütülmüş MgH_2 'nin yapısı da aynı şekilde verilmektedir. Görüldüğü gibi grafit katkılı numunede incelme daha belirgindir. Numunelerde elde edilen incelme ayrıca X-Işınları kırınım yöntemi ile de incelenmiştir.

Elde edilen sonuçlar tüm numeneler için Şekil 6 da verilmektedir. Görüldüğü gibi grafitli sistemde kırınım genişlemesi (yapısal incelme) en yüksek değerine erişmiştir. Grafitli sistemde gözlenen hızlanmanın bu incelme ile ilişkili olduğu düşünülmektedir.

4. SONUÇ

Hidrojenin magnezyum esaslı tozlarda depolanmasını konu alan bu çalışmada magnezyum çeşitli katkı ilaveleri ile işlenmiş ve yapılan çalışma sonucunda Mg-grafit sisteminde (%5 grafit)

1- Depolama ve serbest bırakmanın 0-5 atmosfer 350-400 ^{0}C sıcaklık aralığında yapılabileceğini,

2- Yukarıdaki koşullarda sistemde ağırlıkça %6 oranında hidrojenin depolanmasının mümkün olduğunu,

3- Gene aynı koşullarda depolama ve serbest bırakma hızları için (kg başına) 70 litre/dakika 'lık değerlerin eldesinin mümkün olduğunu

göstermiştir.

Elde edilen bu değerler depolama ve serbest bırakma hızı açısından tatmin edici olmakla beraber, sorblama için gerekli basınç ve sıcaklık aralığı arzu edilen değerlerin üstündedir. Anılan değerlerin 2-3 atmosfer ve 100-200 ^{0}C aralığına düşürülmesi için halen çalışmalar sürdürülmektedir.

Teşekkür

Bu çalışma, **ODTÜ** (AFP 2001-07-02-00-15, BAP 2002-07-02-00-) ve **TÜBİTAK** (MİSAG 213) tarafından desteklenmiştir.

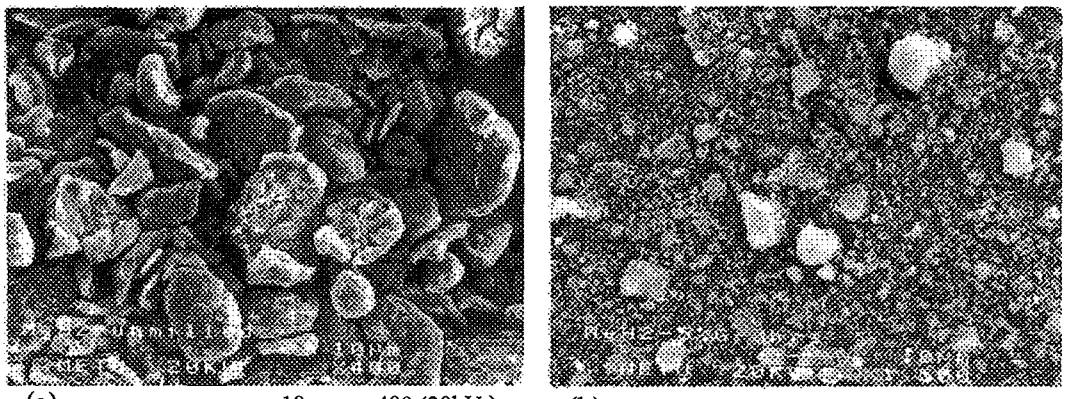

Şekil 5. MgH_2 tozlarının öğütme öncesi (a) ve %5 grafit ilaveli öğütme sonrası (b) yapısı.

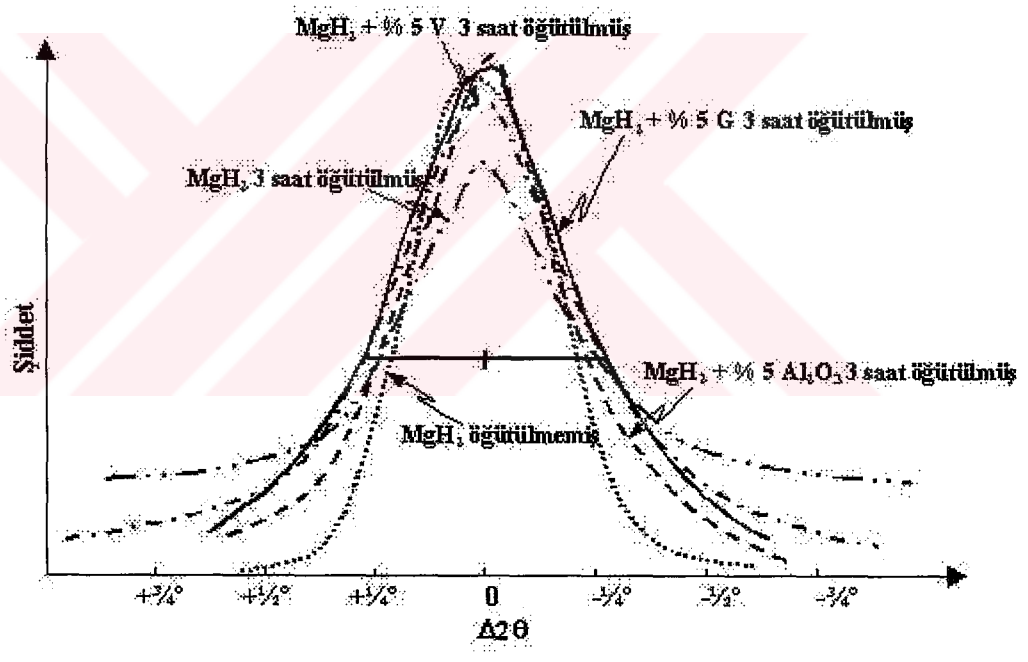

Şekil 6. MgH_2 'de 3 saat katkı ilaveli öğütme sonunda Co Kα ile tespit edilen, açısal olarak kaydırılmış ve yarı şiddetlerinde çakıştırılmış, (211) kırınım profilleri.

KAYNAKÇA

1. Selvam P., Viswanathan B., Swamy C.S., Srinivasan V., (1986), "Magnesium and Magnesium Alloy Hydrides", *Int. J. Hydrogen Energy*, Vol. 11, pp. 169-192.

2. Han E., Eroğlu İ., Türker L., (2000), "Performance of an alkaline fuel cell with single or double layer electrodes" *Int. J. Hydrogen Energy*, Vol. 25(2), pp.157-165

3. Dantzer P, (1997), "Metal Hydride Technology: A Critical Review", *Topics in Applied Physics*, Vol. 73, pp. 273, Springer-Verlag, Berlin Heidelberg.

4. M. Güvendiren, H.E. Ünalan ve Tayfur Öztürk,(2002), "Hidrojen depolama amacıyla magnezyum tozlarının öğütülmesinde katkı maddelerinin etkisi", *Proc. 2002 Int. Powder Metallurgy Conf.* Gazi Universitesi, Ankara.

5. E. Baybörü, (2000), "Magnezyum tozlarının mekanik olarak öğütülmesi ve hidrojen alma/verme özelliklerinin ölçümü", Yüksek Lisans Tezi, ODTÜ, Metalurji ve Malzeme Müh. Böl., Ankara.

6. M. Güvendiren, (2002), "Mekanik alaşımlandırma ile üretilen magnezyum bazlı alaşımların hidrojen sorplama özelliklerinin incelenmesi", Yüksek Lisans Tezi, ODTÜ, Metalurji ve Malzeme Müh. Böl., Ankara.

APPENDIX C

EFFECTS OF ADDITIVES ON MECHANICAL MILLING AND HYDORGENATION OF MAGNESIUM POWDERS*

M. Güvendiren and T. Öztürk
Department of Metallurgical and Materials Engineering
Middle East Technical University
06 531, Ankara, Turkey

ABSTRACT

A study is carried out on the role of additives for structural refinement of magnesium powders in mechanical milling. Additives, namely Al_2O_3, SiC, V and graphite are chosen so as to cover a wide hardness range. Structural refinement after milling are studied both metallographically and in terms of X-ray line broadening. It is found that for efficient structural refinement, the additives should be chosen not on the basis of their hardness but rather whether or not they are preserved with an acceptable size during milling. Thus of the additives, it is found that graphite and Al_2O_3 are most effective. The milled structures are modified upon exposure to hydrogenation temperature, leading to similar structural sizes. In terms of hydrogenation, graphite appears to be the most effective additive. A storage capacity of 6 weight percent is reached with a quite fast sorbing rate.

Keywords: Magnesium hydride; Hydrogen storage; Sorption kinetics; Mechanical milling; Structural refinement; Additives in milling

1. Introduction

In recent years there has been considerable interest in magnesium-based systems for hydrogen storage application [1]. A number of studies have been carried out so as to improve the system, especially to enhance its sorption (absorption and desorption) kinetics [2-6]. As reported in the studies milling or mechanical

---

**Submitted to International Journal of Hydrogen Energy,2003. Accepted in 30 January 2003.*

alloying is a common method. It is well known that magnesium or other hydrogen storage alloys when milled on their own shows a considerable improvement in sorption rate. In order to further enhance the kinetics a variety of additives have been used. For instance, graphite addition to magnesium was studied by Imamura et al [7] and Bouricha et al [8]. Liang et al [9] have studied the transition metal additives. Of these they found that titanium and vanadium is the most efficient in accelerating the sorption rate. Similar improvements are also reported with oxide additions. For instance Oelerich et al [5] have used a variety of oxides as additives and of these Cr_2O_3 and Fe_3O_4 yielded the best absorption and desorption kinetics respectively.

How the use of additives in milling improves the sorption characteristic of magnesium is not clear. With the use of additives such as V there may be a chemical basis for this. Thus Liang et al [9] attribute this to the catalytic effect of vanadium; V acts as "hydrogen pump" by easily dissociating the hydrogen gas into its atomic form and feeding the atoms to the host magnesium. But the fact that similar or sometimes better improvements are obtained with oxide addition implies that the effect may not always have a chemical basis.

Whatever the origin of the improvement, it is clear that an essential requirement for accelerated kinetics is the refinement of particle size in hydrogen storage systems. Thus there is a need to identify conditions of milling that would yield as fine particle size as possible. The current work is undertaken so as to identify the role of additives on structural refinement and subsequent hydrogenation of Mg based systems.

2. Experimental Procedure

Starting material was magnesium hydride (95 wt.% MgH_2, 5 wt.% Mg supplied by Th. Goldmischmidt AG). The hydride form of magnesium was preferred because it is less ductile than magnesium and therefore relatively easy to mill. All millings are carried out for 3 hours with an attritor mill operated at 515 rpm. Stainless steel balls of diameter 6.5 mm were used. Ball to powder ratio was 10:1. The amount of powder milled in each run was 5 g.

Two sets of experiments were carried out. In the first set; samples containing 5 vol.% additives were milled in the presence of alcohol (20 mL). In the second set the samples with additives were prepared on a weight basis (5 wt.%) and milling is carried out within a glove box under argon atmosphere. 1 wt.% graphite is used as anti-sticking agent. Compositions of the samples prepared in both sets are shown in Table 1.

Degree of milling obtained for powders was followed via measurement of X-ray line broadening of selected peaks. Co Kα radiation is used. Peak profiles recorded were used on a comparative basis. Structural sizes of MgH_2 were computed with the use of Scherrer formula from peak profiles recorded for (211) diffraction [10]. Structural size computed in this manner is approximate and refers to diffracting

volume. It should be noted that diffracting volume is not necessarily the particle size [11].

The hydrogen storage properties of milled powders were evaluated using a volumetric method. The mass of the samples was typically 300 mg. Data for pressure-composition isotherms as well as for those of sorption kinetics were recorded after three absorption and desorption cycles. Pressure composition isotherms were recorded at intervals of 1 atmosphere under constant pressure conditions. Absorption rate was followed under an initial pressure of 10 atmospheres and pressure drop is recorded as a function of time. Similarly desorption rate was measured by recording the increase in pressure from the initial pressure set at 1 atmosphere.

3. Results and Discussion

3.1 Structural Refinement

Particulate structure of MgH_2 after 3 hours of milling without any additive are shown in Fig.1 (a). The greater portion of particles is of micron or sub-micron size, though few particles of relatively coarse size e.g. 2-3 microns are also present. MgH_2 when milled with additives develops similar structures. The distribution is however more uniform i.e. coarse particles appear too less in fraction. An example of particulate structure developed is given in Fig.1 (b), which refer MgH_2-Al_2O_3. This is found to be the best as particles obtained are fine with homogeneous distribution.

X-ray line profiles recorded for (211) planes of MgH_2 are given in Fig.2. "Structural size" determined from these profiles are given in Table 2. Structural size obtained with V addition is similar to MgH_2 without addition. There is a pronounced refinement of structural size with other additives. Al_2O_3 and graphite appear to be the most effective additive. They lead to an apparent structural size of approximately 20 nm.

In this part of the study; all samples are prepared with the same volume fraction of additives and thus the samples are similar except for inherent properties of the additives themselves. Under such condition, ratio of additive per host is the same if the additives are of the equal size. In the experiments; Al_2O_3 and SiC additives have approximately the same size (5 microns); V are coarser (13 microns). Graphite had its own flaky form with sizes of approximately 60 microns. Thus it can be stated that samples with Al_2O_3 and SiC additives are milled under similar geometric conditions.

Under similar conditions, it is natural to expect that harder additives will lead to a more efficient milling. However in the current study the observation is just the opposite. The macrostructure with SiC additive as verified with X-ray line broadening are of intermediate fineness and not finer that obtained with Al_2O_3.

This is despite the fact that SiC 1.5 times harder than Al_2O_3. Again the graphite though much softer than Al_2O_3, they both lead to similar structural refinement.

Thus the role of additives in structural refinement is highly complex. The samples are analyzed further with respect to the additives themselves. X-ray line profiles recorded for the additives before and after milling are given in Fig. 3. Graphite has been affected little as it seems to have almost the same width-at-half-maximum. This may be due to layered structure of graphite, which based on SEM observation it is definite that they are broken down into pieces, but the thickness appears to be the same. Alumina shows some broadening after milling but the broadening is not very pronounced. The most pronounced effect is observed in SiC. The additive particles of SiC were milled to such an extent that they seem to have reached to extremely fine size. Thus it can be concluded that in milling graphite and Al_2O_3 remain in the system with almost the same size, but V and especially SiC rather than milling the host particles, i.e. MgH_2, are milled themselves. Therefore the success of additives in milling appears to depend on whether or not their size are preserved during milling. In this respect Al_2O_3 and graphite are more efficient refiner than the other additives studied in this work.

3.2 Sorbing Characteristics

Following the study on structural refinements, three systems are selected for further investigation; MgH_2-Graphite, MgH_2-V and MgH_2. Because in storage, the weights of powders are more important than their volume, the samples are prepared on weight basis, i.e. MgH_2-5 wt.% additive. Structural sizes obtained for these samples in milled condition are included in Table 2.

Pressure-composition isotherms at 623 °K measured for the samples are given in Fig. 4. It is seen that the plateau pressures are in the interval between 2.4 – 6.3 atmospheres. The plateau pressure with graphite is slightly higher than the others.

The capacity i.e. amount of hydrogen stored at the end of plateau is highest with graphite, i.e. 6.0 wt.%. This is higher than the values reported in the literature for graphite additions, which uses Mg rather than MgH_2 as starting material [12]. The capacity reached with V addition and that without addition namely 4.5 and 5.4 % respectively are close to those reported in the literature [4,9].

Prior to measurement of pressure-composition isotherms, samples were subjected to several dehydrating (623°K) and hydrating (673°K) cycles. Naturally structural sizes measured after cycling are different than those measured after milling. In fact for hydrogen storage, "structural size" stabilized after cycling is more relevant than those obtained after milling. Stabilized "structural size" measured for the samples are included in Table 2, and should be compared with those of milling. It should be noted that there is a reverse relationship between the milled sizes and the amount of recovery that occurs upon sorption. For instance in as milled condition the sample with graphite gives the smallest structural size. Upon sorption the amount of recovery is largest for this sample and reaches a structural size of 57

nm. On the other hand the sample without addition yields the largest structural size upon milling and the amount of recovery in this case is much less, see Table 2.

Absorption and desorption kinetics of the samples are given in Fig. 5 (a) and (b) respectively. It is seen that absorption is quite fast in all milled samples, and can store 4 wt.% hydrogen within less than 400 seconds. The values are 250 and 320 seconds for the addition of graphite and vanadium respectively and 380 seconds for the sample without additive. Differences between samples are more pronounced for desorption. Here MgH_2-Graphite has the fastest desorption rate. Similar amount of hydrogen i.e. 4 wt.% can be desorbed within 250 seconds for this sample. The values for MgH_2-V and MgH_2-without additive are 430 and 780 seconds respectively.

Thus of the systems studied in this work MgH_2-graphite appears to be most attractive. This is true for the amount of hydrogen that can be stored in the system as well as for sorption kinetics. It is true that graphite is the most efficient refiner in milling. However, how this is achieved is not clear. Graphite with its layered structure is expected to act as "lubricant". The milling condition with graphite addition should therefore be less severe than for instance in the sample without any additive. Only advantage of graphite is by forming an inert layer-in-between may prevent cold welding of the particles; layers by shearing one over the other may totally envelop the particles and thus prevent particle-particle contact.

It may be argued that improved sorption kinetics with graphite has a physical origin. That is with graphite addition the particle size is less and therefore absorption as well as desorption requires less time. This is however a simplistic argument and not consistent with the current observations. As mentioned above what is relevant here is the structural size after cycling. Though graphite gives the smallest structural size after milling this advantage is lost after cycling. After cycling it is vanadium that gives the smallest structural size, see Table 2.

Thus the fact that graphite gives the highest sorption rate may be due the formation of protective layers around the particles. Similar arguments are advanced by Bouaricha et al [8]. Graphite by encapsulating the metallic particles may form a barrier for oxidation. Thus the freshly created surfaces during milling may be protected in time, in the process minimizing the degree of oxidation.

4. Conclusions

In order to enhance the hydrogen sorption properties, magnesium hydride is milled with the various additives so as to obtain refined particulate size. The current study has shown that

i) for efficient refinement of magnesium hydride, the behavior of the additive during milling is more important than their relative hardness. The additives that preserve their initial size are more effective in producing refined particles of magnesium hydrides. Thus of the

additives investigated in this work graphite and Al_2O_3 are more effective than SiC or V.

ii) with graphite addition system can reach a storage capacity of 6.0 wt.%, highest reached in the current work. The sorption kinetics, especially desorption is enhanced with graphite addition reaching a value of 4 wt.% hydrogen within less than 250 seconds.

It appears that there is no direct relationship between the sorption kinetics and as milled (and sorbed) structural size. Thus chemical factors are perhaps more important than the physical considerations. However for given system i.e. where the chemical factors are the same, fines of structural size in sorbed condition and additives that can achieve this are important for obvious reasons.

Acknowledgement

Support for this work is provided by METU Research Fund (Project numbers AFP-01-07-02-15 and BAP 02-07-47) and TUBITAK (MISAG 213), which authors gratefully acknowledge.

References

[1] Reiser A, Bogdanovic B, Schlichte K. The application of Mg-based metal-hydrides as heat energy storage systems. Int J Hydrogen Energy 2000;25;425-430.

[2] Shultz R, Huot J, Liang G, Boily S,Lalande G, Denis MC, Dodelet JP. Recent developments in the applications of nanocrystalline materials to hydrogen technologies. Mat Sci Eng 1999;A 267;240-245.

[3] Bobet J-L, Akiba E, Nakamura Y, Darriet B. Study of Mg-M (M=Co, Ni and Fe) mixture elaborated by reactive mechanical alloying – hydrogen sorption properties. Int J Hydrogen Energy 2000;25;987-996.

[4] Oelerich W, Klassen T, Bormann R. Comparison of the catalytic effects of V, V_2O_5, VN and VC on the hydrogen sorption of nanocrystalline Mg. J Alloys Comp 2001;322;L5-L9.

[5] Oelerich W, Klassen T, Bormann R. Metal oxides as catalysts for improved hydrogen sorption in nanocrsytalline Mg-based materials. J Alloys Comp 2001;315;237-242.

[6] Khrussanova M, Bobet J-L, Terzieva M, Chevalier B, Radev D, Peshev P, Darriet B. Hydrogen storage characteristics of magnesium mechanically alloyed with $YNi_{5-x}Al_x$(x=0,1 and 3) intermetallics. J Alloys Comp 2000;307;283-289.

[7] Imamura H, Tbata S, Shigetomi N, Takesue Y, Sakata Y. Composites for hydrogen storage by mechanical grinding of graphite carbon and magnesium. J Alloy Comp 2002;330-332; 579-583.

[8] Bouaricha S, Dodolet J-P, Guay D, Huot J, Schulz R. Study of the activation process of Mg based hydrogen storage materials modified by graphite and other carboneceous compounds. J Mat Res 2001; 16; 2893-2905.

[9] Liang G, Huot J, Boily S, Van Neste A, Schulz R. Catalytic effect of transition metals on hydrogen sorption in nanocrystalline ball milled MgH_2-Tm (Tm=Ti, V, Mn, Fe, and Ni) systems. J Alloys Comp 1999;292;247-252.

[10] Warren BE, Biscoe J. J American Ceramic Soc1938; 21;49.

[11] Warren BE, Averbach BL. J Appl Phys 1950;21;595

[12] Bouaricha S, Dodelet JP, Guay D, Huot J, Shulz R. Activation characteristics of graphite modified hydrogen absorbing materials. J Alloys Comp 2001;325;245-251.

Tables

Table 1 Additives in Mg based systems.

	Milled with solvent		Milled under argon	
Additives	(Vol.%)	(Wt.%)	(Wt.%)	(Vol.%)
SiC	5	10	-	-
Al_2O_3	5	13	5	1.88
V	5	18	5	1.24
G (Graphite)	5	8	5	3.29

Table 2 Structural sizes for MgH_2 milled with additives for 3 hours.

	Structural Size, nm		
System	(Milled-solvent)	(Milled-argon)	(Milled and Sorbed)
MgH_2+5wt.%Al_2O_3	20.4	-	-
MgH_2+5wt.%G	21.6	26.1	57.1
MgH_2+5wt.%SiC	23.6	-	-
MgH_2	31.2	32.7	45.4
MgH_2+5wt.%V	31.2	26.5	60.6

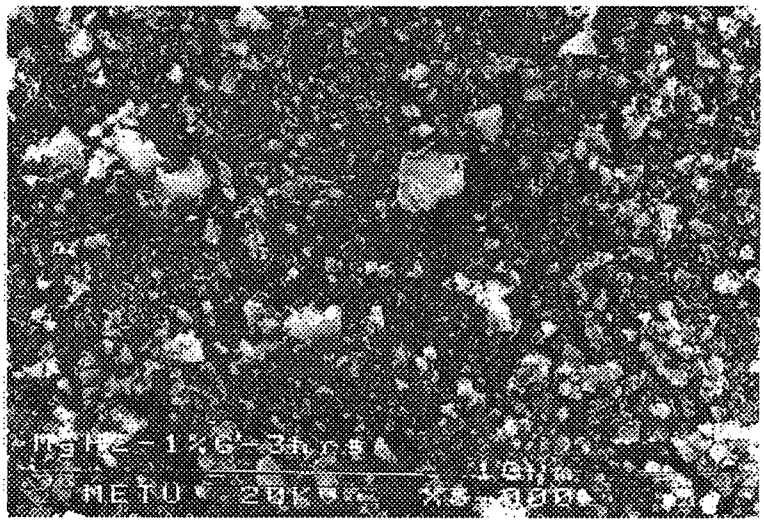

(a)

(b)

Figure 1. SEM micrographs of MgH_2 powders milled for 3 hours; (a) MgH_2, (b) MgH_2- 5 vol.% Al_2O_3.

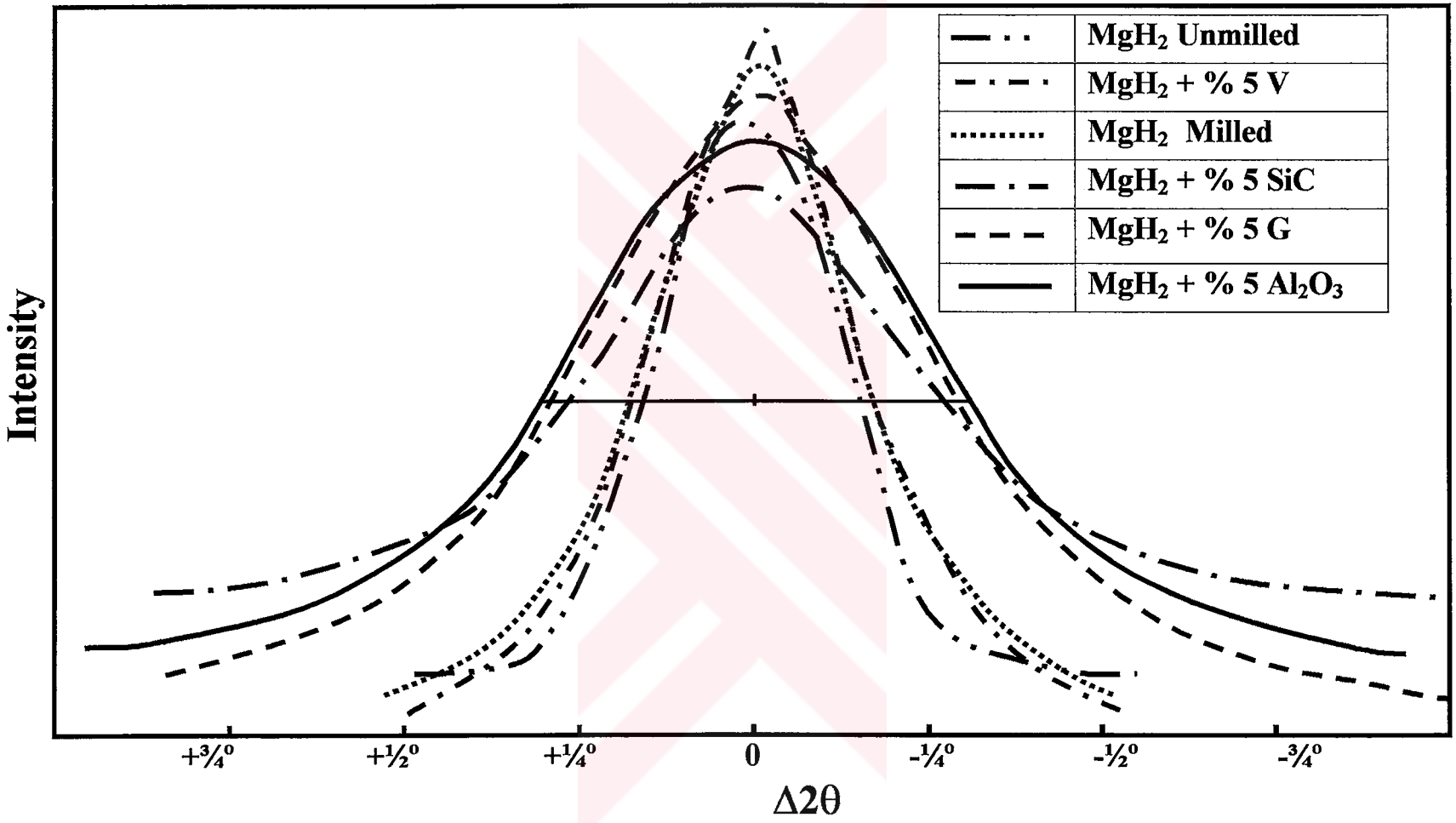

Figure 2. X-Ray line profile of (211) reflection of MgH_2 milled for 3 hours with and without additives. Peaks are moved and superimposed symmetrically at half maximum.

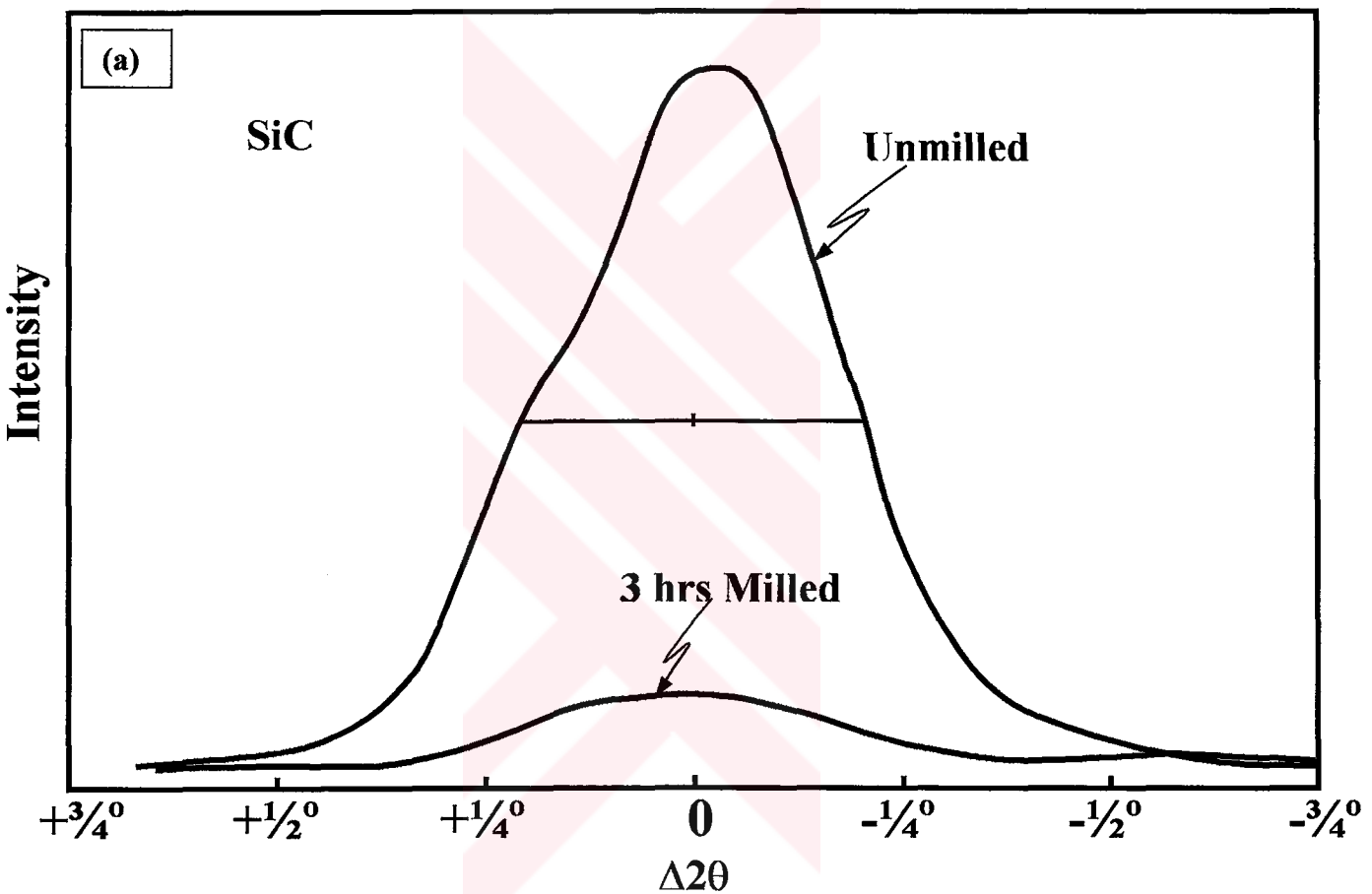

Figure 3 X-ray line profile of additives before and after milling. The peaks -except for SiC- are moved and superimposed symmetrically at half maximum; a) SiC (110), b) Al_2O_3 (116), c) Graphite (002), d) V (110).

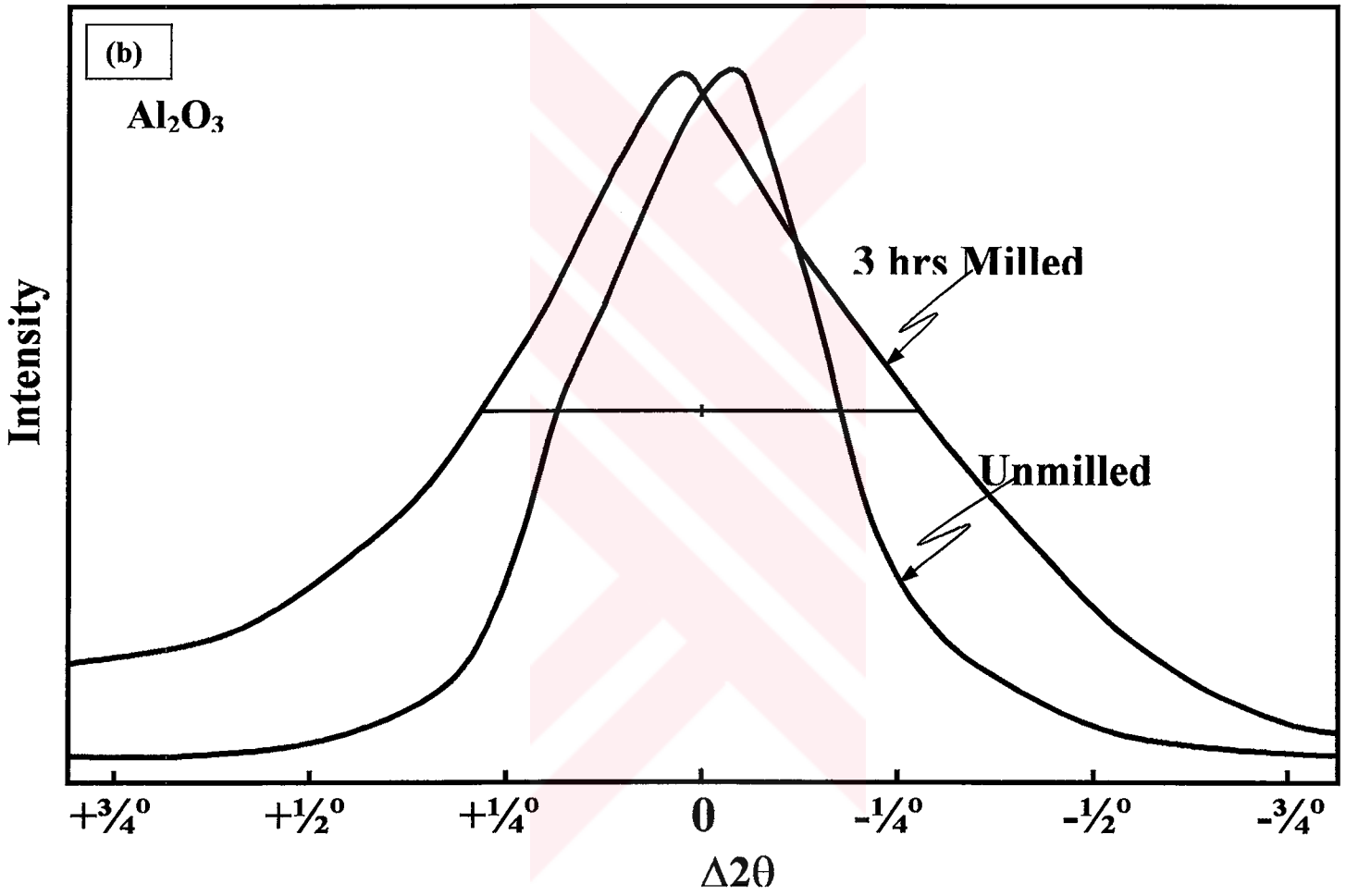

"Figure 3 (continued)"

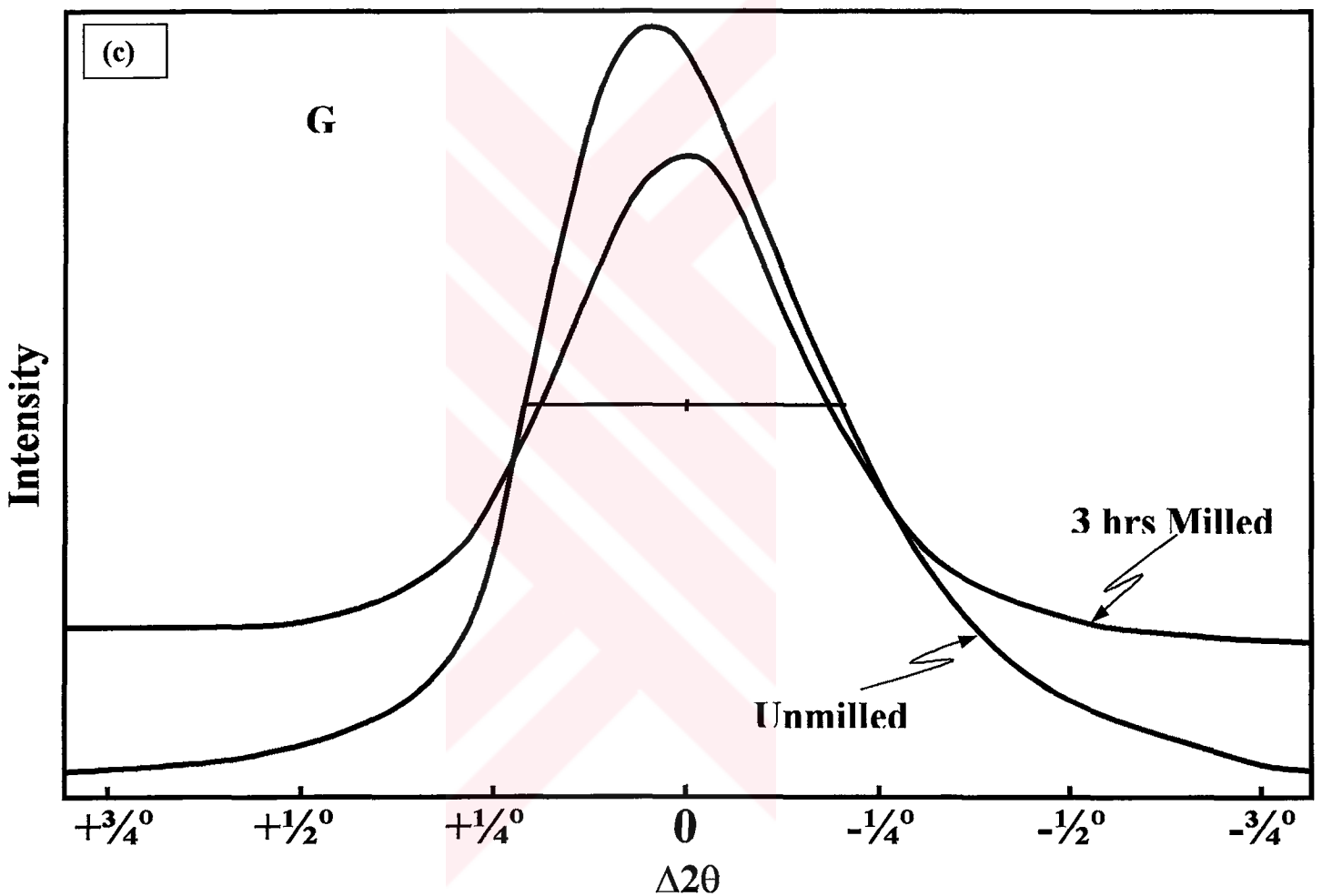

"Figure 3 (continued)"

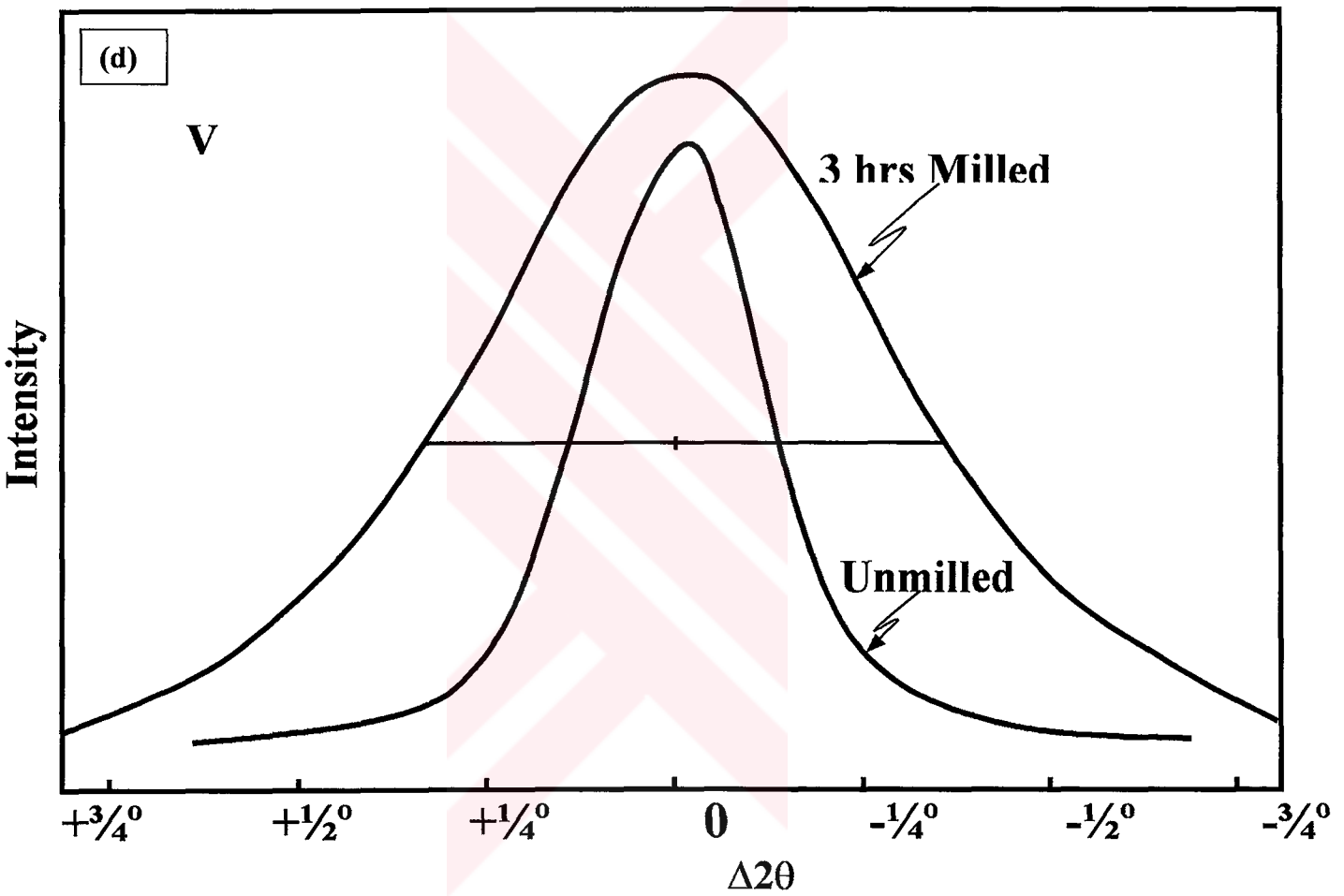

"Figure 3 (continued)"

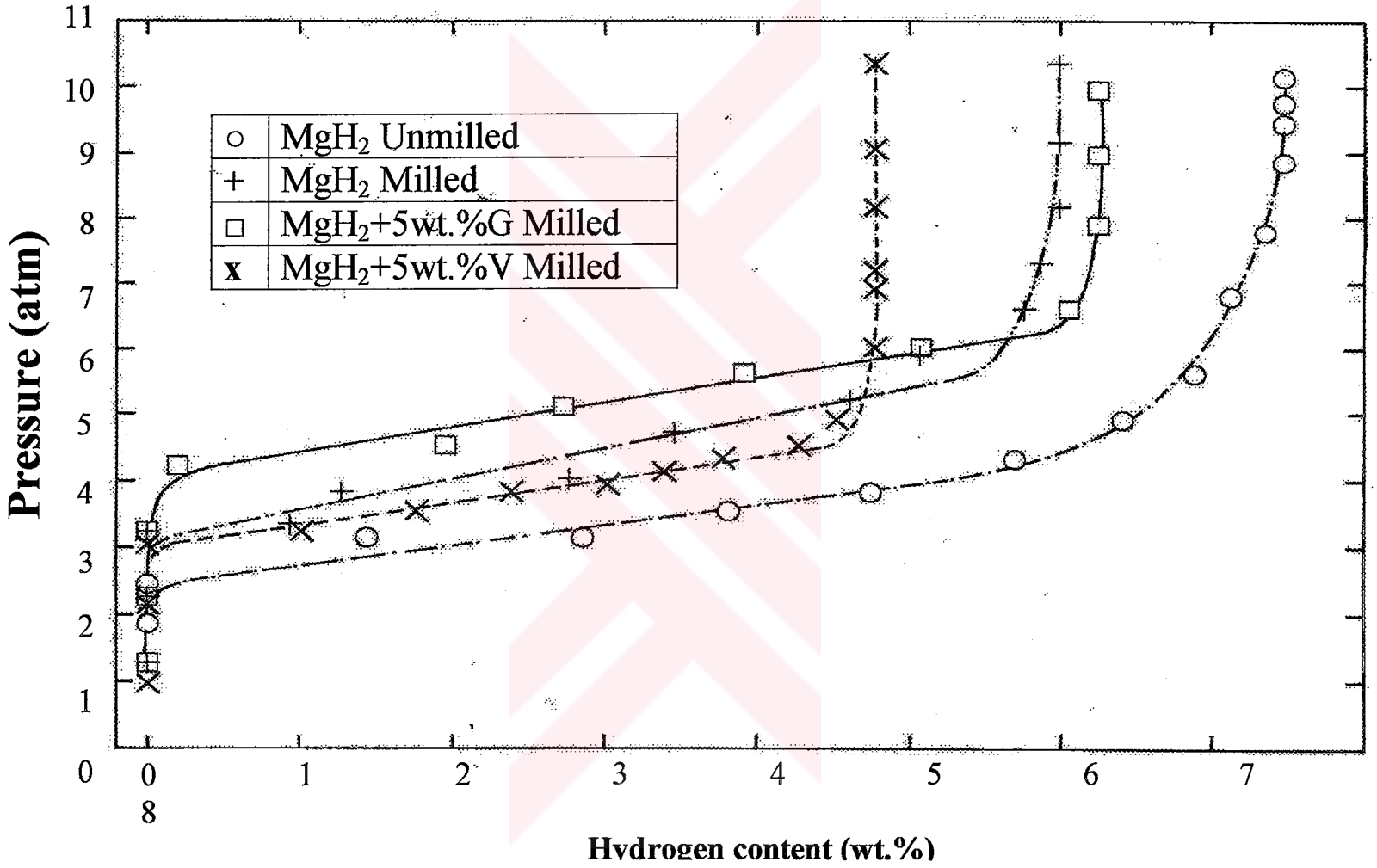

Figure 4. Pressure-composition isotherms of Mg based systems. The isotherms are determined at 623 °K for absorption.

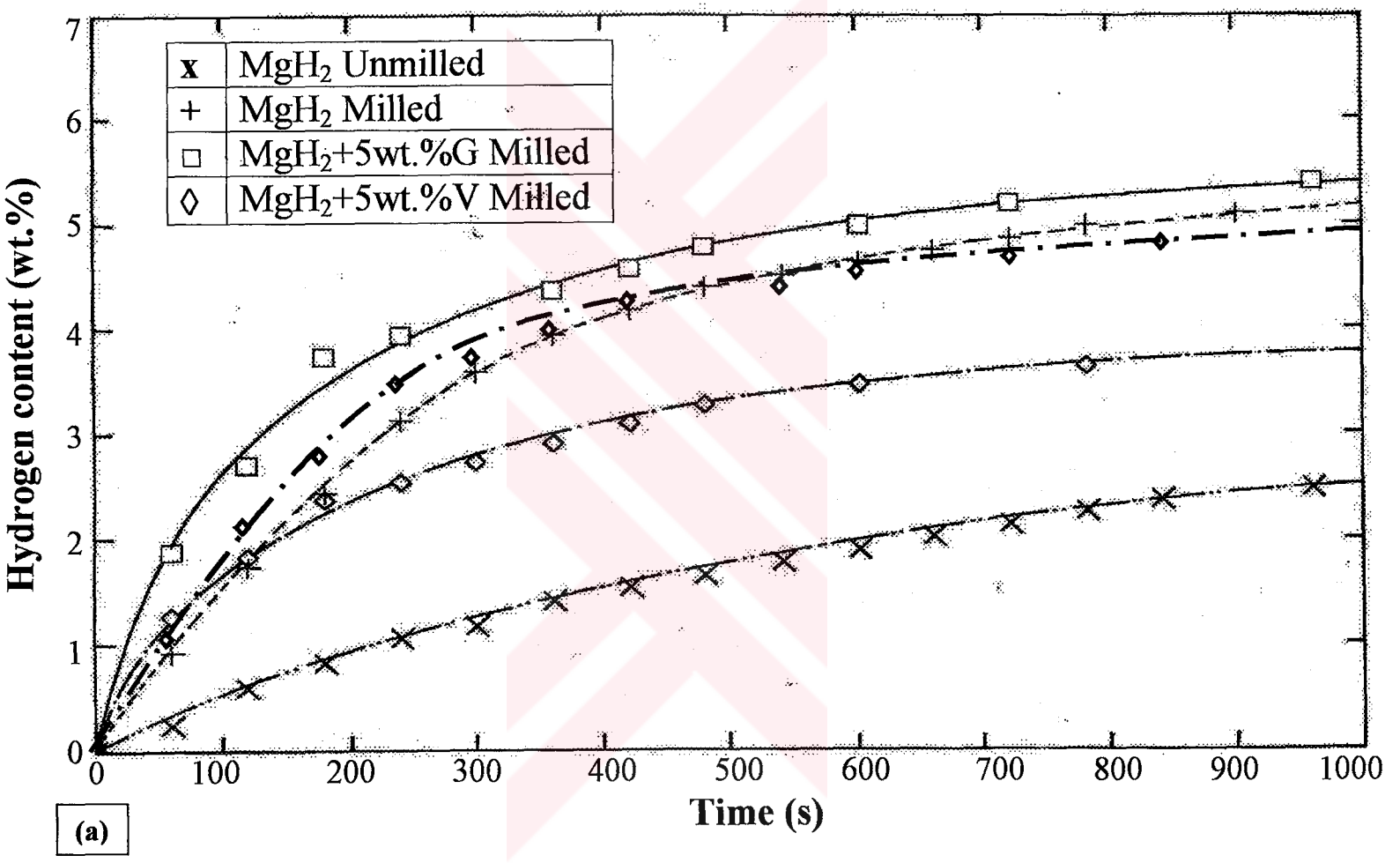

Figure 5. Sorption kinetics for MgH_2 milled for 3 hours with and without additives; (a) for absorption at 623 °K, (b) for desorption at 673 °K.

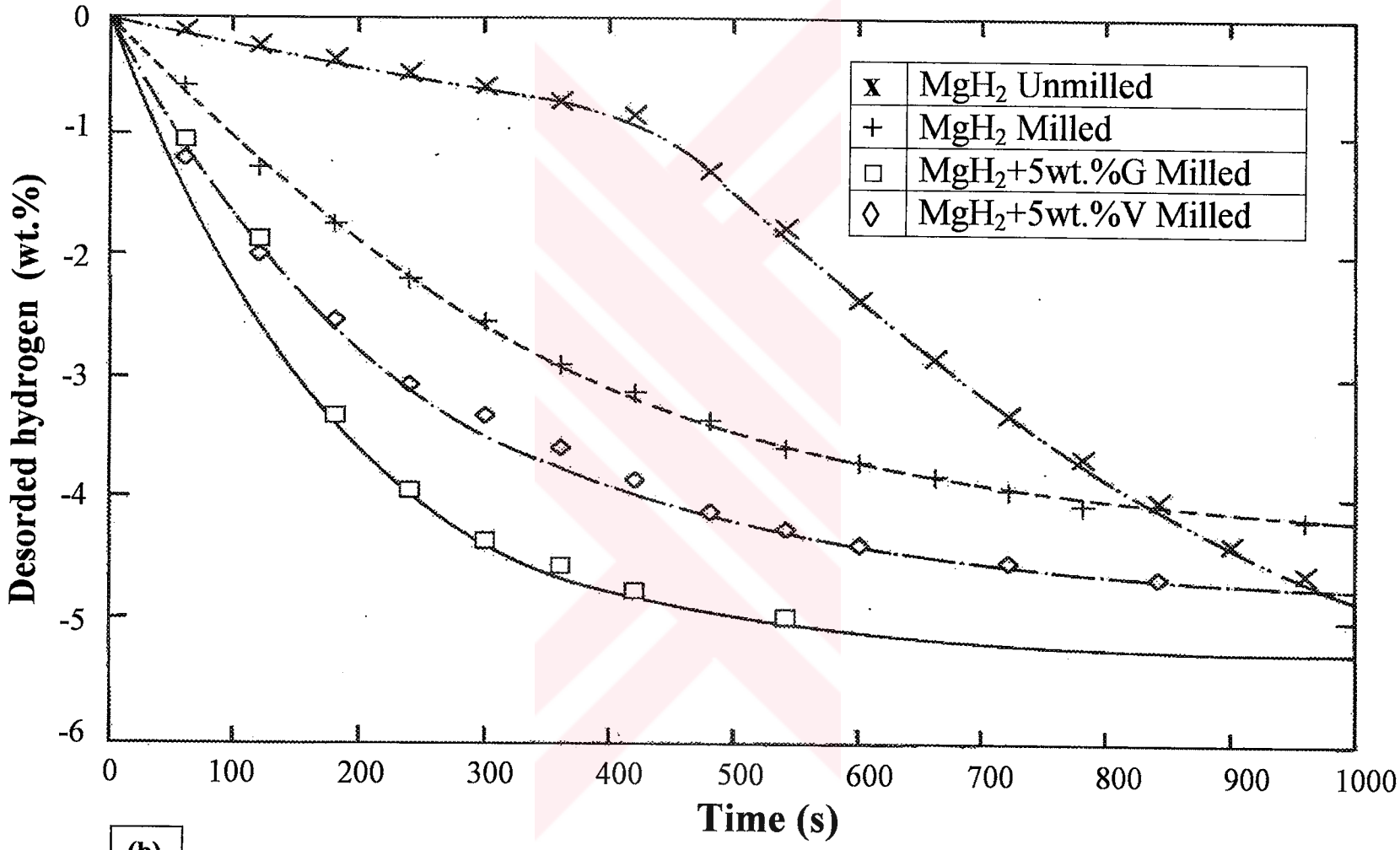

"Figure 5 (continued)"